GDE2-DEPENDENT ACTIVATION OF CANONICAL WNT SIGNALING IN NEURONS REGULATES OLIGODENDROCYTE MATURATION

by
Bo-Ran Choi

A dissertation submitted to Johns Hopkins University in conformity with the requirements for the degree of Doctor of Philosophy

Baltimore, Maryland
May, 2020

Abstract

Neurons and oligodendrocytes communicate to regulate oligodendrocyte development and to ensure appropriate axonal myelination. Here, we show that Glycerophosphodiesterase phosphodiesterase 2 (GDE2) is part of a signaling pathway in neurons that promotes oligodendrocyte maturation through the release of soluble neuronally-derived factors. Mice lacking global or neuronal GDE2 expression have reduced mature oligodendrocytes and myelin proteins but retain normal numbers of oligodendrocyte precursor cells (OPCs). WT OPCs cultured in conditioned medium (CM) from *Gde2* null (*Gde2-/-*) neurons exhibit delayed maturation, recapitulating *in vivo* phenotypes. *Gde2-/-* neurons show robust reduction in canonical Wnt signaling, and genetic activation of Wnt signaling in *Gde2-/-* neurons rescues in vivo and in vitro oligodendrocyte maturation. Phosphacan, a known stimulant of OL maturation, is reduced in CM from *Gde2-/-*neurons but is restored when Wnt signaling is activated. These studies identify GDE2 control of Wnt signaling as a novel neuronal pathway that signals to oligodendroglia to promote oligodendrocyte maturation.

Thesis Advisor: Dr. Shanthini Sockanathan, D.Phil, Professor of Neuroscience, The Solomon H. Snyder Department of Neuroscience, Johns Hopkins University School of Medicine

Reader: Dr. Alex Kolodkin, Ph.D, Professor of Neuroscience, The Solomon H. Snyder Department of Neuroscience, Johns Hopkins University School of Medicine

Table of Contents

List of Tables

List of Figures

Chapter 1
Introduction

1.1 Neural cell-type diversity and oligodendrocyte (OL) development

1.1.1 Diversity of neural cell types in the brain

The brain is comprised of diverse cell types that include neurons, glia, and capillary-associated cells. Neurons are highly polarized cells that conduct electrical signals along axons to transmit information to their terminals for synaptic transmission. Glia are a group of cell types with small soma that can be further classified into astrocytes, microglia, and oligodendrocytes (OLs). Historically, glia were considered to be static and to function as the structural “glue” of the nervous system. However, recent studies indicate that they have varied, specialized functions that are critical for nervous circuit function. Astrocytes are involved in regulating water balance and ion distribution, and for maintaining the blood-brain barrier via the formation of endfeet that contact the vasculature system[1]. In addition, astrocytes have been discovered to modulate synaptic transmission through the release of gliotransmitters from astrocytes that surround the pre- and postsynaptic membranes in the so-called tripartite synapse[2]. Microglia are the resident immune cells in the central nervous system (CNS) that function in immune defense as well as in synaptic pruning[3]. Oligodendrocytes, in contrast, facilitate electrical conductance by their production of myelin sheets that wrap around axons and, in addition, serve to provide nutrients and neurotrophic factors to neurons that are essential for neuronal survival[4]. Thus, the diverse cell types in the brain structurally and functionally interact each other to ensure the appropriate generation and function of

neural circuits. However, there is still much to learn as to how neuronal and glial cells interact to control these events.

1.1.2 Development of OLs

1.1.2.1 OL lineage specification, proliferation, and migration

Glial development initiates after neurogenesis is complete, with OLs being generated before astrocytes. The formation of mature OLs occurs in sequential stages that are characterized by changes in morphology, and changes in gene and protein expression. Oligodendrocytes are produced from three distinct waves of OL progenitor cells (OPCs) in the forebrain[5]. The earliest wave of OPCs is generated at around embryonic day (E)11.5 in the medial ganglionic eminence and anterior entopeduncular area, and these OPCs populate the telencephalon by E14.5. However, these early OPCs are replaced in the cortex by two waves of later-born OPCs that occur first at E15.5 in the lateral ganglionic eminence and then at birth in the cortex[5]. The intermediate and later-born cortical OPCs produce cortical oligodendrocytes in the ratio of 1:4 in the adult, while the first wave of early-born OPCs predominate in the ventral forebrain and corpus callosum[6,7]. OPCs express receptors that are responsive to mitogenic factors such as platelet-derived growth factor (PDGF)[8]. Mitotically active OPCs leave the oligodendrogliogenic zones and radially migrate out throughout the forebrain, including the cortex. Once they reach their destinations, they terminally differentiate into mature OLs and proceed to initiate myelination[7]. A subpopulation of OPCs does not differentiate and retains their proliferative potential into adulthood, and these are referred to as adult OPCs[9]. These adult OPCs constitute up to 10% of the

cells in the CNS, and they have a characteristic uniform distribution across brain regions that span areas that are high and low in myelination.

1.1.2.2 OL maturation

The differentiation of OPCs into mature OLs is tightly regulated both temporally and spatially. For example, within the cortex, OPC differentiation and subsequent myelination initiates in deeper cortical layers before extending to the upper cortical layers even though axons are present throughout all cortical layers[10]. As OPCs undergo maturation, they exhibit distinct changes in their morphology as well as in their gene and protein expression profiles. All OL lineage cells coexpress Olig2 and Sox10[11,12]. Mitotically active proliferating OPCs have branched dendrites, also known as polydendrocytes, and express PDGF receptor alpha (PDGFRα) and neuron/glia antigen 2 (NG2) on the membrane[13]. As they exit the cell cycle and differentiate, cells undergo complex morphological transitions, extending highly branched and elaborate processes that ultimately myelinate axons. Differentiating OPCs decrease the expression of PDGFRα and NG2, and they concomitantly increase the expression of genes and proteins that are involved in OL maturation and myelination. For instance, the expression of TCF4 protein as well as long non-coding RNA 9630013A20Rik is transient and peaks in immature OLs[14,15]. In addition, the expression of CC1 and 2',3'-cyclic nucleotide 3'-phosphodiesterase (CNP) proteins and also *Myelin Basic Protein* (*Mbp*) transcripts increase in maturing OLs[16,17]. As cells mature further, myelinating OLs express myelin proteins including myelin basic protein (MBP), proteolipid protein (PLP), and myelin/oligodendrocyte glycoprotein (MOG) and aspartoacylase (ASPA)[18,19]. The

stage-specific expression of these proteins and transcripts has been utilized to molecularly define different stages of OL development and is commonly used in the field to study OL development (Fig 1.1).

1.1.2.3 OL myelination

Myelination is a process where mature OLs ensheath axons with a multilayered myelin sheet. Myelin consists of a lipid-rich membrane in which myelin-specific proteins such as MBP, PLP, and MOG are deposited.This process involves the spiral and longitudinal extension of OL plasma membrane that is coordinated by the transport of *Mbp* mRNA and local translation[20] (Fig 1.2). The ultrastructure of compact myelin features multilayered periodic alterations of electron-dense lines and intraperiod lines that are formed by the apposition of intracellular and extracellular membrane surfaces, respectively[21]. The myelinated parts of axons are termed internodes while the unmyelinated segments are referred to as the Nodes of Ranvier, which are highly enriched in voltage-gated ion channels[22,23]. The segmental arrangement of myelin facilitates the rapid propagation of electrical signals through saltatory conduction[24]. Unlike Schwann cells in the PNS that myelinate one target axon, OLs myelinate multiple axons, ranging up to 50 axons per OL. The peak period of axonal myelination occurs during the first postnatal month in mice; in humans, this period spans the first 1~2 years after birth[25]. Importantly, *de novo* myelination can still occur in the adult nervous system, and recent studies speak to the plasticity of myelination during learning and social interactions[26,27].

1.1.3 Regulatory mechanisms underlying OL development

1.1.3.1 Diversity in OL development

OPCs and OLs are believed to be heterogeneous populations based on their developmental origins and morphology[7,28]. As discussed in section 1.1.2.1, OPCs in the brain are specified from distinct regional origins at specific time points. The three different waves of OPCs are induced by various morphogens including BMP, Wnt, and SHH that originate from different organizing centers of the forebrain[7]. Further, the timing of OL differentiation and subsequent myelination patterns during development are also heterogeneous. In the cortex, OL maturation and myelination appear in the deep cortical layers prior to the superficial layers[10] and there are more OLs in the white matter than the grey matter. In addition, OLs in the spinal cord make longer internodes than OLs in the brain[21]. Interestingly, single cell RNA sequencing (scRNA-seq) analyses reveal that OPCs derived from different waves of OPCs in the brain have homologous transcriptional signatures, suggesting that OPCs from different spatiotemporal origins are initially equivalent at the transcriptional level[29]. Another study from the same group reported that postnatal OPCs in the spinal cord and brain also have similar gene expression profiles[14]. However, OL lineage cells from different brain regions diverge transcriptionally and in their electrophysiological properties as animals age[30]. These studies suggest that OL diversification likely occurs as OPCs differentiate and imply that OL heterogeneity likely arises as a consequence of local extrinsic cues and interactions with neighboring cells.

1.1.3.2 Neuronal-dependent mechanisms of OL maturation

The initiation of myelination is thought to occur when differentiating OLs directly interact with axons during development. Differentiating OLs dynamically extend and retract their elaborate membrane processes in response to local cues until they make stabilized contacts with a target axon. The establishment of a stable contact is mediated by surface-localized receptors and adhesion molecules that converge to stimulate activity of the non-receptor Src-family tyrosine kinase Fyn in OPCs[31]. Interestingly, many contact-mediated cues appear to inhibit OL differentiation, presumably to ensure the appropriate timing of axonal myelination during development. For example, PSA-NCAM inhibits OPC differentiation and is downregulated to coincide with myelination[32], as is the canonical Notch ligand Jagged, which is expressed on axons and binds the Notch receptor on OPCs to inhibit OL differentiation[33]. The finding that OLs cultured with inert polystyrene fibers exhibit a size-dependent ensheathment of 0.4 μm fibers or more suggests that axonal caliber also contributes to OL myelination[34]. Of note, both myelinated and unmyelinated axons range in diameter from 0.2-0.8μm *in vivo*[35], suggesting the existence of repulsive and instructive axonal cues that integrate axonal caliber with OL developmental mechanisms. One such cue is likely to involve Akt-mTOR signaling, as activation of this pathway increased the caliber of normally unmyelinated cerebellar axons and expanded OPC progenitors and production of myelinating OLs[36]. Another major factor that influences OL proliferation, differentiation and maturation is neuronal activity. Neuronal activity releases adenosine and glutamate, which regulates the proliferation and differentiation of OPCs into myelinating OLs[37,38]. In addition, ATP released by electrically active neurons can stimulate astrocytes to produce leukemia inhibitory factor (LIF), which

promotes OL differentiation[39]. Thus, contact-mediated signals, axon caliber and neuronal activity are important for OL development. However, the role of other neuronal pathways that regulate OL development is still unclear.

1.1.4 Wnt signaling pathway

1.1.4.1 Canonical Wnt signaling pathway

The Wnt signaling pathway is a major regulator of multiple developmental processes that include tissue shaping, cell proliferation, differentiation, and maturation[40-43]. Wnt ligands can activate three main downstream signaling cascades that utilize distinct pathway components. For instance, Wnt signal transduction that involves the stabilization of β-catenin eventually leads to changes in gene expression, and this pathway is known as the canonical Wnt signaling pathway[44]. The two remaining pathways primarily affect the cytoskeleton and the mitotic spindle, and these pathways are mediated through the activation of the Wnt/planar cell polarity pathway and Wnt-Calcium pathways[44]. Among these mechanisms of Wnt signal transduction, the canonical Wnt signaling pathway is the most studied and accordingly, the best understood. In the absence of Wnt ligand, β-catenin is degraded by a destruction complex comprised of proteins that include Axin, APC, and the Ser/Thr kinases GSK3β and CK1, and the E3-ubiquitin ligase βTrCP[43] (Fig 1.3). After phosphorylation and subsequent ubiquitination, modified β-catenin is degraded by the proteasome[45]. In contrast, when Wnt ligand is available, Wnt binds to a multiprotein receptor complex comprising of the Frizzled receptor and the low-density-lipoprotein receptor-related proteins (LRP) 5/6 (Fig 1.3). This results in receptor dimerization, interaction with Wnt

cascade mediators, and subsequent inhibition of the destruction complex, which prevents β-catenin degradation[45]. The stabilization of unphosphorylated free β-catenin results in its translocation into the nucleus. β-catenin does not have a DNA binding -domain; however, it interacts with the TCF/LEF family of transcription factors in the nucleus to regulate the expression of Wnt target genes, including the transcription factor *Lef1*[46,47]. Of note, β-catenin plays a second role as a binding partner for cadherins such as E-adherin in adhesion junctions[48]; however, the adhesive and signaling properties of β-catenin are believed to be independent.

The complexity of Wnt signaling is immense. For instance, there are 19 different Wnt ligands, 10 FZD receptors and 3 LRP co-receptors (Http://web.stanford.edu/group/nusselab). Each Wnt ligand can interact with different combinations of receptors and co-receptors and the type as well as concentration of Wnt ligand can elicit different downstream responses within the same cells. Combinations of Wnt ligands can also synergize with each other to influence cellular responses[49]. Adding further complexity, Wnts are not the only ligands for FZDs; Norrin proteins can also bind and activate FZD receptors[50,51]. Although the FZD/LRP proteins act as the primary Wnt receptors, there are other proteins that can function as receptors for Wnt ligands. In the vasculature system for instance, Wnt7 can interact with not only FZD4 and LRP, but also a multi-receptor complex with Gpr124[52]. In addition, Wnt can directly bind RECK, a GPI-anchored protein that is part of the FZD/LRP/GPR124 complex. Wnt signal transduction cascades can further be tuned by other factors. For example, extracellular proteins such as Notum and Dickkopf (DKK) can modulate Wnt signal transduction[53,54]. Notum directly deacylates Wnt to prevent receptor binding while

DKK antagonizes Wnt signaling activity by binding LRP5/6[55]. Additionally, the GPI-anchored glypican proteins have been shown to modulate Wnt signaling on the plasma membrane via inhibitory or activation mechanisms depending on cellular context[54,56].

1.1.4.2 The roles of canonical Wnt signaling in the postnatal cotex.

Canonical Wnt signaling has fundamental roles in the formation and maintenance of the CNS. In the developing cortex, different Wnts, Wnt receptors, and Wnt regulators are expressed in overlapping patterns in different layers. The expression of Wnt signaling components persists in the postnatal cortex; however, their expression is refined so that specific components are restricted to distinct cortical regions and laminae[47]. In embyonic development, canonical Wnt signaling regulates the rostral-caudal and medial-lateral patterning of the cortex and plays roles in the organization of radial cortical layers[57]. Less is known of the roles of canonical Wnt signaling in the postnatal cortex. Recent studies report that canonical Wnt signaling activity in postmitotic pyramidal neurons is dynamic and temporally regulated during neuronal migration in perinatal and early postnatal cortex (~P6) (Fig 1.4.A) [58,59]. Further, canonical Wnt signaling is implicated in OL development in the postnatal cortex (Fig 1.4.B). For instance, activation of canonical Wnt signaling in cortical neural progenitor cells (NPCs) inhibits neocortical OPC generation[60,61] and this is dependent on the extent and timing of Wnt activation. Specifically, transient downregulation of Wnt signaling activity results in delayed OPC generation[62], while complete ablation of Wnt signaling activity showed a minimal effect on OPC production[61]. Whether canonical Wnt signaling plays a key role in OL differentiation and myelination is still not known. Genetic

and pharmacological studies that activate Wnt constitutively suggest that Wnt activation inhibits the transition of OPCs to OLs[60,63]. However, the physiological roles for Wnt signaling in OL maturation is still unclear as different studies report that ablating Wnt function can inhibit or promote OL maturation, and in one case, has no affect at all[61,64,65]. Nevertheless, these collective studies suggest important roles for canonical Wnt signaling in cortical development and indicate that the strength and duration of Wnt activity are finely regulated in neural cell types at different developmental stages.

1.2 GDE2 in the central nervous system

1.2.1 GDE family proteins

GDE2, GDE3, and GDE6 are six-transmembrane proteins that contain an external enzymatic domain that bears homology to bacterial glycerophosphodiester phosphodiesterases (GDPD)[66]. They are the only known enzymes in vertebrates that function at the cell surface to cleave the glycosylphosphatidylinositol (GPI)-anchor that tethers some proteins to the plasma membrane. There are approximately 150 annotated GPI-anchored proteins in the mammalian genome, and many of these proteins have been shown to play important roles in cell signaling, adhesion and intercellular communication in health and disease[67 68].

GDE2, also known as GDPD5, has important roles in nervous system development . GDE2 is required for the generation of late-born α-motor neurons in the

spinal cord that innervate the limb, and is also essential for the appropriate timing of cortical neuronal differentiation[69]. Supporting roles for GDE2 in promoting neurogenesis, GDE2 is also found to promote the differentiation of neuroblastoma cells and high GDE2 activity is associated with good prognosis for patients with neuroblastoma[70]. GDE2 function in neurogenesis is associated with its ability to cleave and regulate GPI-anchored protein function. For example, GDE2 regulates spinal motor neuron differentiation through cleavage of the GPI-anchored protein RECK[71], while its role in neuroblastoma differentiation occurs through cleavage of the glypican protein GPC6[70]. GDE2 has roles outside the nervous system. GDE2 is required for appropriate pancreatic development in zebrafish models[72]. In addition, GDE2 is also reported to metabolize glycerophosphocholine and is implicated in breast cancer and kidney homeostasis[73].

GDE3 (or GDPD2) was first identified in osteoblasts and was shown to inhibit osteoblast proliferation and induce their differentiation[74]. Consistent with its roles in inhibiting proliferation, GDE3 slows the growth of breast cancer cells and this activity is attributed to its cleavage and regulation of the GPI-anchored protein uPAR[75]. More recently, we have shown that GDE3 inhibits the proliferation of OPCs and that this occurs through the release of the GPI-anchored protein CNTFRα, a component of the multicomplex CNTF receptor that consists of CNTFRα, LIFR and gp130[76]. GDE6 (GDPD4) is also capable of cleaving GPI-anchored proteins; however its function remains unknown.

1.2.2 The mechanism of GDE2 function in neurogenesis

GDE2 is expressed in postmitotic spinal motor neurons and cortical neurons in the developing central nervous system where it regulates the temporal differentiation of specific neuronal subtypes[77,78]. In both cases, GDE2 promotes neuronal differentiation by downregulating Notch signaling, which is required to maintain progenitor cells in an undifferentiated state[77,78]. In the developing spinal cord, Notch signaling in progenitors within the pMN domain is stimulated by binding to the transmembrane Notch ligand Delta (Dll 1), which is expressed on the surface of neighboring newly differentiated motor neurons[79]. The GPI-anchored protein RECK is also expressed in motor neurons and ensures Notch activation by inhibiting the metalloprotease ADAM10 from shedding Dll 1[80]. The initiation of GDE2 expression in motor neurons leads to cleavage and inactivation of RECK, which stimulates ADAM10 shedding of Dll1. This shuts down Notch signaling in neighboring progenitors and initiates their differentiation into postmitotic neurons. This study defined the mechanism of GDE2 function in neurogenesis and identified the six-transmembrane GDEs as the only known GPI-anchor cleaving enzymes in vertebrates that function at the cell surface (Fig 1.5).

GDE2 also regulates the timing of neurogenesis in the developing cortex. The different layers of the cortex are established by the temporal generation and migration of specific neuronal subtypes in an “inside- out” manner. Early born neurons reside in deep cortical layers whereas later-born neurons migrate through the deep layers to populate more superficial layers[81]. Loss of GDE2 in the developing cortex results in an increase in Notch signaling and this leads to a decrease in deep-layer cortical neurons and an expansion of neurons in superficial layers[78]. Collectively, these studies show

that GDE2-mediated regulation of Notch signaling is required for the temporal control of neuronal differentiation in the developing CNS.

1.2.3 GDE2 in the adult nervous system

We have found that GDE2 expression persists in adulthood. Aged mice lacking GDE2 expression show progressive neurogenerative pathology in the spinal cord suggesting that GDE2 is required for neuronal survival[82]. Specifically, motor neurons in mice lacking GDE2 display neuropathologies that include increased vacuolization, gliosis, cytoskeletal protein accumulation, increased deposition of lipofuscin, and motor neuron death[82]. Temporal genetic ablation of GDE2 that preserves its embryonic expression but removes postnatal expression recapitulates motor neuron degenerative pathologies, indicating that GDE2 function in neuronal survival is attributable to its postnatal function. These observations suggest that GDE2 has neuroprotective roles in the adult CNS that are distinct from its roles in embryonic development.

1.3 Summary and Specific Aims

OLs are important regulators of neural circuit function. OLs produce myelin, a lipid-rich extension of their plasma membrane that wraps axons and facilitates the fast, saltatory conduction of action potentials. In addition, OLs serve as a source of metabolic support for neurons that help promote neuronal health and survival[4]. The development of OLs is tightly regulated both spatially and temporally, and this requires the coordinate action of cell-extrinsic and cell-intrinsic factors. This involves in part, communication

between axons and OLs; however, the neuronal pathways that control the timing of OL development are not well understood.

Our laboratory has previously shown that GDE2 is required for embryonic neurogenesis and for adult motor neuron survival. However, roles for GDE2 in early postnatal development have not been defined. We find that GDE2 is primarily expressed in neurons but is also expressed in oligodendrocytes in the postnatal cortex. Based on these observations, I hypothesize that GDE2 regulates the development of OLs in the postnatal brain.

I will test this hypothesis in the following Aims:

Specific Aim 1: To characterize GDE2 expression and requirement in OL development and myelination.

Specific Aim 2: To determine the cell type-specific contributions of GDE2 to OL development and myelination.

Specific Aim 3: To identify the mechanism by which GDE2 regulates OL development and myelination.

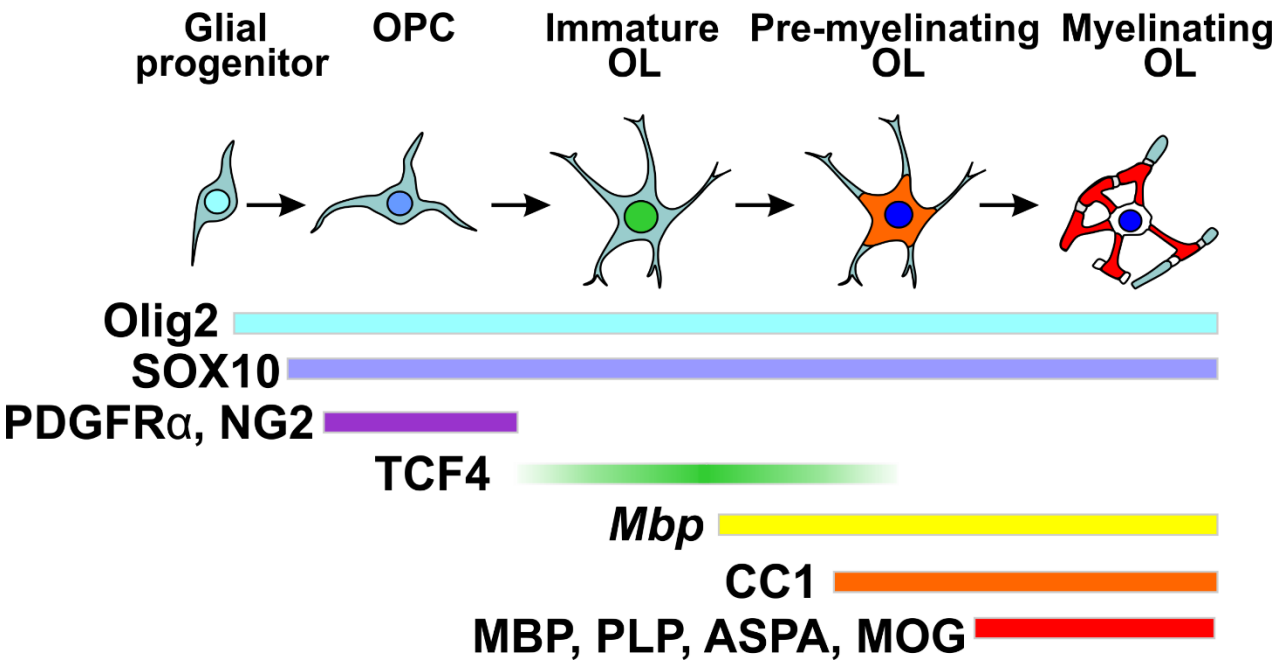

Figure 1.1. Molecular markers that define the stages of OL development

This schematic illustrates the the expression of specific proteins and transcripts that delineate the stages of OL development. The length of the colored bars indicates the duration of marker expression.

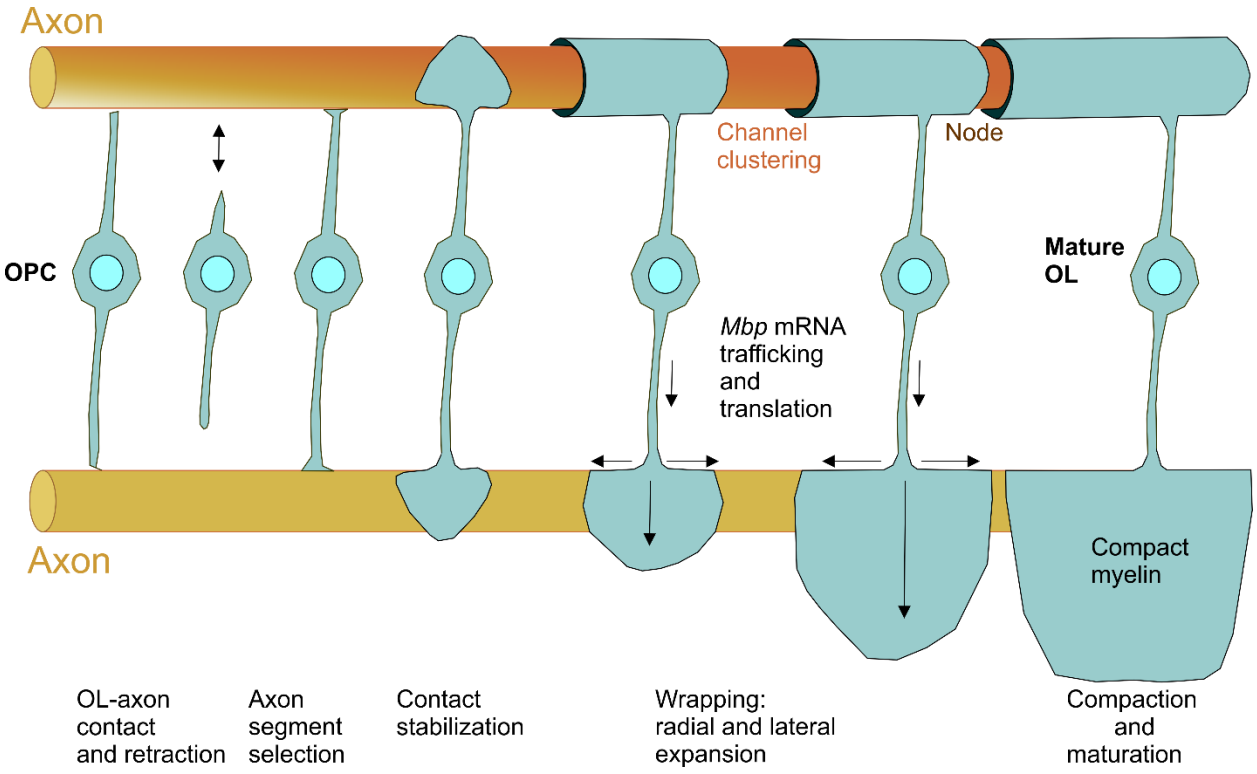

Figure 1.2. The process of axonal myelination

This schematic illustrates the cell biology of axonal myelination. OPCs extend and retract their cellular processes until a stabilized contact with axons is formed. Radial and lateral extension (arrows) of the myelin membrane is accompanied by the deposition of myelin proteins such as MBP. The top axon exemplifies the rolled myelin sheath whereas the lower axon depicts unrolled myelin. Maturation of the node of Ranvier involves the clustering of axonal voltage-gated ion channels. Adapted from [83]

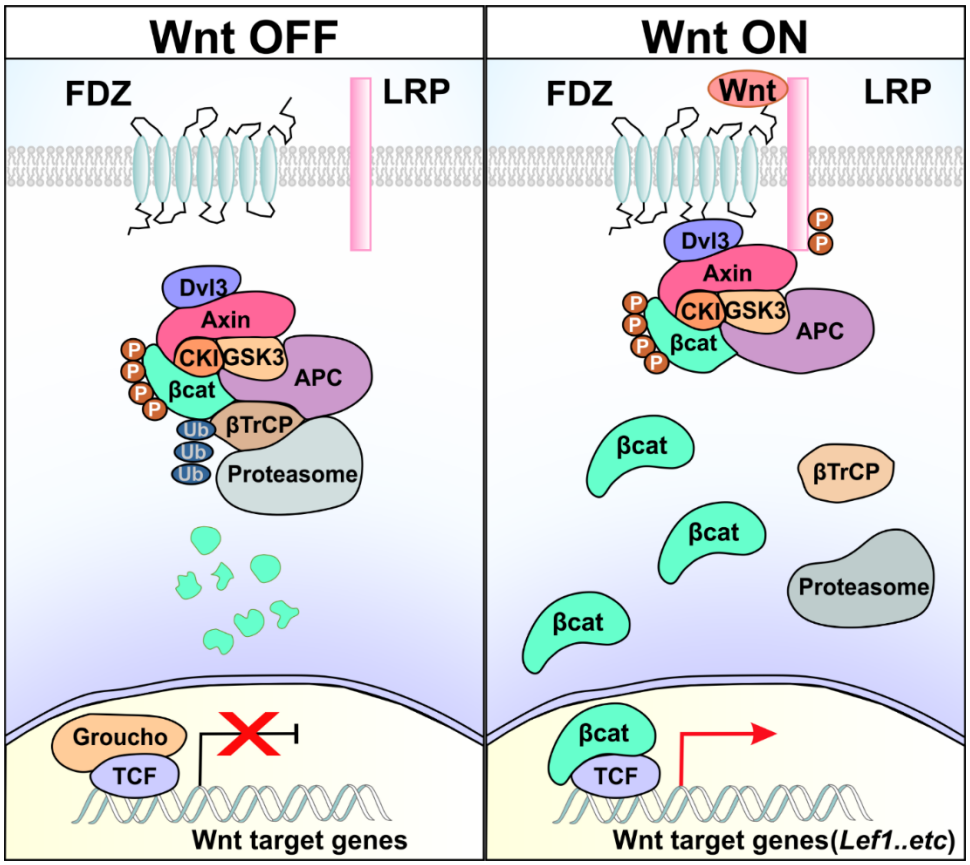

Figure 1.3. Canonical Wnt signaling pathway

The schematic illustrates the canonical Wnt signaling pathway in the absence (left) and the presence (right) of Wnt ligand. Left: In the absence of a Wnt signal, β-catenin is degraded by the destruction complex comprised of Axin, the Ser/Thr kinases GSK3 and CK1, protein phosphatase 2A, and the E3-ubiquitin ligase β-TrCP. After phosphorylation and ubiquitination, β-catenin is degraded by the proteasome. In the nucleus, T cell factor (TCF) is inactive because of interaction with the repressor molecule Groucho. Right: In the presence of Wnt ligand, binding of Wnt to its receptor complex induces destabilization of the destruction complex. This enables β-catenin to be stabilized and translocated into the nucleus where it binds to TCF to upregulate target genes. Adapted from [84]

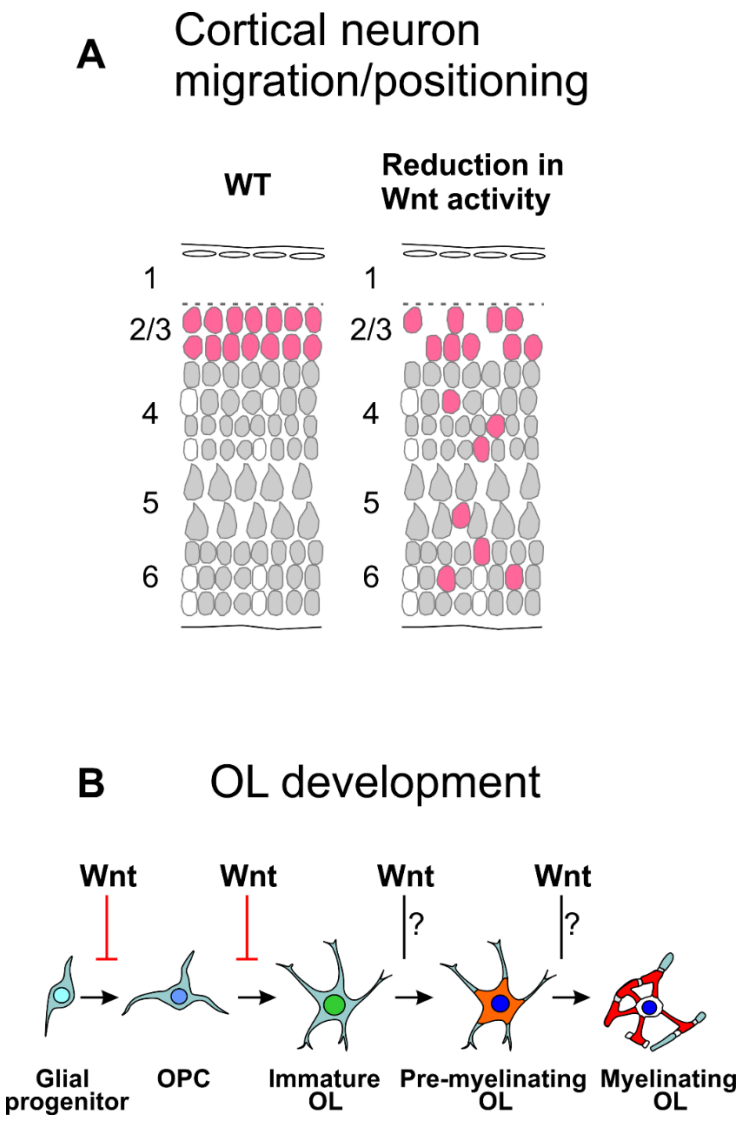

Figure 1.4. Roles of canonical Wnt activity in postnatal cortex

This schematic illustrates the cell-autonomous functions of the canonical Wnt signaling pathway in postnatal cortical neuron migration/positioning (A) and OL development (B). (A) Reduced canonical Wnt signaling activity in cortical neurons (E18) results in delayed neuronal migration and aberrant settling positions of layer 2/3 cortical neurons at P3. (B) Enhanced canonical Wnt signaling at glial progenitor or OPC stages inhibits lineage progression. However, the role of Wnt signaling on OL maturation and myelination is unclear.

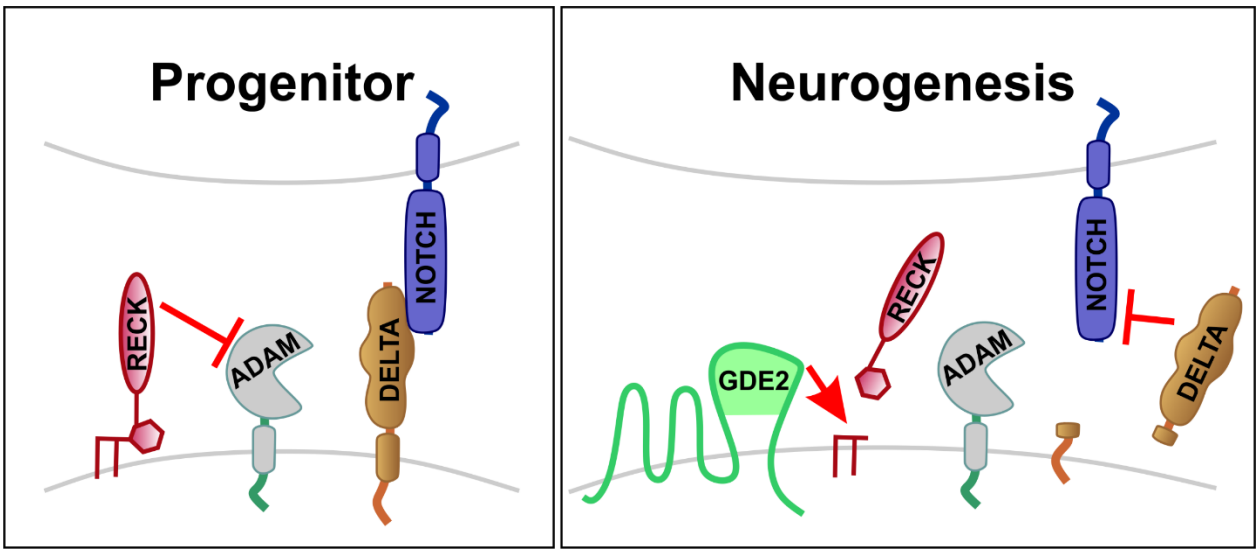

Figure 1.5. Role of GDE2 in neurogenesis

This schematic illustrates a model of GDE2 function in neuronal differentiation. The GPI-anchored protein RECK inhibits ADAM10 proteolytic cleavage and shedding of Delta, a ligand of the NOTCH receptor. Stimulation of Notch signaling by Delta binding maintains cells in a progenitor state. GDE2 expressed in postmitotic neurons cleaves RECK on the plasma membrane, thus promoting ADAM10 proteolytic cleavage of Delta. Loss of Delta on the plasma membrane downregulates NOTCH signaling in neighboring cells and induces them to differentiate into postmitotic neurons.

Chapter 2
Temporal and spatial expression of *Gde2* in the postnatal brain

2.1 Introduction

Previous studies have shown that *Gde2* is expressed in postmitotic neurons in the developing spinal cord and cortex during embryogenesis. Fluorescent in situ hybridization (FISH) analysis of postnatal spinal cord sections revealed that *Gde2* is expressed in neurons but also in Olig2+ oligodendroglia. Large scale profiling studies by others substantiate these observations[85,86]. To better define the expression pattern of *Gde2* in the postnatal brain, we utilized FISH and Western blotting to examine the temporal and cell-specific expression of *Gde2* transcripts and protein. These studies are expected to provide insight into potential functions of GDE2 in the developing postnatal brain.

2.2 Results

2.2.1 *Gde2* is expressed in multiple brain structures.

To visualize *Gde2* transcripts, we performed FISH on wild type (WT) mouse brains at postnatal day (P) 11. Antisense probes against the *Gde2* transcript (exon 12-15) revealed that *Gde2* transcripts were largely detected in the grey matter (NeuN+) with less expression noted in white matter areas (NeuN-Olig2+), such as the fimbria (Fi) and corpus callosum (CC) (Fig 2.1A and Fig 2.1.C). In the grey matter, *Gde2* transcripts were abundantly present in the hippocampus, thalamus, caudoputamen, cortex, and medial habenula (Fig 2.1.A). Sense probes showed little to no signal confirming the specificity of the antisense probes used to detect *Gde2* transcripts (Fig 2.1.B).

In the motor and somatosensory (SS) cortex, *Gde2* mRNA is initially expressed in deep cortical layers V and VI (Fig 2.1.C). At P28, when the cortical laminae have been established, *Gde2* expression was found to expand and include both deep and upper cortical layers (Fig 2.1.D). We next examined GDE2 protein expression to confirm the FISH *Gde2* transcript expression in the cortex. Indeed, Western blot showed GDE2 protein expression in postnatal cortices with increasing GDE2 expression from P7-P14 (Fig 2.1.E).

2.2.2 *Gde2* is primarily expressed in neurons in the postnatal cortex

Previous FISH analysis of *Gde2* transcripts in spinal cord sections showed that *Gde2* is expressed in neurons and oligodendroglia. Likewise, bulk or single cell gene expression profiling on cortical cell types indicate that *Gde2* is expressed in neurons and differentiated OLs[87,88]. To explore the cell-type specific expression of *Gde2*, we first utilized FISH combined with immunohistochemistry for cell type specific markers. We observed abundant expression of *Gde2* transcripts in neurons (NeuN+) at P11 (Fig 2.2.A). Quantification of the intensity of *Gde2* signal in NeuN+ neurons revealed that approximately 98% of NeuN+ neurons expressed *Gde2* mRNA (Fig 2.2.B). Western blot of protein extracts from cultured cortical neurons at DIV 3 confirms neuronal expression of GDE2 protein (Fig 2.2.C). *Gde2* transcripts are also detected in approximately 20% of Olig2+ oligodendroglial cells but, levels of *Gde2* transcript expression in Olig2+ cells are one third of that in neurons (Fig 2.2.A and 2.2.B). To further elucidate at which stage of oligodendroglial development *Gde2* transcript is expressed, we examined *Gde2* expression in proliferating OPCs and OPCs that were cultured and induced to

differentiate for 2 days *in vitro.* Quantitative PCR (qPCR) from cultured OPCs isolated from P6 cortices reveals minimal *Gde2* expression in proliferating OPCs; however, differentiated OLs express both *Gde2* transcripts and GDE2 protein (Fig 2.2.D and 2.2.E). Thus, *Gde2* is predominantly expressed in neurons during early postnatal development, with lower levels of expression in a subset of OLs.

2.2.3 *Gde2* is expressed in the adult cortex

We next examined if *Gde2* is expressed in the adult cortex. Cortical extracts from 1 month and 2 month mouse brain showed equivalent GDE2 protein expression (Fig 2.3.A). At 2 months, when cortices are mature, *Gde2* transcript expression in neurons persists in the upper layers of the motor and SS cortex (Fig 2.3.B. inbox 1). However, *Gde2* transcript expression is perceivably diminished in neurons that reside in deep cortical layers (Fig 2.3.B. inbox 2). These observations indicate that *Gde2* expression persists in the adult cortex albeit enriched in more superficial cortical layers.

2.3 Summary

As observed in the previous studies with the postnatal spinal cord, *Gde2* is expressed in both neurons and oligodendroglia in the postnatal brain; however, we find that GDE2 is primarily expressed in neurons and to a lesser extent in oligodendroglia. Consistent with published gene expression profiling studies[86,87], *Gde2* is expressed in differentiated OLs but not in mitotically active proliferating OPCs. It is worth noting that *Gde2* expression is weighted in neurons over oligodendroglia. This implies a potential role for GDE2 in neurons in the early postnatal brain. Further, the temporal expansion of

Gde2 expression in the cortex resembles the pattern of oligodendrocyte maturation and myelination pattern where OL maturation occurs first in deep cortical layers and then later in upper layers[10]. Taken together, our observations suggest a potential function for GDE2 in oligodendrocyte development in the postnatal brain.

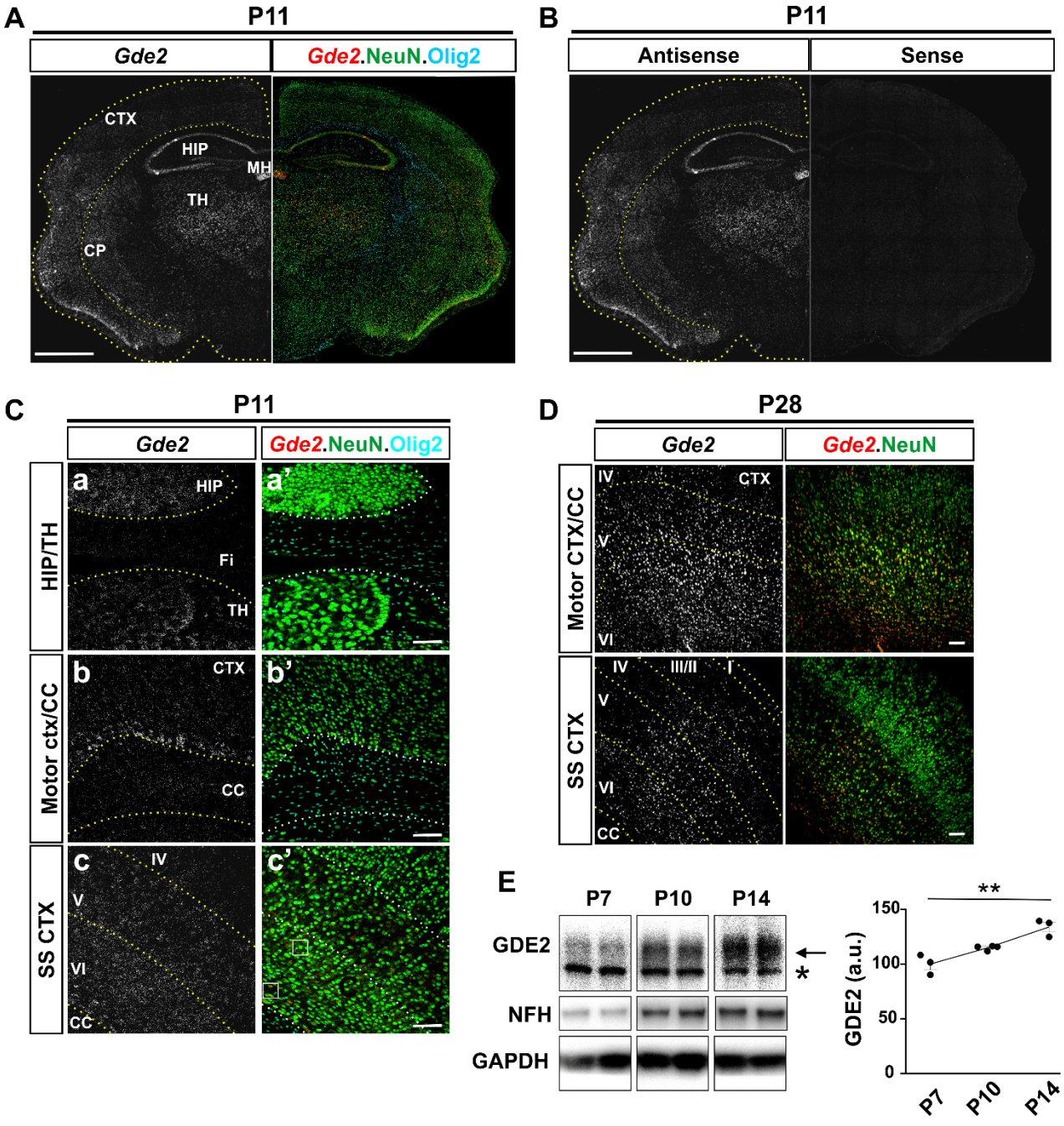
A
P11
Gde2
Gde2.NeuN.Olig2
CTX
HIP
MH
TH
CP
B
P11
Antisense
Sense
C
P11
Gde2
Gde2.NeuN.Olig2
HIP/TH
Motor ctx/CC
SS CTX
a
a'
HIP
Fi
TH
b
b'
CTX
CC
c
c'
IV
V
VI
CC
D
P28
Gde2
Gde2.NeuN
Motor CTX/CC
SS CTX
IV
CTX
V
VI
III/II
I
CC
E
P7
P10
P14
GDE2
NFH
GAPDH
*
**
GDE2 (a.u.)
150
100
50
0
P7
P10
P14

Figure 2.1 *Gde2* transcripts are expressed in the postnatal brain

Coronal sections of postnatal day 11 (P11) mouse brain showing FISH of *Gde2* transcript expression in brain. HIP: hippocampus, TH: Thalamus, CP: Caudoputamen, MH: Medial Habenula. (B) Antisense probe detects specific *Gde2* transcripts compared to sense probe. The images of *Gde2* transcript expression in A and B are identical. (C) Coronal sections of postnatal day 11 (P11) *Gde2* transcript expression in hippocampus and thalamus (panel a), motor cortex (CTX) and corpus callosum (CC) (panel b), and somatosensory (SS) CTX (panel c). Fi: Fimbria. (D) P28 mouse brain showing FISH of *Gde2* transcript expression in motor and SS CTX. Cortical layers I-VI are marked with hatched lines. (E) Western blot of cortical extracts prepared from WT animals at postnatal day 7 (P7), P10 and P14. GAPDH is a loading control, neurofilament heavy chain (NFH) is expressed in axons and provides a readout of neurons in brain tissue. Asterisk indicates a nonspecific band. Graph quantifying Western data shows increase in GDE2 protein expression (arrow) from P7-P14. a.u. = arbitrary units. **p = 0.0013. n = 3 P7, 4 P10, 3 P14, 1-way ANOVA. Scale bars in A-B: 1000 μm and C-D: 100 μm.

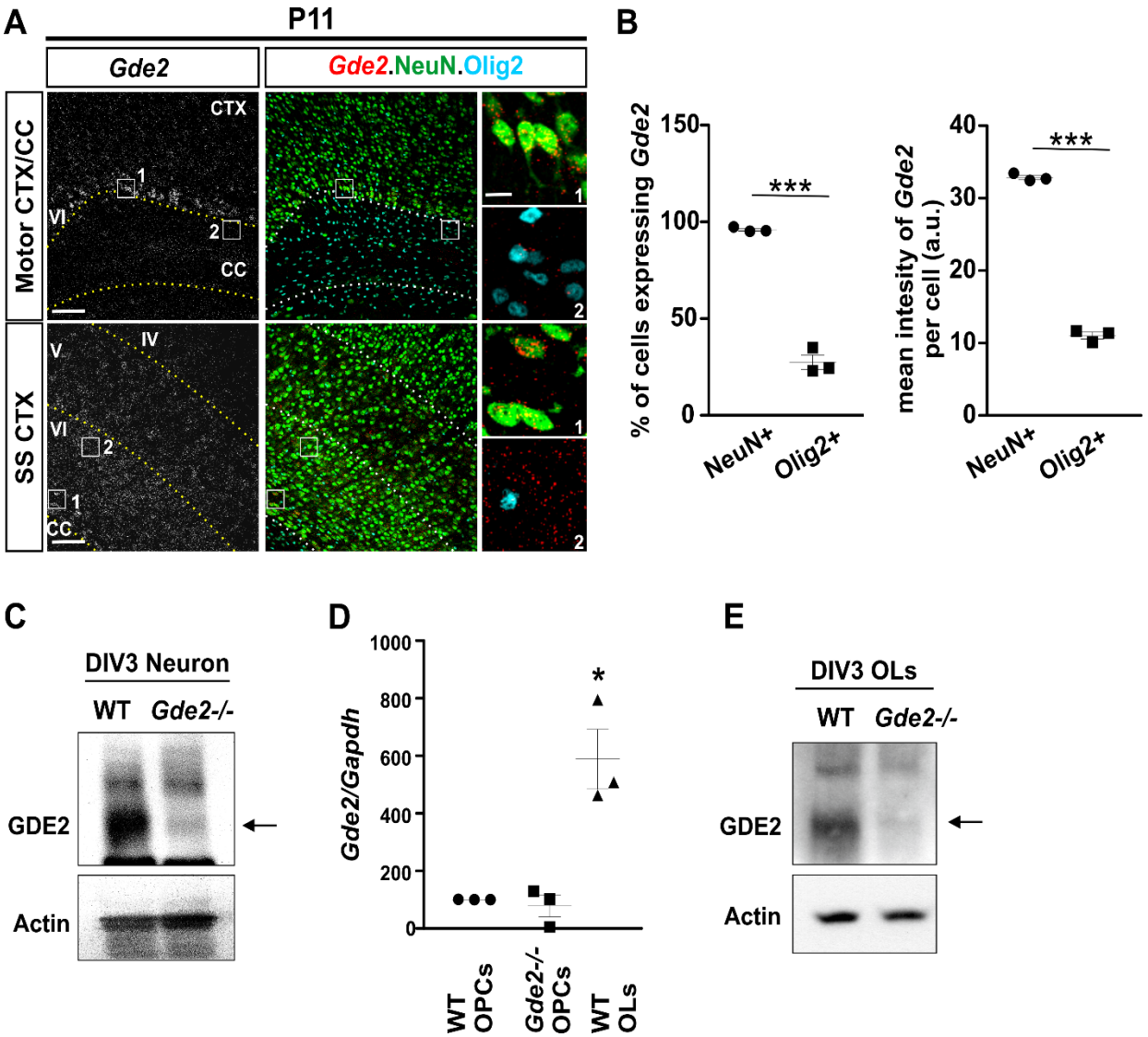
A
P11
Gde2
Gde2.NeuN.Olig2
Motor CTX/CC
SS CTX
CTX
VI
CC
V
IV
B
% of cells expressing Gde2
150
100
50
0
***
NeuN+
Olig2+
mean intesity of Gde2 per cell (a.u.)
40
30
20
10
0
***
NeuN+
Olig2+
C
DIV3 Neuron
WT
Gde2-/-
GDE2
Actin
D
Gde2/Gapdh
1000
800
600
400
200
0
*
WT OPCs
Gde2-/- OPCs
WT OLs
E
DIV3 OLs
WT
Gde2-/-
GDE2
Actin

Figure 2.2 *Gde2* is expressed in neurons and OLs in postnatal brain

(A) Coronal sections of postnatal day 11 (P11) showing FISH of *Gde2* transcript expression in relation to neurons (NeuN) and oligodendroglia (Olig2) in motor and SS CTX and CC. Boxes 1 and 2 are magnified in corresponding right-hand side panels, showing *Gde2* transcript expression in neurons and oligodendroglia. *Gde2* transcript images of motor and SS CTX in A are identical to the image in Figure 2.1.C. Scale bar: 100 μm. (B) Graphs quantifying *Gde2* transcript expression shows *Gde2* is expressed primarily in NeuN+ neurons (***p <0.0001) and that NeuN+ neurons express higher levels of *Gde2* transcripts than Olig2+ oligodendroglia (a.u.: Arbitrary units, ***p <0.0001). n = 3 WT, 3 *Gde2-/-*; two-tailed unpaired Students t-test. (C) Western blot of DIV3 cortical neuronal cultures. Arrow marks GDE2. Actin is a loading control. (D) qPCR of *Gde2* transcripts normalized to *Gapdh* mRNA. *Gde2* is not expressed in OPCs but is detected in OLs (*p = 0.0021. n = 3 sets of WT, *Gde2-/-* OPCs, and WT OLs, 1-way ANOVA. (E) Western blot shows GDE2 is expressed in WT OLs (marked by arrow). Actin is a loading control. All graphs: Mean $\pm$ sem.

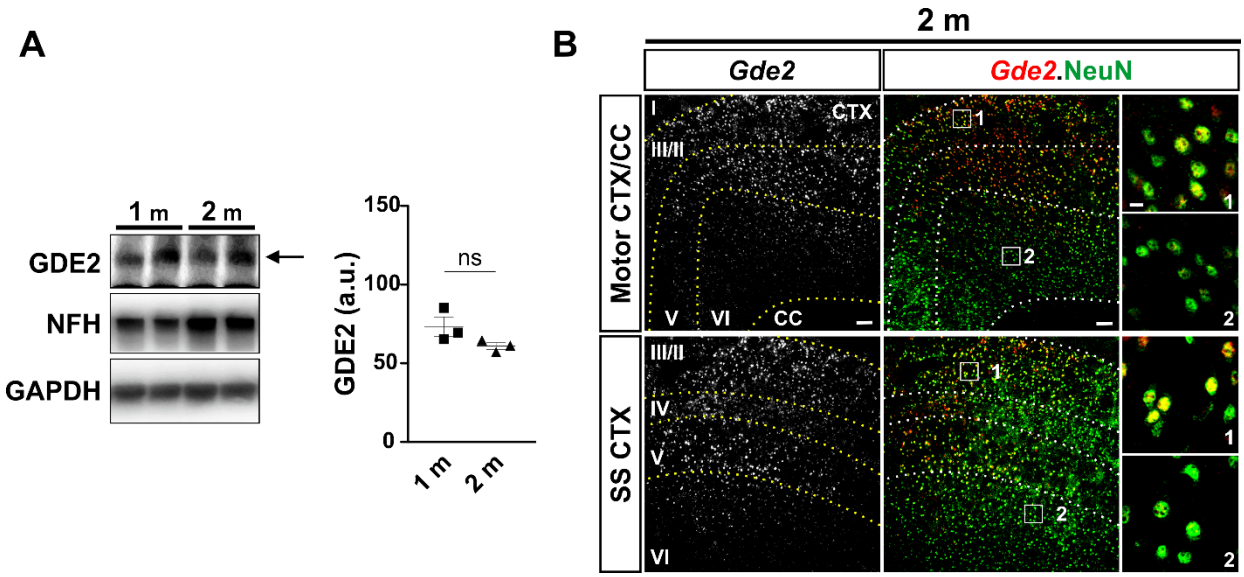

Figure 2.3 *Gde2* is expressed in the adult brain

(A) Western blot of cortical extracts prepared from WT animals at 1 month (1 m) and 2 months (2 m). GAPDH is a loading control, NFH is expressed in axons and provides a readout of neurons in brain tissue. Graph quantifying Western data shows equivalent levels of GDE2 protein expression at 1 and 2 m of age. a.u. = arbitrary units. **ns p=0.182. n = 3 for each timepoint, two-tailed unpaired Students t-test. Mean ± sem. (B) Coronal sections of 2 m brain showing FISH of *Gde2* transcript expression in motor and SS CTX. Boxes 1 and 2 are magnified in corresponding right-hand side panels, showing *Gde2* transcript expression in neurons. *Gde2* transcript expression remains abundant in the upper layers but perceivably less in the deep layers. Scale bar: 100 µm, insets 10 µm.

Chapter 3
GDE2 regulates OL maturation *in vivo*

3.1 Introduction

Our *Gde2* expression studies provide evidence that *Gde2* is expressed primarily in neurons in postnatal cortices and that the temporal expression pattern of *Gde2* resembles the maturation pattern of OLs in the developing postnatal cortex. Further, the period of increased GDE2 expression in mouse cortex (P7-P14, Fig 2.1.E) coincides with the peak periods of OL development. These observations suggest a potential function for GDE2 in OL development in the postnatal cortex. To test this hypothesis, we utilized constitutive *Gde2* knock out (*Gde2-/-*) mice in which the deletion of *Gde2* exon 11 leads to the generation of a nonfunctional truncated GDE2 protein[77]. We examined OL development in *Gde2-/-* cortices compared to WT littermate cortices using FISH, Western blot, and immunohistochemistry. These *in vivo* studies allowed us to identify a physiological role for GDE2 in regulating OL maturation in the early postnatal cortex.

3.2 Results

3.2.1 GDE2 ablation does not impact OPC proliferation

A previous study in our laboratory reported that *Gde2-/-* mice show altered timing of cortical progenitor differentiation that resulted in the delayed production of deep layer neurons and increased production of superficial cortical neurons during embryonic development[78]. To examine if the aberrant cortical neurogenesis persists in the postnatal *Gde2-/-* cortex, we visualized cortical neuronal lamination using two antibodies that specifically detect laminae-specific antigens (Cux1 and Ctip2). Cux1 is a transcription

factor specifically expressed in layer 2, 3 and 4 cortical neurons. In contrast, Ctip2 is expressed in cortical neurons of layer 5 and 6. We did not observe any discernible differences in cortical lamination in *Gde2-/-* animals compared with WT littermates at P15 when neuronal migration is complete, suggesting that early perturbations in neurogenesis have normalized by this timepoint (Fig 3.1.A). Milestones of OL development were examined by visualization of stage-specific molecular marker expression in cortices at P7, P11, P14, and P28 (Fig 3.2.A). For immunohistochemical analysis, we focused specifically on the corpus callosum (CC) and adjacent motor and retrosplenial cortex (CTX) that bear unique anatomical features to enable consistent comparison of OL development between the groups (Fig 3.2.B). I also took into consideration the potential regional heterogeneity in OL development between grey matter and white matter by analyzing the CTX and CC respectively[89] (Fig 3.2.B). To examine OPC proliferation in *Gde2-/-* animals at P7, sections were stained for Olig2 and Sox10. Although Olig2 and Sox10 are OL lineage determinants, their individual expression does not identify OL lineage cells. For instance, glial progenitors as well as a subpopulation of cortical astrocytes express Olig2, while Sox10 is also expressed in pericytes[90,91]. Therefore, we specifically and reliably identified oligodendroglia by co-expression of Olig2 and Sox10 (Fig 3.3.A). Quantification of the number of Olig2+Sox10+ cells per unit surface area (mm^2) showed no difference between *Gde2-/-* and WT mice (Fig 3.3.B). Further, OPCs that are actively proliferating, identified by coexpression of the proliferation marker Ki67 showed equivalent numbers of proliferating OPCs (Ki67/SOX10/Olig2+) in WT and *Gde2-/-* CC and CTX at P7. These observations suggest that loss of GDE2 does not affect OPC proliferation (Fig 3.3.C).

3.2.2 GDE2 ablation impairs OL maturation

OPCs stop dividing and differentiate into premyelinating and myelinating OLs, which express CC1 and *Mbp* transcripts[16,17] (Fig 3.2.A). At P11, overall numbers of OL lineage cells (Olig2+) in CC and CTX were equivalent between *Gde2-/-* animals and WT controls (Fig 3.4.A and 3.4.B). However, *Gde2-/-* animals exhibited a 30% reduction of Olig2+ CC1+ cells in CC and CTX compared with WT (Fig 3.4.A and 3.4.C middle region). Importantly, the number of CC1+ cells in *Gde2-/-* cortices was reduced in rostral, medial and caudal regions, indicating a requirement for GDE2 in CC1+ OL generation across the rostral-caudal axis (Fig 3.1.A and Fig 3.4.C). Likewise, FISH *Mbp* transcript expression showed a decrease in *Gde2-/-* cortices compared with WT (Fig 3.4.D). Notably, no change in the number of immature, newly differentiating, OLs (TCF4+/CC1-) was found between WT and *Gde2-/-* brains (Fig 3.1.A and Fig 3.5.A). These observations suggest that GDE2 is not required for the initiation of OPC differentiation but is instead required for OL maturation. In support of this notion, the number of mature OLs, identified by expression of ASPA protein[19], a marker of later OL maturation, was markedly reduced in P15 *Gde2-/-* mice compared with WT littermates (Fig 3.6.A and 3.6.B). Western blot analysis of P14 cortical extracts revealed robust reduction of myelin proteins MBP and MOG[18] in *Gde2-/-* mutants but equivalent levels of Olig2 and PDGFRα (Fig 3.7.A and 3.7.B). Also, no gross change in Neurofilament Heavy Chain (NFH) expression was observed. (Fig 3.7.A) Our biochemical observations indicate that impaired OL maturation in *Gde2-/-* cortices results in the reduction in myelin protein synthesis and supports our

earlier observations that GDE2 loss does not alter production of OPCs, overall numbers of oligodendroglia, or axonal contents.

Mature OLs synthesize myelin protein to wrap around target axons. Deficits in OL maturation and myelin protein synthesis elicited by the loss of GDE2 have the potential to impact myelination. To test this possibility, we analyzed myelin sheath ultrastructure in the CC using transmission electron microscopy (TEM). The lipid-rich myelin sheath is electron-dense and accordingly displays dark and ring-like appearances around a myelinated axon. For myelin imaging and analysis, the sagittal surface near the midline of the CC beneath the CTX was used. Images were acquired from 10~13 regions from three animals per genotype with the operator blinded. We found that P14 *Gde2-/-* CC showed a significant reduction in the number of myelinated axons compared with age-matched WTs (Fig 3.8.A and B). G-ratios, which are derived from a ratio of the diameters of axons and outer myelinated axons, are the gold standard for measurement of myelin sheath thickness. We found that there was a significant increase in the g-ratio in *Gde2-/-* mutants compared to WT (Fig 3.8.C and D), consistent with hypomyelination in the *Gde2-/-* condition. Notably, axon diameters of myelinated axons between the groups were equivalent (Fig 3.8.E), suggesting that the deficits in myelination in *Gde2-/-* animals are not a consequence of altered axon caliber. These observations suggest that GDE2 is required for OL maturation in the postnatal brain.

3.2.3 GDE2 ablation delays timely OL maturation

Loss of GDE2 displays deficits in OL maturation and myelination in the postnatal cortex at the time of active OL maturation. We next asked if these impairments persist in

adulthood. At P28, there was no change in the number of ASPA+ mature OLs in WT and *Gde2-/-* cortices (Fig 3.9.A and 3.9.B), indicating that OL maturation deficits in *Gde2-/-* animals had recovered to WT. Supporting this notion, expression of myelin proteins (MBP and MOG) showed equivalent levels between WT and *Gde2-/-* mice (Fig 3.9.C and 3.9.D). However, TEM analysis in the CC of 10 week animals showed that there was a considerable reduction in the number of myelinated axons with diameters larger than 2μm in *Gde2-/-* animals compared to WT (Fig 3.10.A and D). In contrast, there was no change in the number of myelinated axons with diameters larger than 1.5 μm and smaller than 2 μm (Fig 3.10.C). The observed changes in myelination was intriguing because both measurements of axon diameter and g-ratio of axons greater than 1.5 μm were equivalent between genotypes (Fig 3.10.E and F). Our data are consistent with the model that the precise temporal control of OL maturation by GDE2 is necessary for appropriate myelination in the postnatal cortex.

3.3 Summary

To determine if GDE2 is required for OL development, we characterized the different stages of OL development, myelin protein synthesis, and myelin sheath ultrastructure in *Gde2-/-* cortices at multiple timepoints. We find that global ablation of GDE2 results in the delay of OL maturation and myelin protein synthesis, and hypomyelination but has no impact on OPC proliferation or the initiation of OPC differentiation. The recovery of mature OLs by P28 in *Gde2-/-* animals is consistent with known compensatory pathways that ensure OL homeostasis. Nevertheless, the loss of GDE2 leads to a dramatic reduction in the number of myelinated large-diameter axons

in adulthood. These observations suggest that GDE2-dependent mechanisms that regulate the pace of OL maturation during development are critical for appropriate axonal myelination.

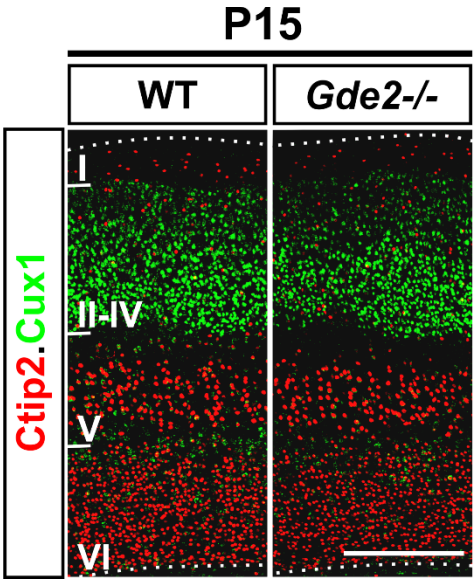

Figure 3.1. Cortical lamination is recovered in the *Gde2-/-* postnatal cortex

Coronal section of P15 mouse SS cortex, hatched lines mark cortical boundaries. Cux1 marks cortical neurons in layer II and III (green) and Ctip2 marks cortical neurons in layers IV through VI. Cortical layers I-VI are marked. Scale bar: 100 μm

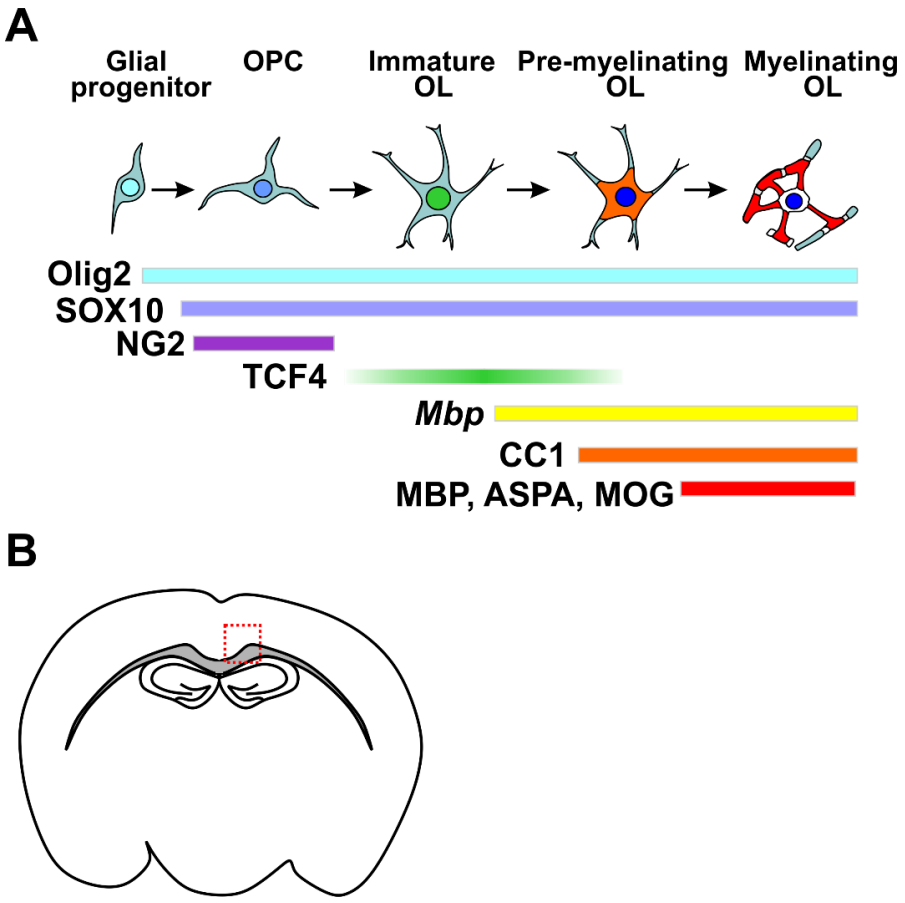

Figure 3.2. OL development lineage markers and regions studied

(A) Schematic showing the progression of OL development coincident with expression of markers used in this study. (B) Schematic showing the region of interest in red boxed area encompassing CC and adjacent CTX used in this study.

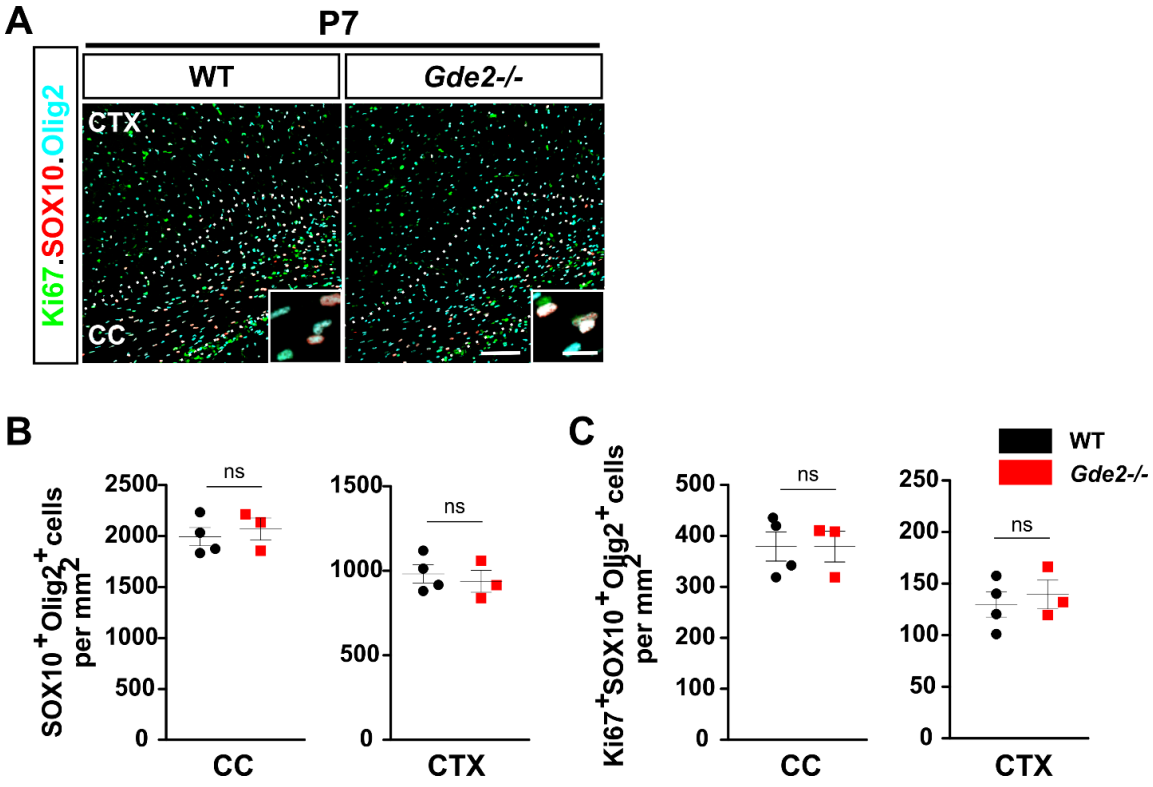

Figure 3.3. GDE2 does not influence OPC proliferation

(A) Coronal section of P7 mouse motor cortex (CTX) and corpus callosum (CC). Hatched line marks the boundary between cortex and corpus callosum. Inset box shows magnified image of proliferating OPCs (white, Ki67+Sox10+Olig2+). (B) Graphs quantifying the number of oligodendroglia (Sox10+Olig2+) shows no change between WT and *Gde2-/-* CC (ns =0.6153) and CTX (ns = 0.6198). (C) Graphs quantifying the number of proliferating OPCs (Ki67+Sox10+Olig2+) shows no change between WT and *Gde2-/-* CC (ns =0.9981) and CTX (ns = 0.6352). n = 4 WT, 3 *Gde2-/-*. Two tailed unpaired Student's t-test. Scale bar: 100 μm

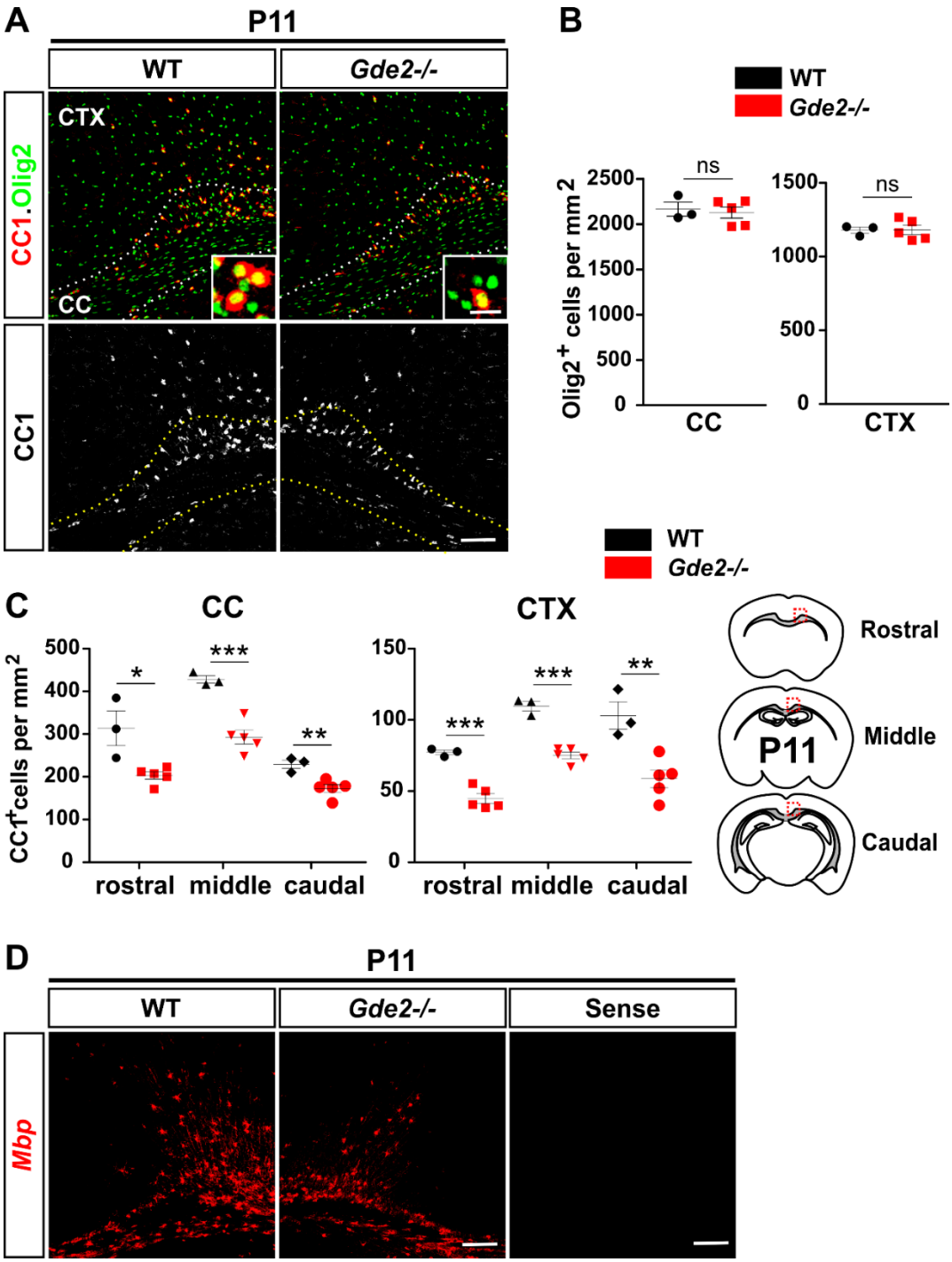
A
P11
WT
Gde2-/-
CTX
CC
CC1.Olig2
CC1
B
WT
Gde2-/-
Olig2+ cells per mm2
2500
2000
1500
1000
500
0
ns
ns
CC
CTX
C
WT
Gde2-/-
CC
CTX
CC1+cells per mm2
500
400
300
200
100
0
150
100
50
0
*
***
**
***
***
**
rostral
middle
caudal
rostral
middle
caudal
Rostral
Middle
P11
Caudal
D
P11
WT
Gde2-/-
Sense
Mbp

Figure 3.4. GDE2 loss impairs oligodendrocyte maturation

(A) Coronal sections of P11 mouse motor cortex (CTX) and corpus callosum (CC). Hatched lines delineate the CC. Inset shows high magnification of premyelinating and myelinating CC1+ Olig2+ oligodendrocytes (OLs). (B) Graphs quantifying numbers of Olig2+ in CC and CTX in WT and *Gde2-/-* P11 animals. Olig2+ cells are equivalent between genotypes in CC (n.s., p = 0.714) and CTX (n. s., p = 0.9903). (C) Graphs quantifying number of CC1+ cells in boxed areas in rostral, middle and caudal regions of mouse P11 CC and CTX shown in schematic. The data in A and B are from the middle region. CC: *p rostral = 0.013 ***p middle = 0.0007 **p caudal = 0.0072; CTX: *p rostral = 0.0004 ***p middle = 0.0035 **p caudal = 0.0063. n = 3 WT 5 *Gde2-/-*. Two tailed unpaired Student's t-test. All graphs: Mean ± sem. (D) FISH *Mbp* expression in coronal sections of P11 brains show perceivable reduction in *Gde2-/-* mice. Sense probes show minimal to no signal, indicating high specificity of antisense probes on *Mbp* transcripts. Scale bars: 100 μm, inset: 5 μm.

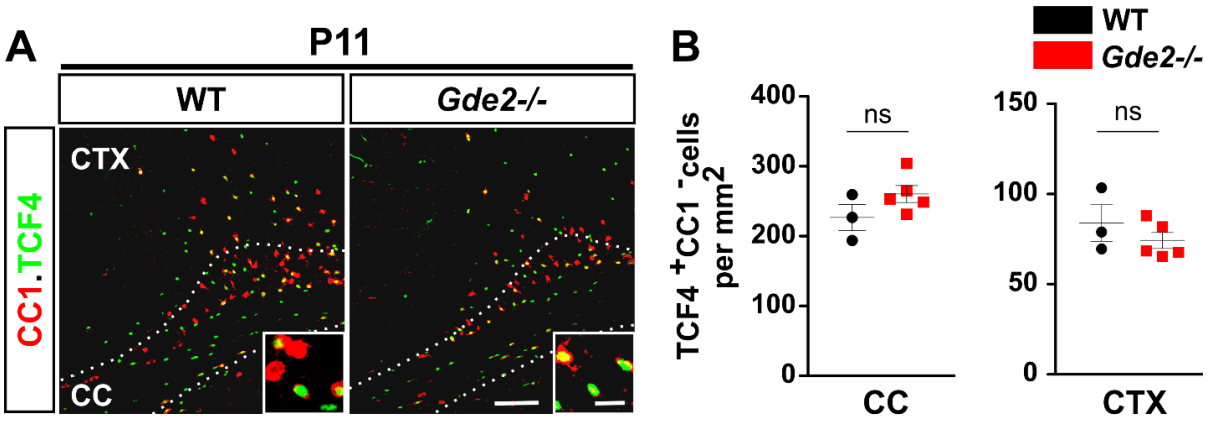

Figure 3.5. GDE2 does not influence OPC differentiation into immature OLs

(A) Coronal section of P11 mouse motor cortex (CTX) and corpus callosum (CC). Hatched line demarcates the corpus callosum. Inset box shows magnified image of immature (TCF4+CC1-) and mature OLs (CC1+). (B) Graphs quantifying the number of immature OLs (TCF4+CC1-) shows no change between WT and *Gde2-/-* CC (ns = 0.2306) and CTX (ns = 0.8021) n = 3 WT, 5 *Gde2-/-*. Two tailed unpaired Student's t-test. Scale bars: 100 μm, inset: 5 μm.

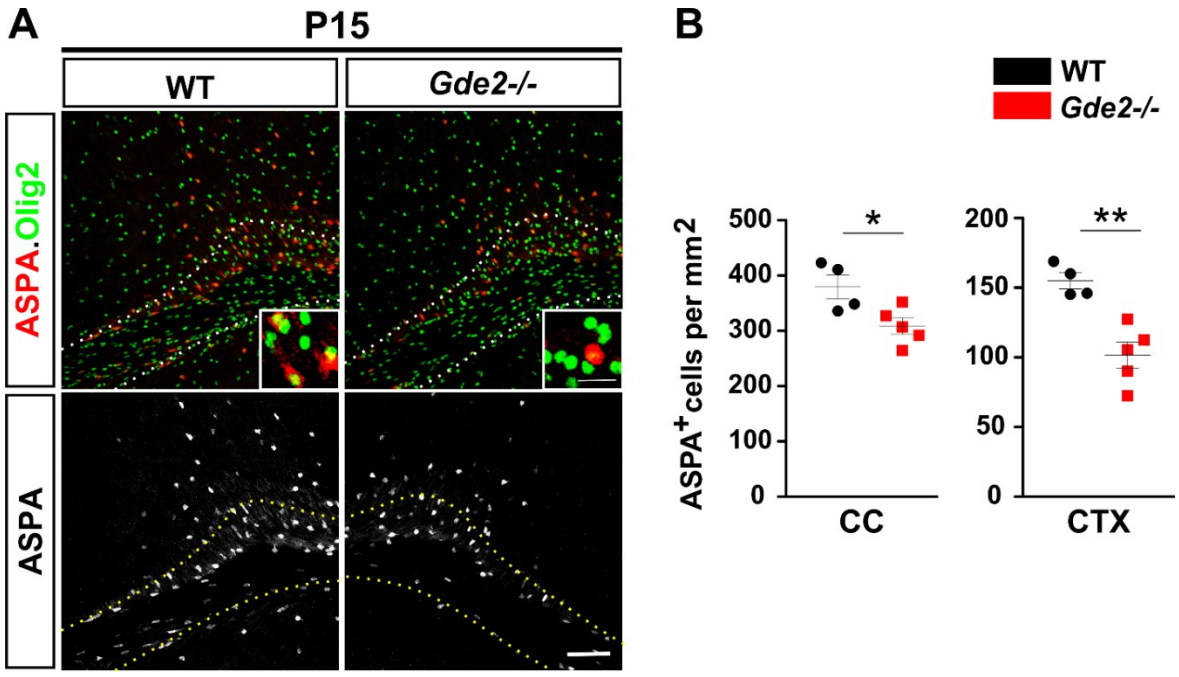

Figure 3.6. GDE2 ablation shows deficits in OL maturation at P15

(A) Coronal sections of P15 mouse motor cortex and corpus callosum. Hatched lines delineate the CC. Inset shows high magnification of mature OLs co-expressing ASPA, a later stage OL maturation marker, and Olig2. (B) Graphs quantifying numbers of ASPA+ OLs in CC and CTX in WT and *Gde2-/-* P15 animals. ASPA+ OLs are decreased in *Gde2-/-* condition in CC (*p = 0.0275) and CTX (**p = 0.0028). n = 4 WT, 5 *Gde2-/-*. Scale bars: 100 μm, inset: 5 μm.

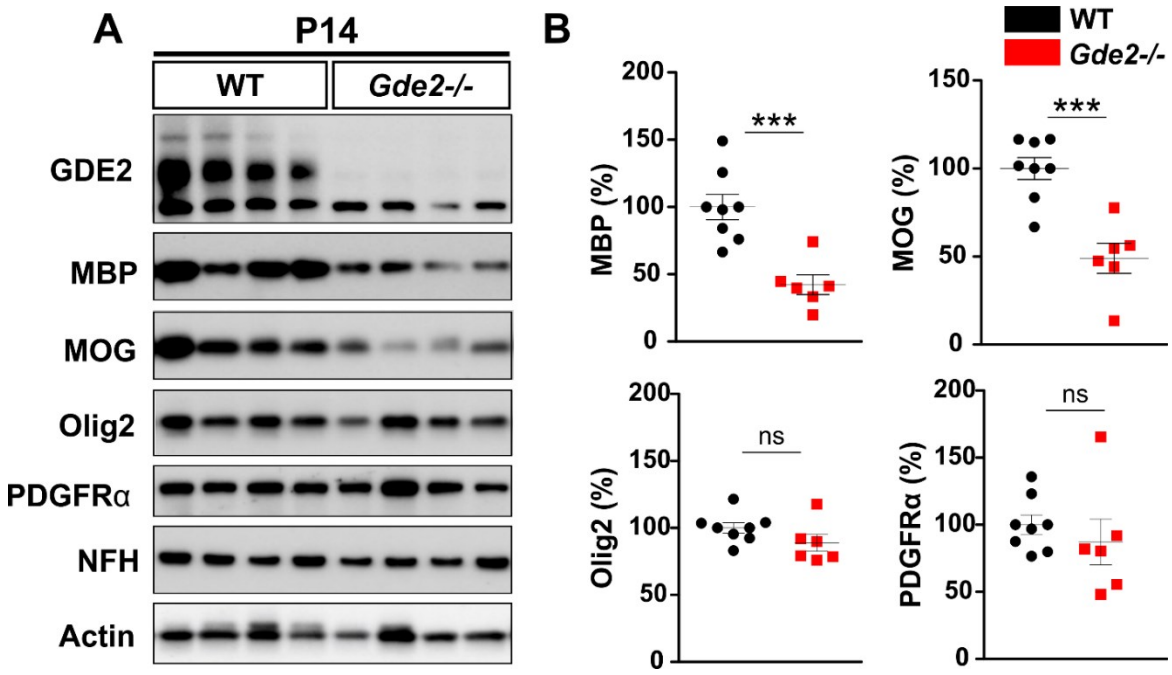

Figure 3.7. Loss of GDE2 shows impaired myelin protein synthesis

(A) Western blot of cortical extracts from P14 WT and *Gde2-/-* animals. Actin is used as loading control. Neurofilament-heavy chain (NFH) expression shows equivalent axonal contents between the groups. (B) Graphs quantifying Western blots show reduction of MBP (***p = 0.0005) and MOG (***p = 0.0009) proteins in *Gde2-/-* cortical extracts compared with WT. Levels of Olig2 and PDGFRα are equivalent between genotypes (Olig2, ns = 0.1745 ; PDGFRα, ns = 0.5163). n = 8 WT, 6 *Gde2-/-*. All graphs: Mean ± sem, two-tailed unpaired Students t-test.

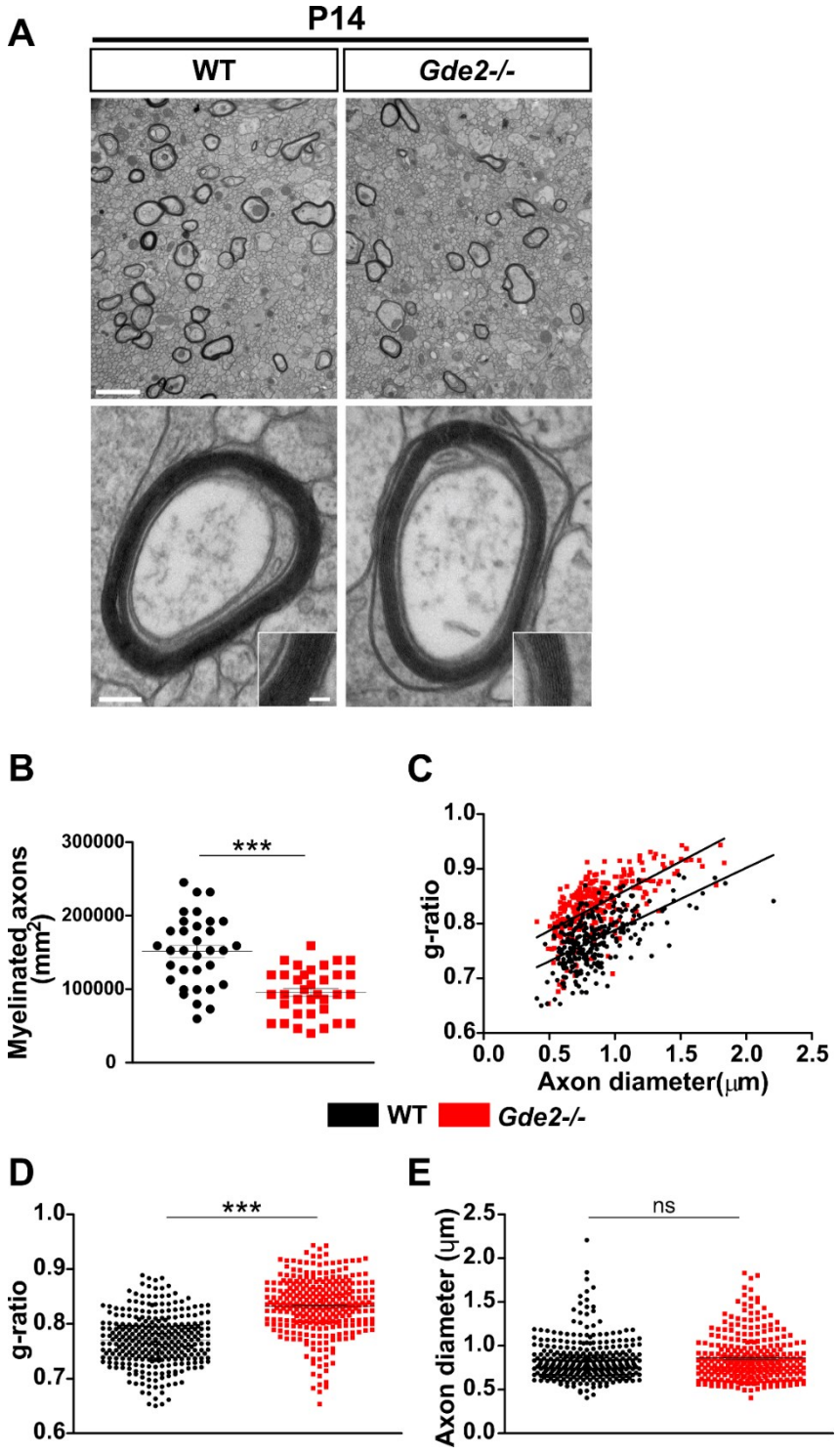
A
P14
WT
Gde2-/-
B
Myelinated axons (mm²)
300000
200000
100000
0
***
C
g-ratio
1.0
0.9
0.8
0.7
0.6
0.0
0.5
1.0
1.5
2.0
2.5
Axon diameter(μm)
WT
Gde2-/-
D
g-ratio
***
E
Axon diameter (μm)
ns

Figure 3.8. Loss of GDE2 results in hypomyelination

(A) Transmission electron microscopy (TEM) of P14 CC of WT and *Gde2-/-.* Scale bars: 2 µm (top), 100 nm (bottom), inset 50 nm. (B) Dot plot quantifying myelinating axons over surface (mm^2) shows a significant reduction in the loss of GDE2 (***p <0.0001; points refer to individual ROIs from 3 WT and 3 *Gde2-/-* animals). (C) Scatter plot showing g-ratio (ratio of diameter of an axon to outer diameter of the myelinated axon) as a function of axon diameter. (D) Graph showing an increase in g-ratio in *Gde2-/-* compared to WT (***p <0.0001; points refer to individual myelinated axons; 3 WT, 3 *Gde2-/-* animals). (E) Graph quantifying axon diameter shows no change in axon diameter of the myelinated axons in (D) between WT and *Gde2-/-* (ns p = 0.5523; 3 WT, 3 *Gde2-/-*). All graphs: Mean ± sem, two-tailed unpaired Students t-test.

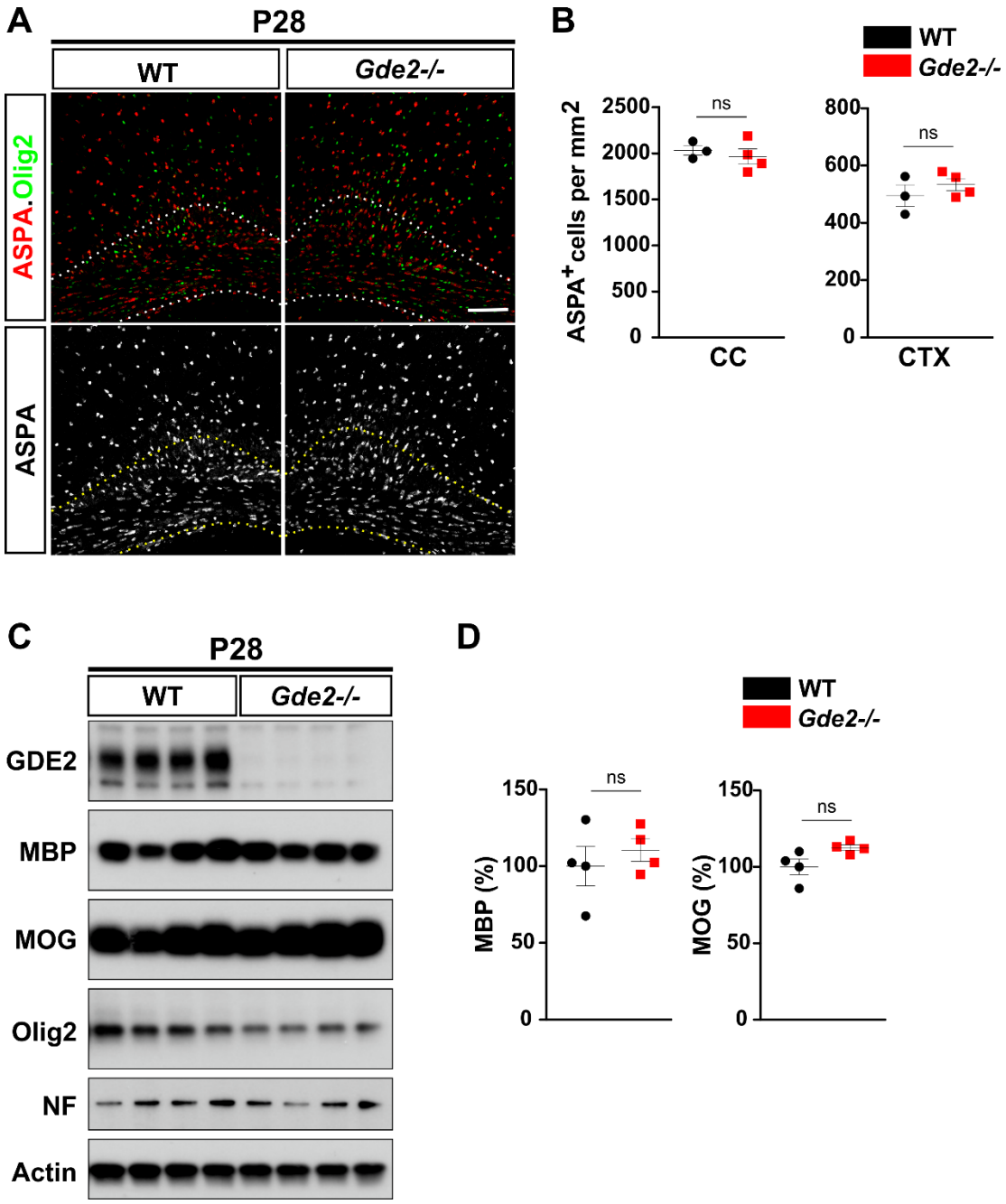
A
P28
WT
Gde2-/-
ASPA.Olig2
ASPA
B
WT
Gde2-/-
ASPA+cells per mm2
2500
2000
1500
1000
500
0
ns
CC
800
600
400
200
0
ns
CTX
C
P28
WT
Gde2-/-
GDE2
MBP
MOG
Olig2
NF
Actin
D
WT
Gde2-/-
MBP (%)
150
100
50
0
ns
MOG (%)
150
100
50
0
ns

Figure 3.9. Deficits in OL maturation and myelin protein synthesis in *Gde2-/-* mice are normalized at P28

(A) Coronal section of P28 mouse motor cortex (CTX) and corpus callosum (CC). Hatched line marks the boundary between cortex and corpus callosum. Mature OLs are marked by ASPA+. (B) Graphs quantifying the number of mature OLs (ASPA+) shows no difference between WT and *Gde2-/-* CC (ns =0.5390) and CTX (ns = 0.4373). n = 3 WT, 4 *Gde2-/-*. Scale bar: 100 μm. (C) Western blots of P28 cortical extracts of WT and *Gde2-/-* mice. Actin is used as loading control. Neurofilament-heavy chain (NFH) expression shows equivalent axonal contents between the groups. (D) Quantification of MBP and MOG in C. Percent of MBP and MOG expression in *Gde2-/-* after normalization to WT shows no difference between the genotypes (MBP, ns = 0.5198 and MOG, ns = 0.1035). n = 4 WT, 4 *Gde2-/-*. All graphs: Mean ± sem, two-tailed unpaired Students t-test.

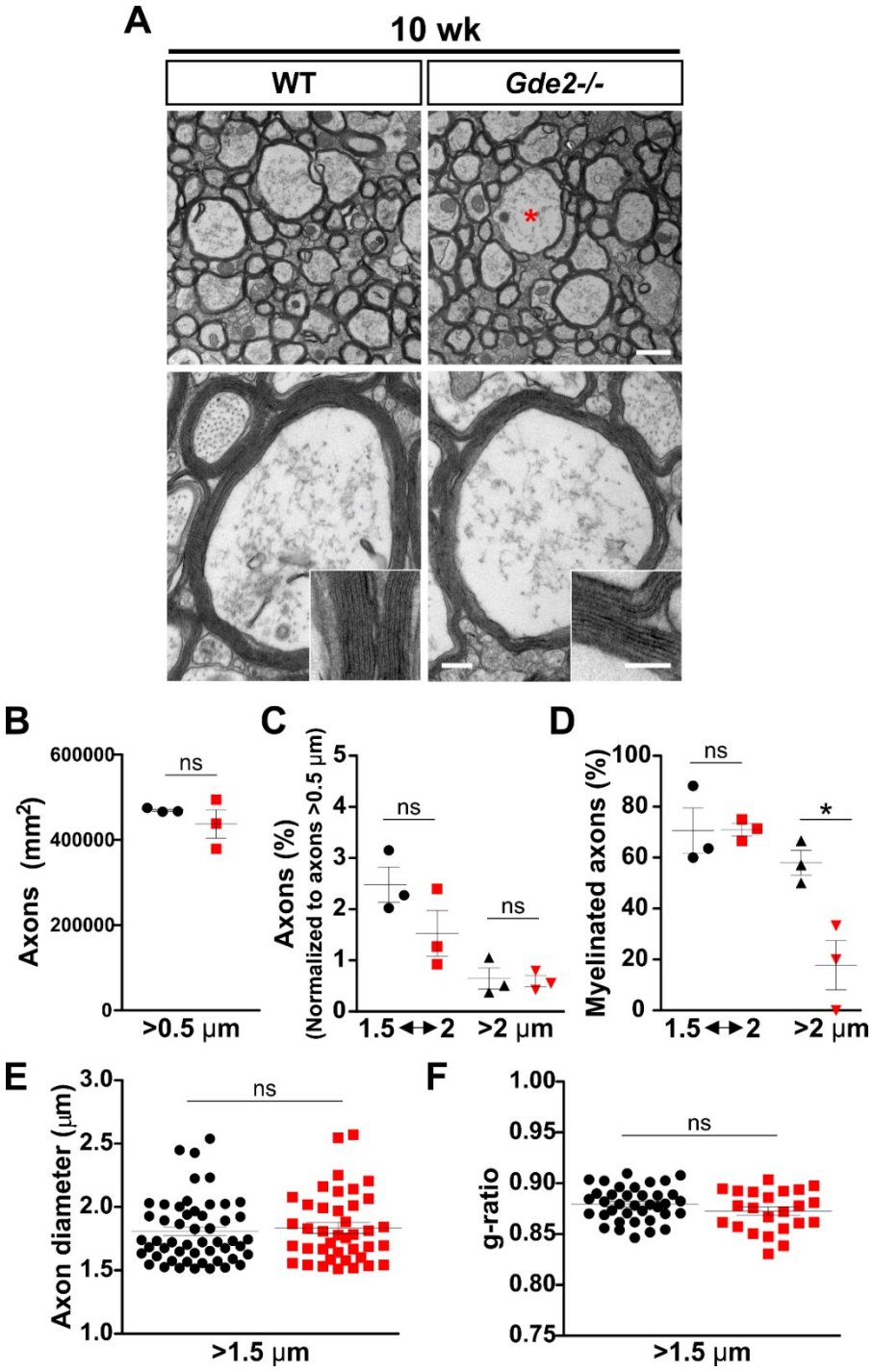
A
10 wk
WT
Gde2-/-
B
Axons (mm²)
600000
400000
200000
0
ns
>0.5 µm
C
Axons (%)
(Normalized to axons >0.5 µm)
5
4
3
2
1
0
ns
ns
1.5↔2
>2 µm
D
Myelinated axons (%)
100
80
60
40
20
0
ns
*
1.5↔2
>2 µm
E
Axon diameter (µm)
3.0
2.5
2.0
1.5
1.0
ns
>1.5 µm
F
g-ratio
1.00
0.95
0.90
0.85
0.80
0.75
ns
>1.5 µm

Figure 3.10. Loss of GDE2 results in an increase in unmyelinated large axons

(A) Representative Transmission electron microscopy (TEM) images of 10 week CC of WT and *Gde2-/-.* * marks exemplar unmyelinated larger-diameter axon in *Gde2-/-* condition. Scale bars: 1 μm (top), 200 nm (bottom), inset 100 nm. (B) Dot plot quantifying axons (both myelinated and unmyelinated) with diameters greater than 0.5 μm over surface area (mm^2) shows no change in the loss of GDE2 (ns p =0.3905; datapoints refer to average number of axons per animal from 3 WT and 3 *Gde2-/-*). (C) Graph quantifying the percentage of axons with diameters between 1.5 μm and 2 μm and greater than 2 μm among the axons in (B) shows no change in the loss of GDE2 (ns p=0.1649 and p=8323, respectively). (D) Graph quantifying the percentage of myelinated axons among the axons with diameter between 1.5 μm and 2 μm and greater than 2 μm. Although the percentage of myelinated axons between 1.5 and 2μm is equivalent between WT and *Gde2-/-* animals (ns p = 0.9667), the percentage of myelinated axons with diameters larger than 2μm is dramatically reduced (*p = 0.0206). Each datapoint represents the average percentage of myelinated axons per animal from n = 3 WT, 3 *Gde2-/-.* Diameter of axons larger than 1.5μm (E) and g-ratio of myelinated axons with diameter larger than 1.5μm (F) are unchanged between WT and *Gde2-/-* animals (ns p = 0.5977 and p = 0.156 respectively). Data points refer to individual ROIs from 3 WT and 3 *Gde2-/-* animals (E and F). All graphs: Mean ± sem, two-tailed unpaired Students t-test.

Chapter 4
Cell type-specific roles of GDE2 in OL development

4.1 Introduction

Our analysis of *Gde2-/-* mice suggests that GDE2 is required for OL maturation but not for OPC proliferation in the early postnatal cortex. GDE2 is expressed in neurons and in a subpopulation of differentiated OLs; accordingly, it remains unclear as to the contribution of neuronal and oligodendroglial GDE2 to the control of OL maturation. To clarify the cell-type specific contributions of GDE2 to OL maturation, we took advantage of Cre-lox genetics to ablate GDE2 function in either neurons or oligodendroglia by utilizing mice harboring a conditional allele of *Gde2* (*Gde2lox/-*). We examined OL development using similar methodologies as described in Chapter 3, specifically immunohistochemistry and Western blotting. These studies provide insight into cell-type specific roles of GDE2 in regulating the timing of OL maturation.

4.2 Results

4.2.1 Neuronal GDE2 promotes OL maturation

To ablate GDE2 function in neurons, we used *Nex-Cre* mice that express Cre recombinase under the control of the endogenous promoter of the gene encoding the NEX transcription factor that targets Cre expression in cortical excitatory pyramidal neurons and hippocampus but not in proliferating neural progenitors, interneurons, oligodendrocytes or astrocytes[92]. To achieve Cre-mediated abrogation of GDE2 expression and function, we used *Gde2lox* mice that carry *lox* sequences flanking exon 11 of *Gde2*[77]. Excision of exon 11 of *Gde2* generates a truncated GDE2 protein, which was validated to be nonfunctional[77]. Thus, *Gde2lox/-; Nex-Cre* mice will lack GDE2

expression and function in pyramidal neurons but will retain GDE2 function in OLs. I first examined GDE2 protein expression in *Gde2+/-*; *Nex-Cre* and *Gde2lox/-; Nex-Cre* mice to ensure efficient cre-mediated recombination of the *Gde2lox* allele. Western blot analysis of P14 cortical extracts shows that GDE2 is significantly reduced by 80% in *Gde2lox/-; Nex-Cre* mice compared with *Gde2+/-*; *Nex-Cre* controls (Fig 4.1.A and 4.1.B). This confirms efficient ablation of GDE2 expression and supports our earlier observation that GDE2 is predominantly expressed in neurons (Fig 2.2).

To determine the contributions of neuronal GDE2 to OL maturation, we quantified the number of Olig2+ CC1+ cells in *Gde2lox/-; Nex-Cre* and control *Gde2+/-*; *Nex-Cre* P11 brains (Fig 4.2.A). *Gde2lox/-; Nex-Cre* animals showed a 15% reduction in Olig2+ CC1+ OLs in the CC and a more marked 30% reduction of Olig2+ CC1+ OLs in the CTX compared with *Gde2+/-*; *Nex-Cre* controls (Fig 4.2.B). In addition, Western blots of P14 cortical extracts showed robust reduction of myelin proteins MBP and MOG in *Gde2lox/-; Nex-Cre* mice compared with control littermates (Fig 4.3.A and 4.3.B). Both genotypes showed equivalent levels of Olig2 and PDGFRα, which are expressed primarily in oligodendroglial cells and OPCs, respectively, suggesting that overall numbers of oligodendroglia or OPCs are not disrupted when neuronal GDE2 functions are ablated (Fig 4.3.B). Consistent with this observation, quantification of the number of Olig2+SOX10+ oligodendroglia (Fig 4.4.A and 4.4.B) and KI67+Olig2+SOX10+ proliferating OPCs (Fig 4.4.C) in P7 brains as well as NG2+ OPCs in P11 brains showed no difference between *Gde2lox/-; Nex-Cre* and *Gde2+/-*; *Nex-Cre* animals. Moreover, the amounts of axonal NFH protein are similar between *Gde2lox/-; Nex-Cre* and *Gde2+/-*; *Nex-Cre* animals, confirming earlier observations that cortical neuronal

lamination is grossly intact in both cases (Fig 4.3.A). Taken together, our data in *Gde2lox/-; Nex-Cre* brain recapitulate the OL developmental phenotypes of *Gde2-/-* animals and provide strong genetic evidence that GDE2 neuronal function is required to promote OL maturation. We note that quantification of the number of ASPA+ mature OLs (Fig 4.5.A and 4.5.B) in P28 cortices showed no difference between *Gde2lox/-; Nex-Cre* and *Gde2+/-*; *Nex-Cre* animals, suggesting that neuronal GDE2 function is required for regulating the timing of OL maturation.

4.2.2 OL GDE2 inhibits OL maturation

Gde2 transcripts and protein are expressed in OLs but not in OPCs (Chapter 2). To examine cell-autonomous functions of GDE2 in OL maturation, we utilized *PDGFαR-CreER* animals, where administration of 4 hydroxytamoxifen (4-HT) induces expression of Cre recombinase under the control of *PDGFα* receptor regulatory sequences to activate Cre expression in OPCs[93]. Thus, crossing *PDGFαR-CreER* mice into *Gde2lox/-* mice will generate *Gde2lox/-; PDGFαR-CreER* mice in which GDE2 expression and function are ablated in oligodendroglia but are retained in other cell types. 4-HT was administered once per day intraperitonially into *Gde2+/-*; *PDGFαR-CreER* and *Gde2lox/-; PDGFαR-CreER* pups at P1 and P2, when OPCs are normally generated. I first examined the extent of Cre-mediated recombination of the *Gde2lox* allele in the genome of OPCs that were freshly isolated from *Gde2+/-*; *PDGFαR-CreER* and *Gde2lox/-; PDGFαR-CreER* P6 cortices. Genomic DNAs from the sample groups were subject to PCR amplification using specific primers that detect the unrecombined *Gde2lox* allele (Lox), the WT *Gde2* allele (WT), and the recombined *Gde2lox* allele

(KO). Control DNAs consisting of *Gde2lox/-* and *Gde2-/-* DNAs were also amplified by PCR. Specifically, different serial dilutions of *Gde2lox/-* DNA with increasing amount of *Gde2-/-* DNA were made so that the total DNA amount was the same across the DNA mixtures (Fig 4.6). The standard curve of the control DNA PCR product is shown to be linear as a function of input DNA[77,94]. We observed that the amount of Lox PCR product in *Gde2lox/-; PDGFαR-CreER* OPCs was similar to the amount amplified when a 2:8 ratio of *Gde2lox/-* and *Gde2+/-* DNAs was utilized, suggesting that approximately 80% of the *Gde2lox* alleles had undergone recombination in *Gde2lox/-; PDGFαR-CreER* OPCs (Fig 4.6). This analysis suggests that GDE2 expression is efficiently abrogated in OPCs using the 4-HT administration regime.

Quantification of the number of Olig2+SOX10+ oligodendroglia (Fig 4.9.A and 4.9.B) and KI67+Olig2+SOX10+ proliferating OPCs (Fig 4.9.C) in P7 cortices was equivalent between *Gde2lox/-; PDGFαR-CreER* and *Gde2+/-*; *PDGFαR-CreER* animals, suggesting that GDE2 expression in OLs is not required for the production of oligodendroglial or OPC proliferation. This is supported by our observation that at P11, both genotypes showed equivalent levels of Olig2 and PDGFRα by Western bloting (Fig 4.3.B). In addition, the amounts of axonal NFH protein are similar between *Gde2lox/-; PDGFαR-CreER* and *Gde2+/-*; *PDGFαR-CreER* animals, suggesting that loss of GDE2 in OLs does not impact axonal numbers (Fig 4.3.A). To determine the contributions of GDE2 expressed in OLs to the control of OL maturation, we quantified the number of Olig2+ CC1+ cells in *Gde2lox/-; PDGFαR-CreER* and *Gde2+/-*; *PDGFαR-CreER* P11 brain (Fig 4.7.A). Strikingly, *Gde2lox/-; PDGFαR-CreER* animals showed a 50% increase in Olig2+ CC1+ OLs in the CC and a marked increase of Olig2+ CC1+ OLs in

the CTX compared with *Gde2+/-*; *PDGFαR-CreER* controls, suggesting that the loss of GDE2 in OLs results in enhanced OL maturation (Fig 4.7.B). In support of this notion, Western blots of P14 cortical extracts revealed a robust increase in MBP and MOG in *Gde2lox/-; PDGFαR-CreER* mice compared with control littermates (Fig 4.8.A and 4.8.B). To test if precocious OL maturation persists when developmental myelination is complete, I quantified the number of ASPA+ mature OLs in P28 cortices but observed no difference between the groups. This observation suggests that GDE2 functions in OLs to inhibit the timing of OL maturation during the developmental phase of myelination (Fig 4.10.A and 4.10.B). Thus, our data in *Gde2lox/-; PDGFαR-CreER* cortices suggest that the GDE2 function in OLs is to prevent precocious OL maturation.

4.3 Summary

We examined OL development and myelin protein synthesis in mice where GDE2 expression and function were conditionally abrogated in neurons or OLs using the Cre-lox system. We determined that GDE2 exerts cell-type specific functions in OL maturation. Specifically, loss of GDE2 function in neurons results in delayed OL maturation, recapitulating the phenotypes in *Gde2-/-* animals. However, loss of GDE2 function in OLs causes earlier onset of OL maturation, contrasting with the phenotypes observed in *Gde2-/-* animals. This suggests that neuronal GDE2 pathways that regulate OL maturation likely operate upstream of GDE2-mediated pathways in OLs. Together, these observations provide genetic evidence that GDE2 functions in both neurons and oligodendroglia to regulate OL maturation and that neuronal GDE2 is required for the

promotion of OL maturation.

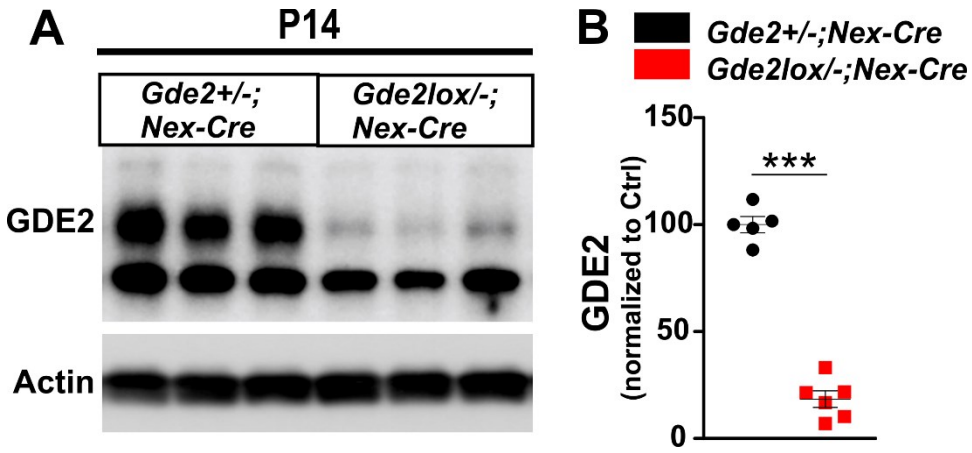

Figure 4.1. *Nex-Cre* mediated deletion of GDE2 in neurons

(A) Western blot of cortical extracts from P14 *Gde2lox/-; Nex-Cre* and *Gde2+/-*; *Nex-Cre* animals. Actin is used as loading control. (B) Graphs quantifying Western blots show efficient Cre-mediated removal of GDE2 (***p <0.0001) in *Gde2lox/-; Nex-Cre* animals. Percent of GDE2 in *Gde2lox/-; Nex-Cre* is normalized to the GDE2 in *Gde2+/-*; *Nex-Cre*. n = 5 *Gde2+/-; Nex-Cre* control, 6 *Gde2lox/-; Nex-Cre*. Mean ± sem, two-tailed unpaired Students t-test.

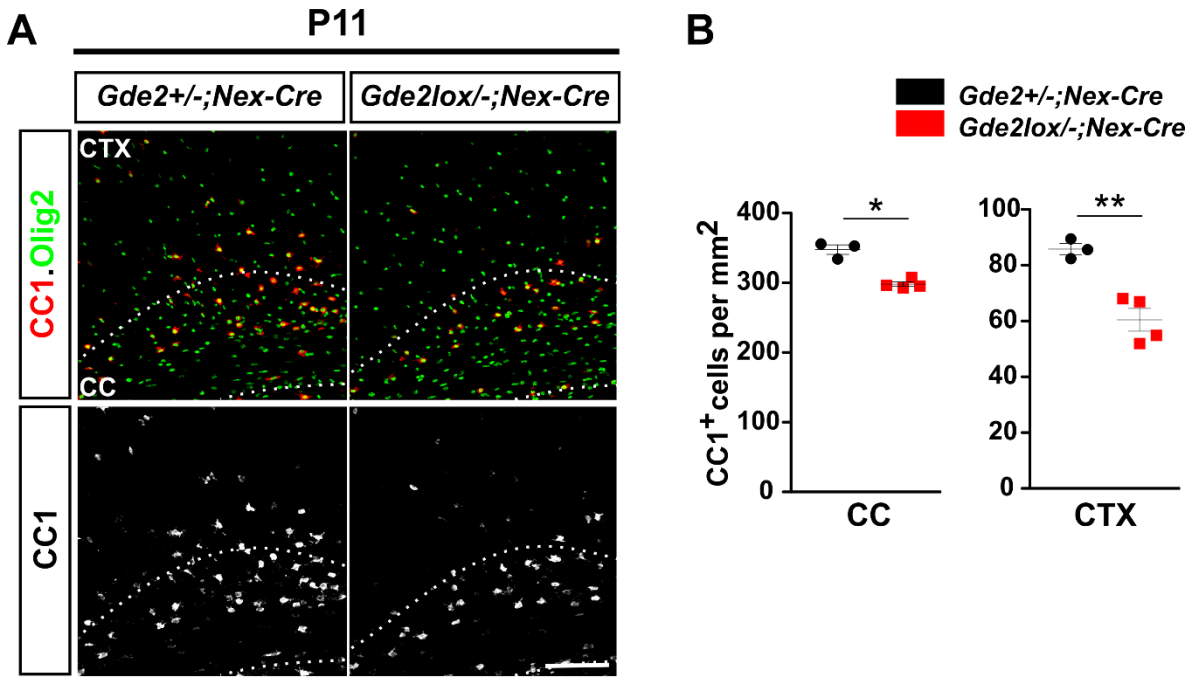

Figure 4.2. Loss of neuronal GDE2 impairs OL maturation

(A) Coronal sections of P11 mouse motor cortex (CTX) and corpus callosum (CC). Hatched lines delineate the CC. (B) CC1+ cells in CC and CTX in *Gde2+/-; Nex-Cre* control and *Gde2lox/-; Nex-Cre* P11 littermates. CC1+ OLs are decreased in animals deleted for neuronal GDE2 (*Gde2lox/-; Nex-Cre*) in CC (*p = 0.0227) and CTX (**p = 0.0052). n = 3 *Gde2+/-; Nex-Cre* control, 4 *Gde2lox/-; Nex-Cre.* Mean ± sem, two-tailed unpaired Students t-test. Scale bar: 100 μm

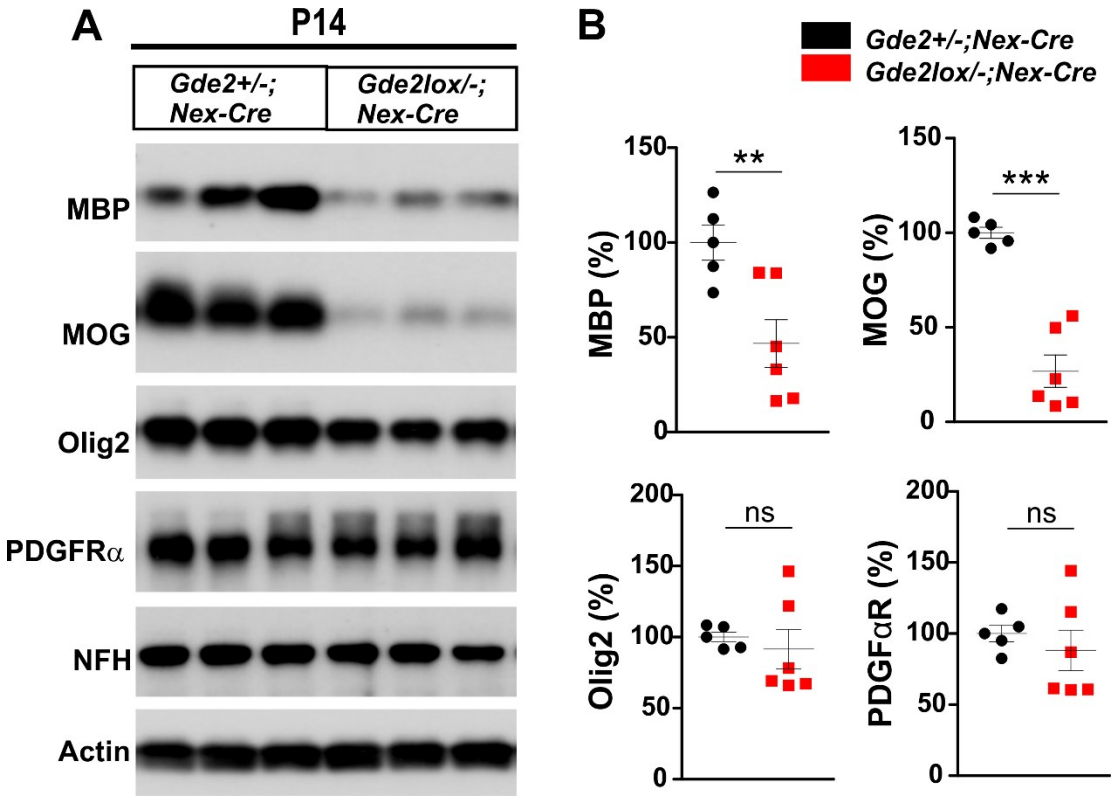

Figure 4.3. Loss of neuronal GDE2 results in impaired OL maturation

(A) Western blot of cortical extracts from P14 *Gde2+/-; Nex-Cre* control and *Gde2lox/-; Nex-Cre* P11 littermates. Actin is used as a loading control. Neurofilament-heavy chain (NFH) expression shows equivalent axonal contents between the groups. (B) Graphs quantifying Western blots show reduction of MBP (**p = 0.0091) and MOG (***p = 0.0002) proteins in *Gde2lox/-; Nex-Cre* cortical extracts compared with WT. Levels of Olig2 (p = 0.5804) and PDGFRα (p = 0.4708) are unchanged between genotypes. n = 5 *Gde2+/-; Nex-Cre* control, 6 *Gde2lox/-; Nex-Cre.* All graphs: Mean ± sem, two-tailed unpaired Students t-test.

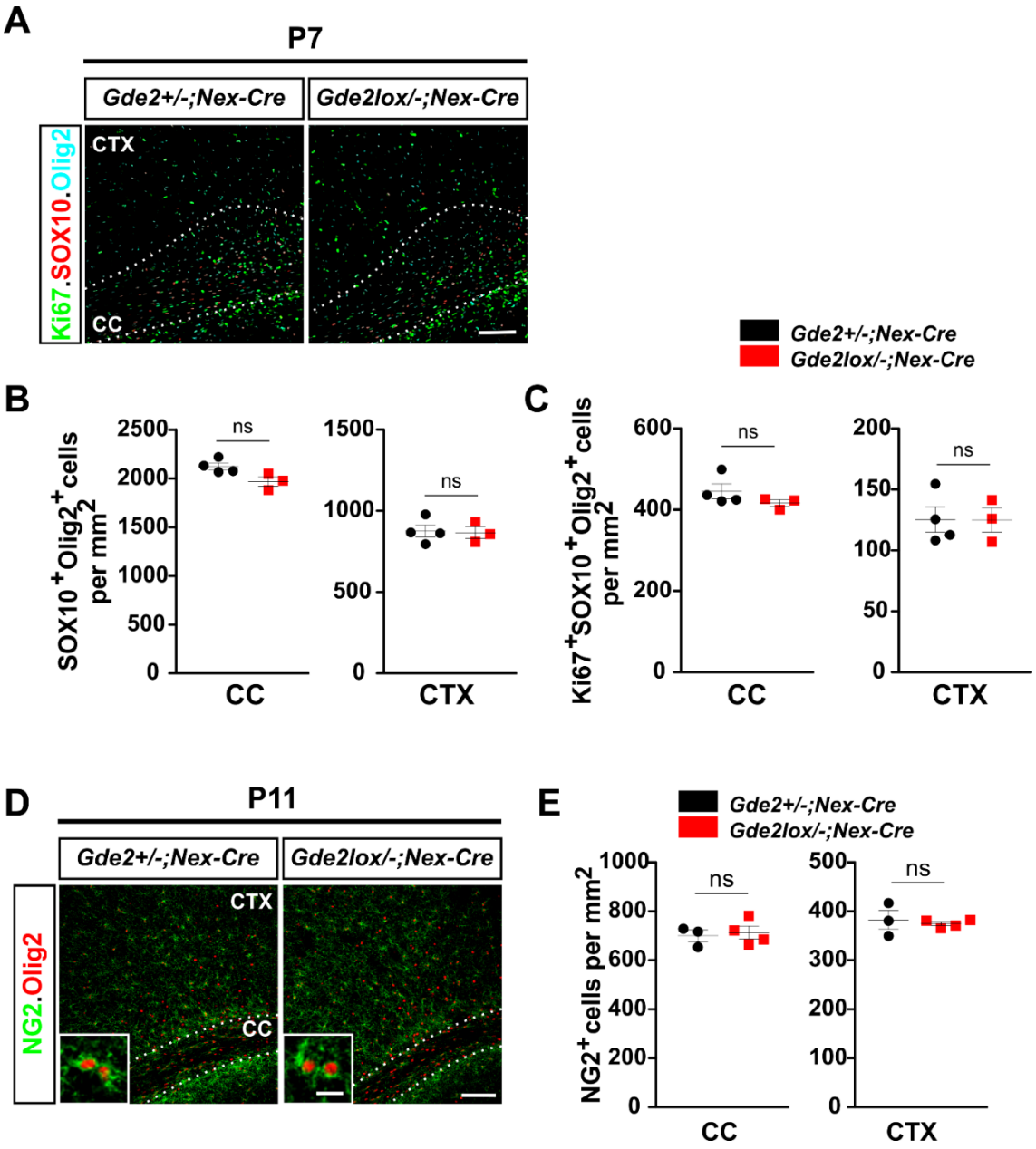
A
P7
Gde2+/-;Nex-Cre
Gde2lox/-;Nex-Cre
CTX
CC
Ki67.SOX10.Olig2
Gde2+/-;Nex-Cre
Gde2lox/-;Nex-Cre
B
SOX10+Olig2+cells per mm2
2500
2000
1500
1000
500
0
ns
1500
1000
500
0
ns
CC
CTX
C
Ki67+SOX10+Olig2+cells per mm2
600
400
200
0
ns
200
150
100
50
0
ns
CC
CTX
D
P11
Gde2+/-;Nex-Cre
Gde2lox/-;Nex-Cre
CTX
CC
NG2.Olig2
E
Gde2+/-;Nex-Cre
Gde2lox/-;Nex-Cre
NG2+cells per mm2
1000
800
600
400
200
0
ns
500
400
300
200
100
0
ns
CC
CTX

Figure 4.4. Loss of neuronal GDE2 does not influence OPC generation

(A) Coronal section of motor cortex (CTX) and corpus callosum (CC) from *Gde2+/-; Nex-Cre* control and *Gde2lox/-; Nex-Cre* P7 animals. Hatched line marks the boundary between cortex and corpus callosum. (B) Graphs quantifying the number of oligodendroglia (Sox10+Olig2+) show no change between *Gde2+/-; Nex-Cre* control and *Gde2lox/-; Nex-Cre* CC (ns =0.0811) and CTX (ns = 0.8631). (C) Graphs quantifying the number of proliferating OPCs (Ki67+Sox10+Olig2+) show no change between WT and *Gde2-/-* CC (ns =0.2221) and CTX (ns = 0.9791). n = 4 *Gde2+/-; Nex-Cre* control, 3 *Gde2lox/-; Nex-Cre.* (D) Coronal sections of P11 mouse motor cortex (CTX) and corpus callosum (CC). Hatched lines delineate the CC. (E) Graphs quantifying NG2+ OPCs cells in CC and CTX in *Gde2+/-; Nex-Cre* control and *Gde2lox/-; Nex-Cre* P11 littermates. Levels of NG2+ OPCs are equivalent between genotypes (CC ns p = 0.7221, CTX ns p = 0.6844). All graphs: Mean $\pm$ sem, two-tailed unpaired Students t-test. Scale bar: 100 μm, inset (A) 10 μm.

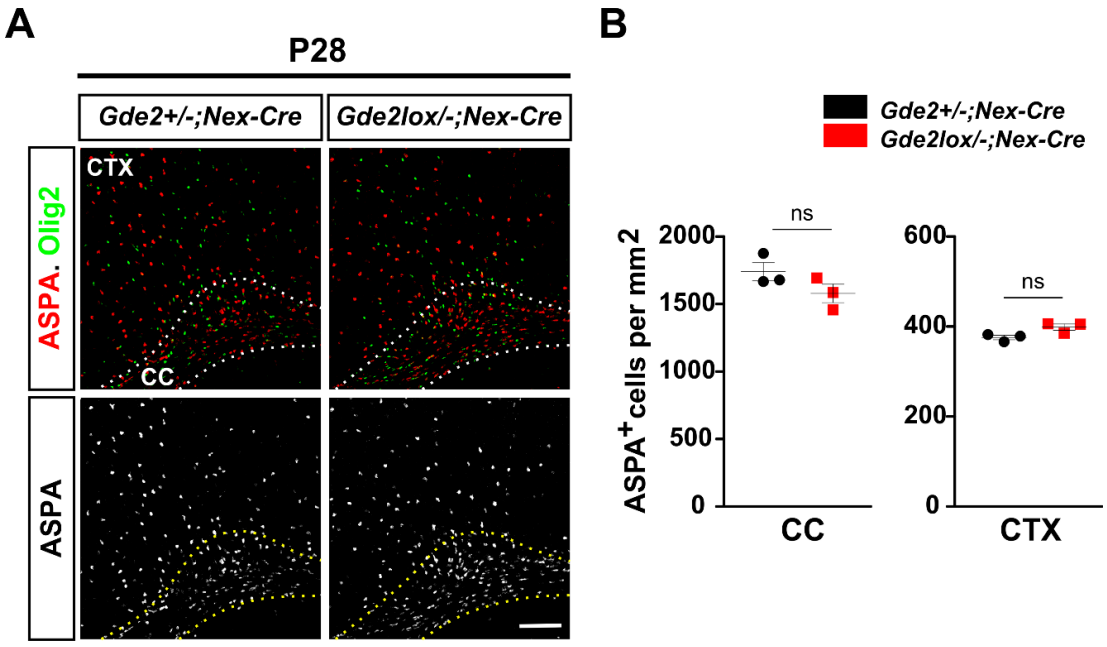

Figure 4.5. Impaired OL maturation from the loss of neuronal GDE2 is normalized by P28

(A) Coronal sections of mouse motor cortex (CTX) and corpus callosum (CC) from *Gde2+/-; Nex-Cre* control and *Gde2lox/-; Nex-Cre* P28 animals. Hatched lines delineate the CC. (B) Graphs quantifying the number of mature OLs (ASPA+) show no difference between *Gde2+/-; Nex-Cre* control and *Gde2lox/-; Nex-Cre* CC (ns =0.9704) and CTX (ns = 0.1929). n = 3 *Gde2+/-; Nex-Cre* control, 3 *Gde2lox/-; Nex-Cre*. Mean ± sem, two-tailed unpaired Students t-test. Scale bar: 100 μm

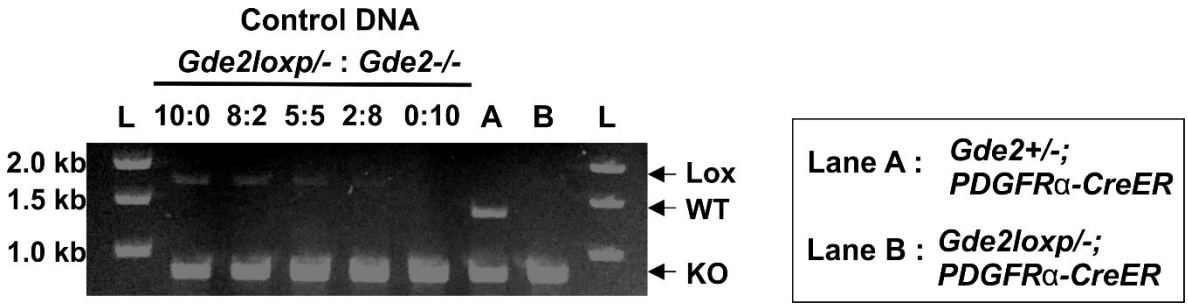

Figure 4.6. *PDGFRα-Cre* -mediated excision of floxed *Gde2* in OPCs

Competitive PCR analysis for *Gde2* sequences in genomic DNAs of freshly isolated OPCs from 4-HT injected *Gde2lox/-; PDGFαR-CreER* and *Gde2+/-*; *PDGFαR-CreER* pups. In parallel, genomic DNAs with 5 different ratios of *Gde2lox/-* and *Gde2-/-* DNAs were also amplified by PCR. The *Gde2* primers used in PCR amplification (primer sequences can be found in the Materials and Methods) can amplify unrecombined *Gde2lox* (Lox), WT *Gde2* (WT), and recombined *Gde2lox* (KO) alleles. *Gde2lox/-; PDGFαR-CreER* (lane B) shows a marked reduction in the Lox band, which shows similar band intensity to the Lox band of 2:8 ratio of mixed genomic DNAs. L indicates DNA ladder.

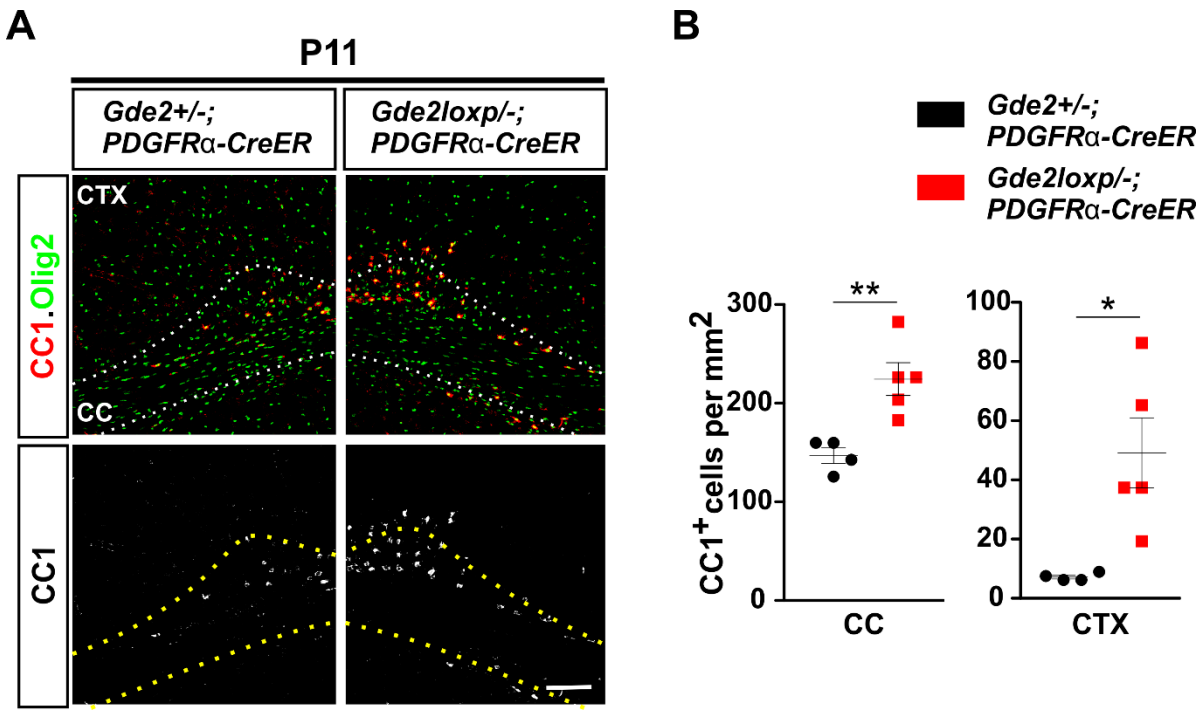

Figure 4.7. Loss of OL GDE2 results in early OL maturation

(A) Coronal sections of motor cortex (CTX) and corpus callosum (CC) of P11 *Gde2lox/-; PDGFαR-CreER* and *Gde2+/-*; *PDGFαR-CreER* mice. Hatched lines delineate the CC. (B) CC1+ cells in CC and CTX in *Gde2lox/-; PDGFαR-CreER* and *Gde2+/-*; *PDGFαR-CreER* P11 littermates. CC1+ OLs are increased in animals deleted for OL GDE2 (*Gde2lox/-; PDGFαR-CreER*) in CC (**p = 0.0087) and CTX (*p = 0.0242). n = 4 *Gde2+/-*; *PDGFαR-CreER* control, 4 *Gde2lox/-; PDGFαR-CreER.* Mean ± sem, two-tailed unpaired Students t-test. Scale bar: 100 μm

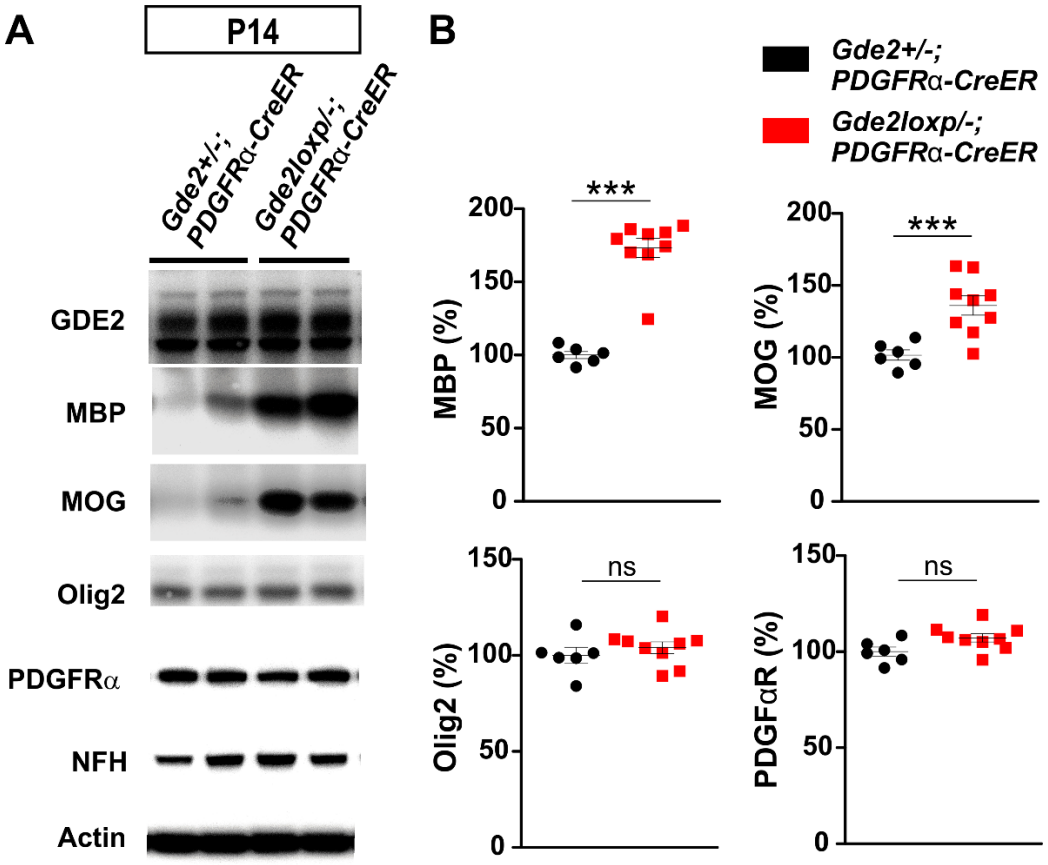

Figure 4.8. Loss of OL GDE2 results in precocious myelin protein synthesis

(A) Western blot of cortical extracts from P14 *Gde2lox/-; PDGFαR-CreER* and *Gde2+/-; PDGFαR-CreER* P11 littermates. Actin is used as a loading control. NFH expression shows equivalent axonal content between the groups. (B) Graphs quantifying Western blots show increase of MBP (***$p < 0.0001$) and MOG (***$p = 0.0007$) proteins in *Gde2lox/-; PDGFαR-CreER* cortical extracts compared with *Gde2+/-; PDGFαR-CreER*. Levels of Olig2 ($p = 0.4388$) and PDGFRα ($p = 0.4855$) are unchanged between genotypes. n = 6 *Gde2+/-; PDGFαR-CreER* control, 9 *Gde2lox/-; PDGFαR-CreER*. All graphs: Mean ± sem, two-tailed unpaired Students t-test.

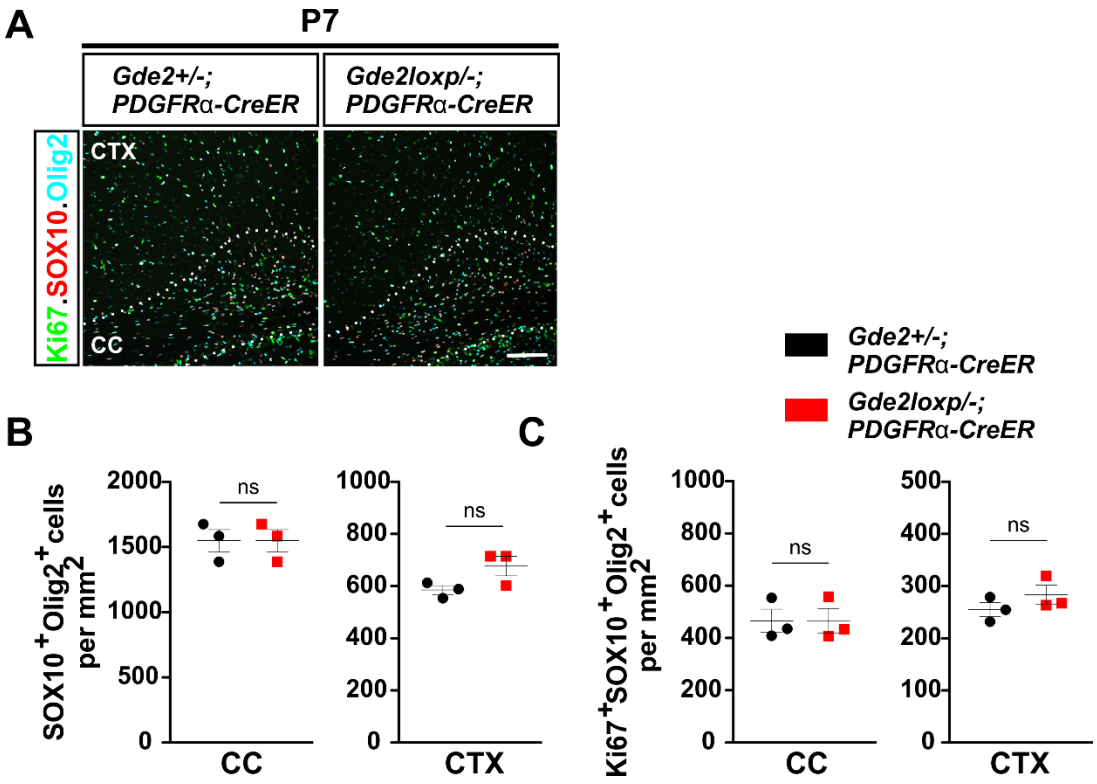

Figure 4.9. Loss of OL GDE2 does not influence OPC proliferation

(A) Coronal section of motor cortex (CTX) and corpus callosum (CC) from *Gde2+/-*; *PDGFαR-CreER* control and *Gde2lox/-; PDGFαR-CreER* P7 animals. Hatched lines mark the boundary between cortex and corpus callosum. (B) Graphs quantifying the number of oligodendroglia (Sox10+Olig2+) show no change between *Gde2+/-*; *PDGFαR-CreER* control and *Gde2lox/-; PDGFαR-CreER* CC (ns =0.0857) and CTX (ns = 0.1555). (C) Graphs quantifying the number of proliferating OPCs (Ki67+Sox10+Olig2+) show no change between WT and *Gde2-/-* CC (ns =0.5147) and CTX (ns = 0.2971). n = 3 *Gde2+/-*; *PDGFαR-CreER* control, 3 *Gde2lox/-; PDGFαR-CreER*. All graphs: Mean ± sem, two-tailed unpaired Students t-test. Scale bar: 100 μm

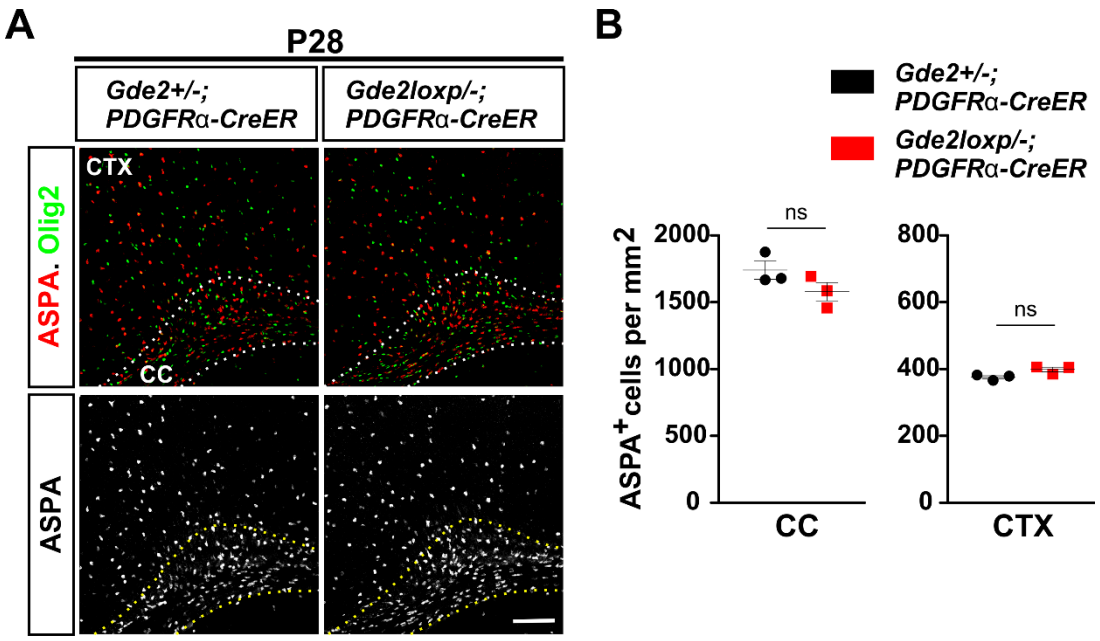

Figure 4.10. Impaired OL maturation from the loss of OL GDE2 is recovered by P28

(A) Coronal sections of mouse motor cortex (CTX) and corpus callosum (CC) from *Gde2+/-*; *PDGFαR-CreER* control and *Gde2lox/-; PDGFαR-CreER* P28 animals. Hatched lines delineate the CC. (B) Graphs quantifying the number of mature OLs (ASPA+) show no difference between *Gde2+/-*; *PDGFαR-CreER* control and *Gde2lox/-; PDGFαR-CreER* CC (ns =0.1922) and CTX (ns = 0.0721). n = 3 *Gde2+/-*; *PDGFαR-CreER* control, 3 *Gde2lox/-; PDGFαR-CreER*. Mean ± sem, two-tailed unpaired Students t-test. Scale bar: 100 μm

Chapter 5
Neuronal GDE2 releases factors to promote OL maturation

5.1 Introduction

The ablation of neuronal GDE2 expression results in impaired OL maturation that mimics the OL phenotypes observed upon global deletion of GDE2. This observation suggests that neuronal GDE2 function is responsible for the regulation of OL maturation. To understand the mechanism by which neuronal GDE2 enhances OL maturation, we took advantage of *in vitro* culture systems in which OL maturation occurs relatively synchronously in contrast to *in vivo* conditions. Using the culture system, we tested whether GDE2 expression in neurons regulates OL maturation through contact-mediated mechanisms or through the release of neuronally-derived soluble factors.

5.2 Results

5.2.1 *Gde2-/-* neuron-WT OPC coculture recapitulates *in vivo Gde2-/-* phenotypes

To better understand the mechanisms by which neuronal GDE2 enhances OL maturation, we first established a culture system in which purified WT and *Gde2-/-* cortical neurons were co-cultured with WT OPCs *in vitro*. Specifically, cortical neurons were derived from E16.5 embryos prior to the onset of astrocyte generation[95]. Neurons were cultured for 3 days *in vitro* (DIV); at this stage, neurons are immature and are undergoing active axonal and dendritic growth similar to neurons in the postnatal brain at the time of OL maturation[96]. The percentage of DAPI+ cells expressing β-tubulin type III, which marks both immature and mature neurons, was approximately 95% in cultures prepared from WT and *Gde2-/-* neurons (Fig 5.1.A). Neuronal cultures from WT and *Gde2-/-* animals contained approximately 2% astrocytes (GFAP+) (Fig 5.1.B), confirming that

these cultures are highly enriched in neurons with little astrocyte contamination. At DIV3, OPCs purified from P6 WT cortices were plated on WT and *Gde2-/-* cultured neurons. Mitogenic factors including PDGFAA are potent molecules that maintain OPCs in proliferative states; accordingly[97], OPCs were plated on neurons in the absence of exogenous mitogenic factors and these OPC-neuronal co-cultures were maintained for an additional 3 days (Fig 5.2.A). Cultures were then fixed and examined for OL maturation by morphology and MBP expression. When compared with OPCs cocultured with WT neurons, OPCs cocultured with *Gde2-/-* neurons showed a marked 33% reduction in the number of mature MBP+ OLs (Fig 5.2.B). Total numbers of Olig2+ OL lineage cells were equivalent between the two conditions (Fig 5.2.B). These observations recapitulate our *in vivo* data indicating that GDE2 neuronal function is required for OL maturation.

5.2.2 Neuronal GDE2 releases promaturation factors

WT OPCs cocultured with *Gde2-/-* neurons showed deficits in OL maturation. To examine if GDE2 regulation of OL maturation involves contact-mediated signals between neurons and OLs or, alternatively, involves the release of factors from neurons that stimulate OL maturation, we treated freshly purified WT OPCs with conditioned medium (CM) collected from WT or *Gde2-/-* neurons at DIV3 and DIV4. Specifically, WT OPCs were cultured for 1 day in DIV3 CM and, on the next day, cultured with CM collected between DIV3 and DIV4 for a further 2 days; they were then fixed and analyzed for OL maturation (Fig 5.3.A). The total number of MBP+ OLs in cultures treated with *Gde2-/-* neuronal CM was reduced by approximately 25% compared with WT neuronal CM (Fig 5.3.B). In addition, we observed a concomitant increase in the number of MBP- Olig2+

cells in WT OPCs cultured in *Gde2-/-* neuronal CM (Fig 5.3.B) CM prepared from DIV3 *Gde2-/-* neurons alone recapitulated these changes in OL maturation (Fig 5.3.C and 5.3.D). These observations suggest that neuronal GDE2 does not utilize contact-mediated signals to regulate OL maturation. Instead, GDE2 stimulates the release of soluble factors from neurons that promote OL maturation.

As OLs mature *in vitro*, they undergo stereotypic morphological changes, increase expression of myelin proteins such as MBP, and shift from actin assembly to disassembly coincident with myelination[98]. We defined 3 stages of OL maturation based on their morphology, MBP expression, and F-actin network visualized by phalloidin staining[98] (Fig 5.4.A). Differentiating Olig2+ OLs *in vitro* initially show arborized morphology with weak cell body MBP expression and robust phalloidin labeling throughout the cell body and in distal processes (Stage 1, immature). Partially differentiated OLs show increased MBP expression and strong phalloidin labeling in distal processes, with occasional flattening of the myelin sheath in distal structures (Stage 2, premyelinating). In contrast, more mature OLs show ring-like or lamellar morphology with strong MBP expression throughout the membrane sheath and near complete disappearance of the actin cytoskeleton (Stage 3, myelinating). WT OPCs co-cultured with *Gde2-/-* neurons after 3 days in culture showed a 20%, 40%, and 50% reduction in the number of OLs at Stage 1, Stage 2, and Stage 3 of maturation, respectively. (Fig 5.4.B). Similarly, WT OPCs grown in DIV3+4 CM showed a 25% and 50% reduction in the number of OLs at Stage 2 and Stage 3 of maturation, respectively, when treated with *Gde2-/-* neuronal CM, but no change in the number of Stage 1 OLs (Fig 5.4.B). Taken together, these observations suggest that GDE2-

dependent pathways in neurons lead to the release of soluble factors that promote the maturation of OLs.

5.2.3 Neuronal activity does not affect GDE2-regulated OL maturation

Neuronal activity has been shown to positively regulate OL maturation. To determine if GDE2-dependent release of OL maturation factors is mediated by neuronal activity, we utilized optical recording of intracellular calcium via the calcium indicator Fluo-4. The cell-permeable calcium indicator increases fluorescence excitation at 488nm upon binding free Ca2+. When neurons loaded with Fluo-4 undergo neuronal activity, extracellular Ca2+ flows into cells and binds to the calcium indicator resulting in an increase in fluorescence intensity[99]. Cultured WT and *Gde2-/-* neurons were loaded with Fluo-4 at DIV3. This timepoint corresponds to when cultured neurons release OL promaturation factors through GDE2-dependent mechanisms (Fig 5.3.). Analysis of calcium transients (ΔF/Fo), over a 3.5-minute recording period showed that both DIV3 WT and *Gde2-/-* neurons showed no detectable signals (Fig 5.5). To confirm that Fluo-4 was loaded appropriately in neurons, WT and *Gde2-/-* neurons were treated with the ionophore ionomycin at the end of recording, which increases calcium internalization[100]. Both WT and *Gde2-/-* neurons treated with ionomycin showed an instant and robust increase in the fluorescence signal, confirming that Fluo-4 was efficiently loaded in neurons. These observations indicate that DIV3 WT and *Gde2-/-* neurons are immature and largely inactive at this stage, suggesting that GDE2 regulation of OL maturation is unlikely to involve neuronal activity-dependent mechanisms. To test the possibility that neuronal activity can influence GDE2 expression at the time when neurons are electrically

active, DIV14 WT cortical neurons were treated with bicuculine for various indicated times (Fig 5.6). Bicuculine stimulates neuronal activity through blocking inhibitory actions of $GABA_A$ receptors[101]. Western blots of neuronal lysates show equivalent GDE2 expression over the time course of bicuculine treatment (Fig 5.6), suggesting that neuronal activity does not influence GDE2 expression.

5.3 Summary

To determine how GDE2 neuronal function regulates OL maturation, we utilized *in vitro* culture models where WT OPCs were either cocultured with WT and *Gde2-/-* neurons or cultured in CM collected from WT and *Gde2-/-* neurons. Both culture systems not only recapitulated the OL maturation phenotypes observed in *Gde2-/-* animals *in vivo*, but they also elucidated functions of neuronal GDE2 at a cellular level. Accordingly, we conclude that GDE2 function in neurons promotes OL maturation through the release of neuronally-derived soluble pro-maturation factors.

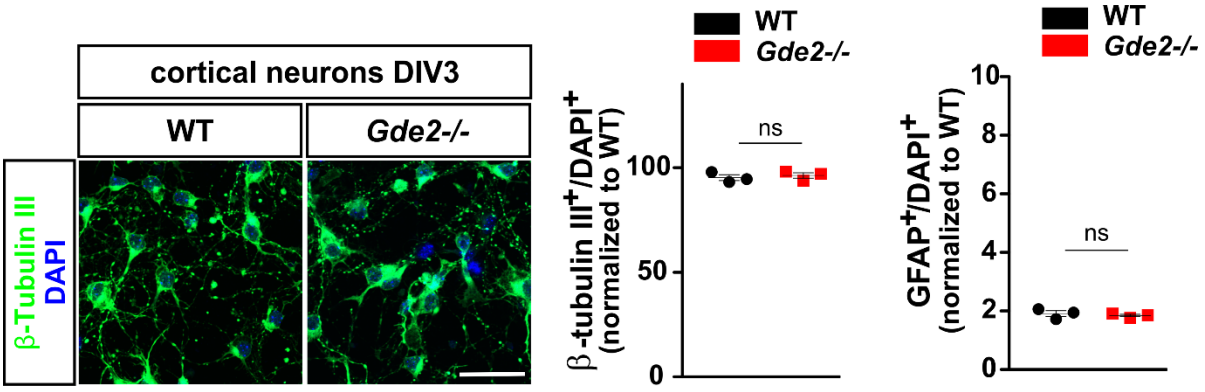

Figure 5.1. Characterization of cortical neuronal cultures

Immunocytochemical staining of DIV3 cortical neuronal culture. Graphs quantifying the number of β-tubulin type III+ neurons and GFAP+ astrocytes show equivalent expression between WT and *Gde2-/-* neurons. A typical culture contains ~95 % β-tubulin type III+ neurons and ~2 % GFAP+ astrocytes. β-tubulin III+ ns p = 0.6243; GFAP+ ns p = 0.6093; n = 3 WT 3 *Gde2-/-*. Scale bar: 50 μm.

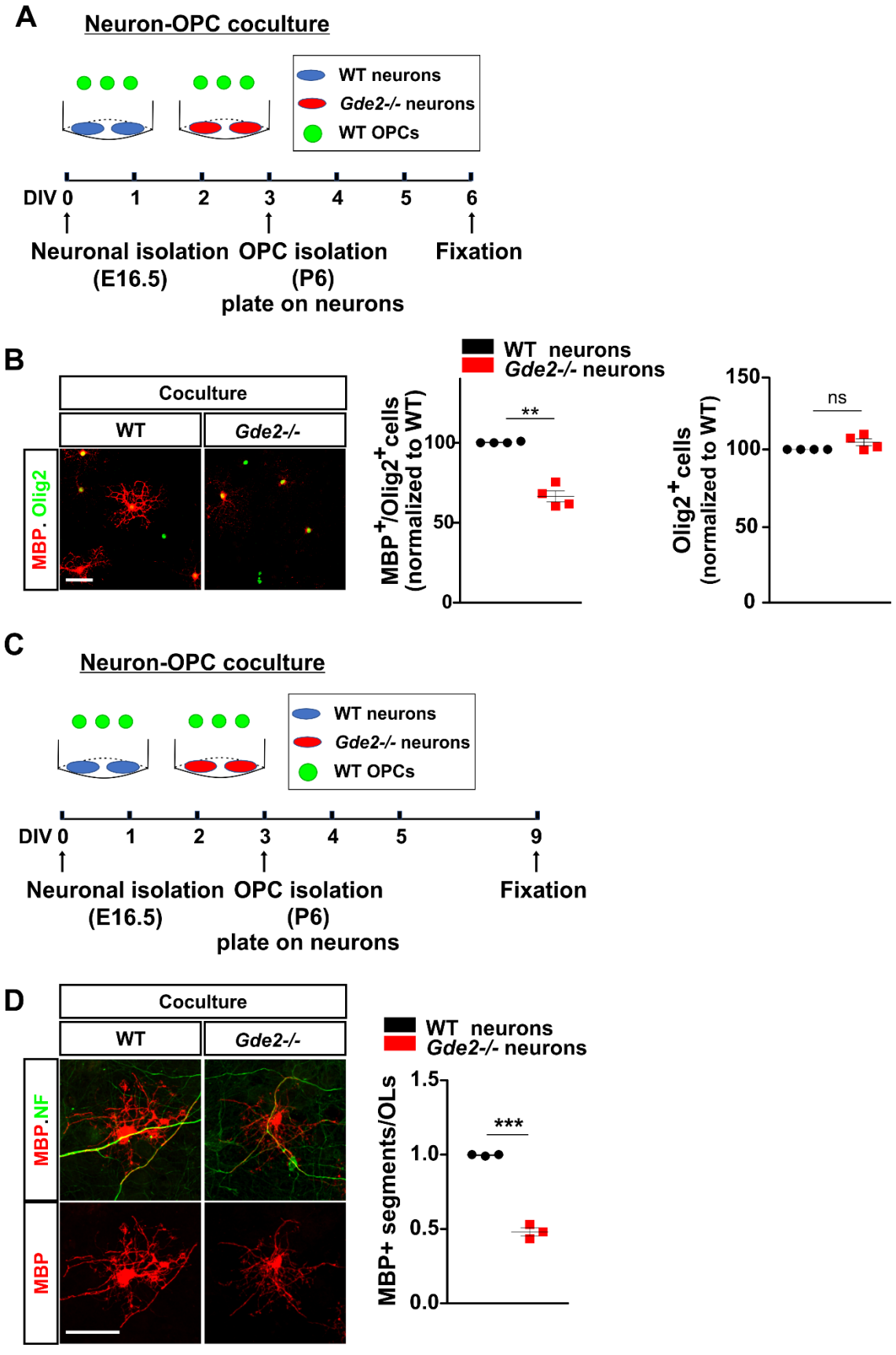
A
Neuron-OPC coculture
WT neurons
Gde2-/- neurons
WT OPCs
DIV 0 1 2 3 4 5 6
Neuronal isolation (E16.5)
OPC isolation (P6)
plate on neurons
Fixation
B
Coculture
WT
Gde2-/-
MBP. Olig2
WT neurons
Gde2-/- neurons
MBP+/Olig2+cells (normalized to WT)
**
Olig2+cells (normalized to WT)
ns
C
Neuron-OPC coculture
WT neurons
Gde2-/- neurons
WT OPCs
DIV 0 1 2 3 4 5 9
Neuronal isolation (E16.5)
OPC isolation (P6)
plate on neurons
Fixation
D
Coculture
WT
Gde2-/-
MBP.NF
MBP
WT neurons
Gde2-/- neurons
MBP+ segments/OLs
***

Figure 5.2. *Gde2-/-* neuron-WT OPC cocultures recapitulate *Gde2-/- in vivo* phenotypes

(A) Schematic illustrating neuron-OPC co-culture paradigm. Cortical neurons are grown for 3 days, co-cultured with purified WT OPCs for another 3 days fixed and analyzed. (B) Immunocytochemical detection of MBP+ OLs in WT neuron-WT OPC and *Gde2-/-* neuron-WT OPC co-cultures. Graphs quantifying the percentage of MBP+Olig2+ OLs and Olig2+ cells in WT neuron-WT OPC and *Gde2-/-* neuron-WT OPC cocultures (normalized to WT). OPCs co-cultured with *Gde2-/-* neurons showed significant decrease in the number of MBP+Olig2+ OLs compared to OPCs cocultured with WT neurons (**p = 0.0019). Numbers of Olig2+ cells are equivalent between co-cultures with WT or *Gde2-/-* neurons (ns p = 0.1235, total number of 2959 Olig2+ cells in WT and 3030 Olig2+ cells in *Gde2-/-* were counted). n = 4 WT neuron-WT OPC co-cultures, 4 *Gde2-/-* neuron-WT OPC co-cultures. (C) Schematic illustrating neuron-OPC co-culture paradigm. Cortical neurons are grown for 3 days, co-cultured with purified WT OPCs for another 6 days fixed and analyzed. (D) Immunocytochemical detection of MBP+ myelin segments. Numbers of MBP+ segments were reduced in *Gde2-/-* condition (***p <0.0001, n = 3 WT, 3 *Gde2-/-*). Two tailed unpaired Student's t-test. All graphs: Mean ± sem.

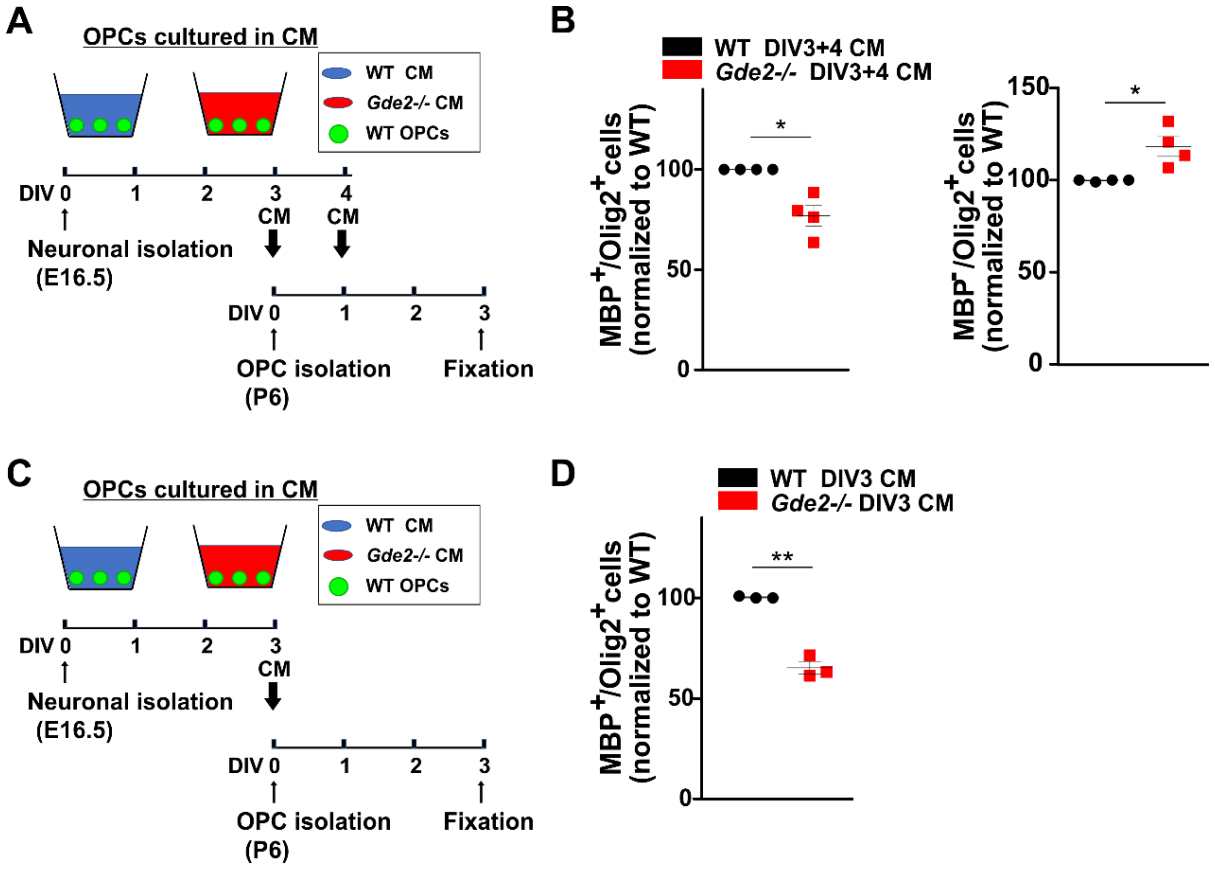
A
OPCs cultured in CM
WT CM
Gde2-/- CM
WT OPCs
DIV 0
1
2
3
4
CM
CM
Neuronal isolation
(E16.5)
DIV 0
1
2
3
OPC isolation
(P6)
Fixation
B
WT DIV3+4 CM
Gde2-/- DIV3+4 CM
MBP+/Olig2+cells
(normalized to WT)
100
50
0
*
MBP-/Olig2+cells
(normalized to WT)
150
100
50
0
*
C
OPCs cultured in CM
WT CM
Gde2-/- CM
WT OPCs
DIV 0
1
2
3
CM
Neuronal isolation
(E16.5)
DIV 0
1
2
3
OPC isolation
(P6)
Fixation
D
WT DIV3 CM
Gde2-/- DIV3 CM
MBP+/Olig2+cells
(normalized to WT)
100
50
0
**

Figure 5.3. GDE2 functions in neurons to release neuronally-derived promaturation factors

(A) Schematic illustrating OPCs cultured with neuronal conditioned medium (DIV3+4 CM). CM prepared from DIV3 and DIV4 neurons were added to OPCs purified from P6 pups. OPCs were cultured in CM for 3 days before analysis. (B) Graphs quantifying the percentage of MBP+ Olig2+ OLs and MBP-Olig2+ cells (normalized to WT) with DIV3+4 neuronal CM (DIV3 and DIV4 neurons). DIV3+4 CM from *Gde2-/-* neurons shows reduction in MBP+ Olig2+ OLs with an increase in MBP-Olig2+ cells (MBP+ Olig2+ *p = 0.0209 ; MBP- Olig2+ , *p = 0.0140 n = 4 WT DIV3+4 CM, 4 *Gde2-/-* DIV3+4 CM,). Similar to DIV3+4 CM, CM from DIV3 *Gde2-/-* neurons show decreased MBP+ Olig2+ OLs (**p = 0.0078, n = 3 WT CM, 3 *Gde2-/-* DIV3 CM,), suggesting that GDE2 functions in DIV3 neurons is required for the release of factors to promote OL maturation. Two tailed unpaired Student's t-test. All graphs: Mean $\pm$ sem.

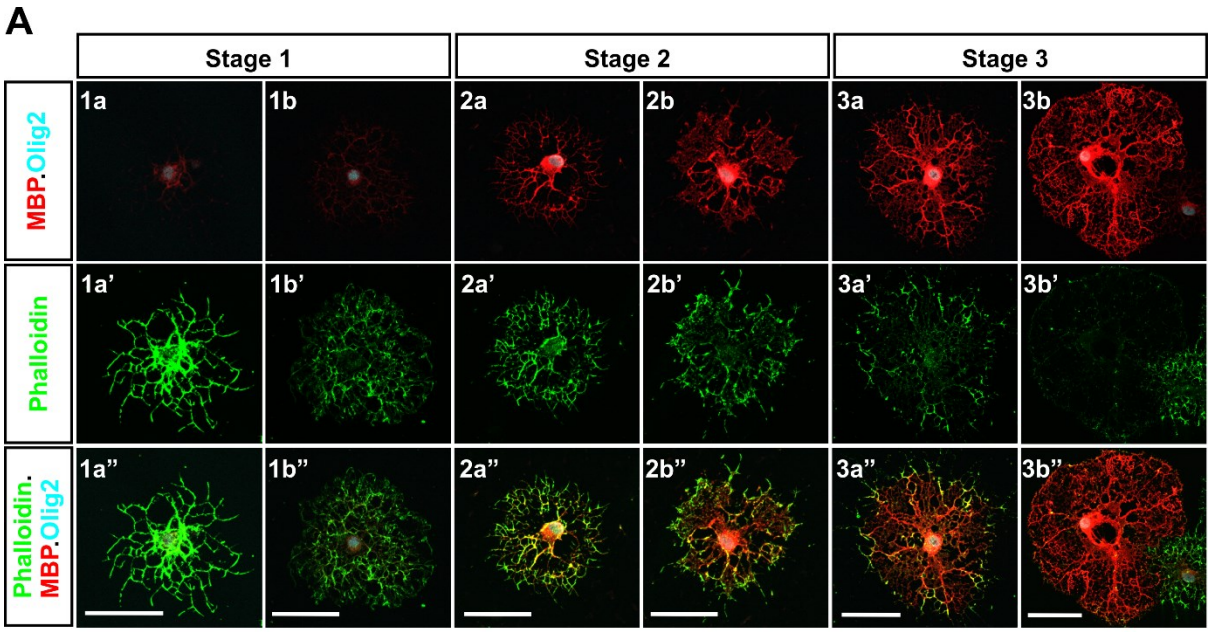
A
Stage 1
Stage 2
Stage 3
MBP.Olig2
Phalloidin
Phalloidin.
MBP.Olig2
1a
1b
2a
2b
3a
3b
1a'
1b'
2a'
2b'
3a'
3b'
1a''
1b''
2a''
2b''
3a''
3b''

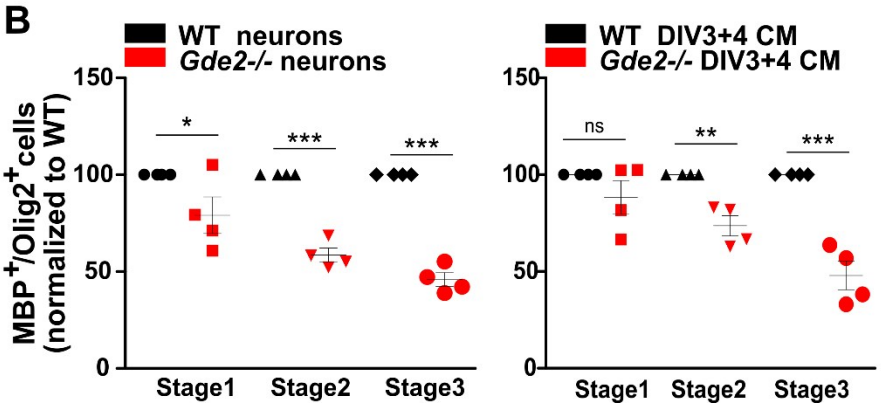
B
WT neurons
Gde2-/- neurons
WT DIV3+4 CM
Gde2-/- DIV3+4 CM
MBP+/Olig2+cells
(normalized to WT)
150
100
50
0
*
***
***
ns
**
***
Stage1
Stage2
Stage3

Figure 5.4. Neuronal GDE2 releases factors to promote maturation of stage 2, premyelinating OLs

(A) Representative images of immunocytochemical staining of cultured OLs to define 3 stages of OL maturation *in vitro*. Two examples (a, b) are shown per stage. (B) Graphs quantifying percentage of MBP+Olig2+ OLs corresponding to each Stage in co-cultures (left) and OPC cultures in DIV3+4 CM (right). For quantification of OLs in cocultures, morphology and MBP expression intensity and pattern were used. WT OPCs co-cultured with WT vs *Gde2-/-* neurons: 2-way ANOVA ***p <0.0001 (Bonferroni correction Stage 1 *p <0.05; Stage 2 ***p <0.001; Stage 3 ***p <0.001; n = 4 WT, 4 *Gde2-/-*; see B for Olig2+ and MBP+ cell numbers; WT MBP+ Stage 1= 159, Stage 2= 116, Stage 3= 53; *Gde2-/-* MBP+ Stage 1= 89, Stage 2= 43, Stage 3= 18). WT OPCs cultured with WT DIV3+4 CM vs *Gde2-/-* DIV3+4 CM: 2-way ANOVA ***p < 0.0001 (Bonferroni correction Stage 1 ns p >0.05; Stage 2 **p <0.01; Stage 3 ***p <0.001; n = 4 WT CM, 4 *Gde2-/-* CM). All graphs: Mean ± sem, two-tailed unpaired Students t-test. Scale bars: 50 μm.

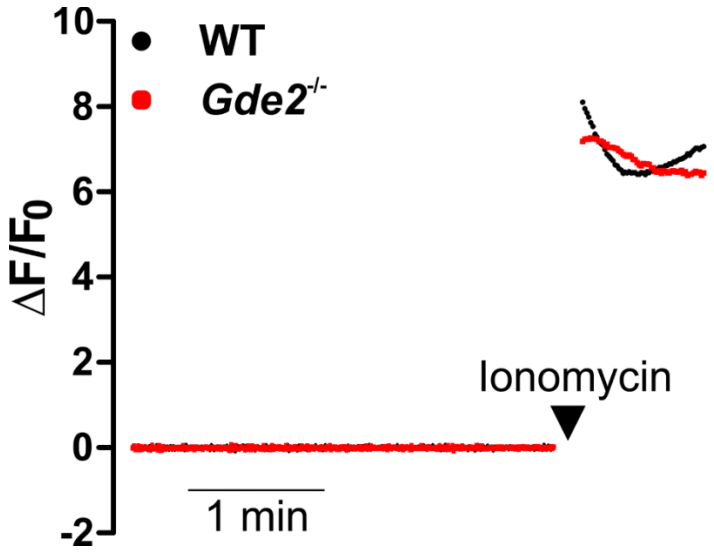

Figure 5.5. DIV3 WT and *Gde2* KO neurons show no neuronal activity

Graph of fluorescence changes (Δ F/F0) in DIV3 WT and *Gde2-/-* neurons loaded with the calcium indicator Fluo-4 over a 3.5 minute period. Each data point represents mean value of $\Delta F/F_0$ from 11 recordings per group at a given time. Arrowhead marks the time of Ionomycin addition, which permeabilizes the membrane and acts as a positive control.

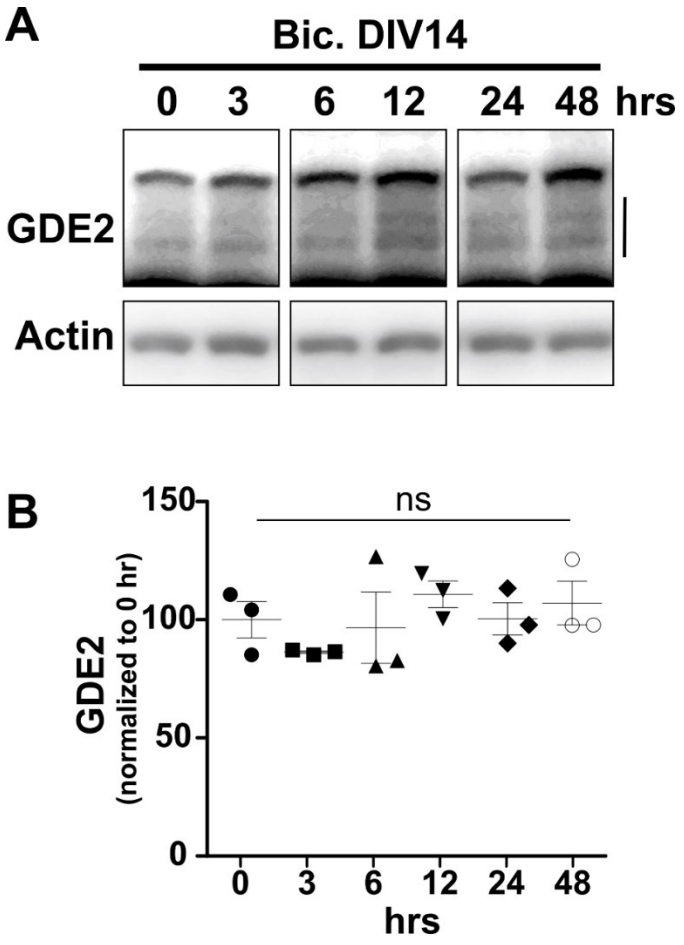

Figure 5.6. Bicuculine treatment does not influence GDE2 expression

(A) Western blot of DIV14 WT cortical neurons treated with bicuculine for specified time periods. Actin is used as loading control. Bar indicates GDE2. (B) Graph quantifying GDE2 protein levels show no change in expression after stimulation. 1 way ANOVA ns $p = 0.4692$, $n = 3$ for each timepoint.

Chapter 6
GDE2 maintains canonical Wnt signaling

6.1 Introduction

Studies with conditional GDE2 deletion in neurons (chapter 4) and *in vitro* neuronal cultures (chapter 5) indicate that GDE2 functions in neurons to promote OL maturation. The major neuronal factors that have been shown to regulate OL maturation are contact-mediated signals[83], axon diameter[34,35], and neuronal activity[27]. Intriguingly, my studies suggest that GDE2-mediated pathways that promote OL maturation are independent of these known neuronal factors (Fig 5.3, Fig 5.5, and Fig 3.8). This finding suggests that GDE2 acts through a separate pathway in neurons to regulate OL maturation. To gain insight into potential pathways that mediate GDE2 regulation of OL maturation, we analyzed bulk RNA-sequencing of WT and *Gde2*-/- nervous tissue and discovered that canonical Wnt signaling pathways are altered in the absence of GDE2. To test the hypothesis that GDE2 might control Wnt signaling pathways in neurons to stimulate OL maturation, we first assessed canonical Wnt signaling pathway components and known downstream target gene expression in cultured neurons using qPCR, Western blot, and immunocytochemistry. To gain further insight into the role of GDE2 in regulating Wnt signaling activity *in vivo*, we utilized canonical Wnt-reporter animals (*Rosa26 Tcf/Lef H2B-eGFP*) in which nuclear expression of a reporter eGFP protein directly reflects canonical Wnt signaling activity. These approaches allowed me to conclude that GDE2 functions to maintain canonical Wnt signaling in the postnatal brain, and that loss of GDE2 function leads to reduced Wnt signaling activity in neurons and oligodendroglia.

6.2 Results

6.2.1 Loss of GDE2 shows altered canonical Wnt signaling pathway

A previous study in our laboratory included bulk RNA-seq of WT and *Gde2-/-* spinal cord tissue. 454 genes were found to be differentially expressed in *Gde2-/-* tissues compared with WT (Table 1), and Gene Ontology (GO) analysis using the STRING database (v.11) highlighted altered pathways associated with Wnt signaling (Fig 6.1.A and Fig 6.1.B). Further, known canonical Wnt signaling target genes, whose expression are upregulated upon activation of canonical Wnt signaling, (https://web.stanford.edu/group/nusselab/cgi-bin/wnt/target_genes), were down-regulated in *Gde2-/-* mutants, implying that GDE2 normally potentiates Wnt pathway activation (Fig 6.1.C). The Wnt signaling pathway plays a wide range of roles in development and disease. Canonical Wnt signaling is characterized by the stimulation of β-catenin-dependent regulation of target gene expression. Briefly, in the absence of Wnt ligands, β-catenin is phosphorylated by GSK3β and targeted for degradation by the cytosolic destruction complex that is comprised of proteins including, but not limited to, Axin, GSK3β, and APC[84]. In the presence of Wnt ligands however, the destruction complex is inactivated in part by its interaction with cognate receptors, which ultimately stabilizes and promotes nuclear translocation of β-catenin[102]. β-catenin does not have a DNA binding-domain; however, by interacting with specific transcription factors in the nucleus, activated β-catenin (ABC) can regulate the expression of Wnt target genes, which include the transcription factor *Lef1*[46,47]. To validate the RNA-seq results, I first quantified the expression of *Lef1* transcripts by qPCR using cDNAs prepared from P10 WT and *Gde2-/-* corticies. *Lef1* expression from P10 *Gde2-/-* cortical cDNA samples

showed a 32% reduction compared with WT, and this decrease was recapitulated in DIV3 *Gde2-/-* cultured cortical neurons (Fig 6.2.A). Further, levels of ABC detected by antibodies specific to β-catenin that is dephosphorylated on residues Ser37 or Thr41[103], are decreased by 20% in *Gde2-/-* DIV3 neuronal extracts compared to WT, while total levels of β-catenin are unchanged between genotypes (Fig 6.2.B). β-catenin subcellular localization dictates biological functions of β-catenin[104]. To test if the decrease in *Lef1* expression can be attributed to reduced levels of nuclear ABC, I examined nuclear ABC expression in fixed cortical neurons or fractionated cortical neuron protein extracts using ABC-specific antibodies. Immunohistochemical and biochemical analyses reveal that ABC levels in both nuclear and cytoplasmic compartments of *Gde2-/-* DIV3 neurons are decreased (Fig 6.3.A and Fig 6.3.B). These observations collectively indicate that levels of canonical Wnt signaling in neurons are reduced when neuronal GDE2 function is disrupted.

6.2.2 GDE2 maintains canonical Wnt activity in the postnatal brain

To gain deeper insight into the temporal and spatial changes in canonical Wnt pathway activation during OL development, we utilized *Rosa26 Tcf/Lef H2B-eGFP* mice, which harbor a cassette knocked-in to the *Rosa26* locus that consists of a histone H2B-GFP fusion protein placed under control of TCF/LEF dependent regulatory sequences[105]. This mouse reporter line has been shown to report *in situ* Wnt pathway activation through expression of eGFP[105]. Although studies provide mounting evidence of the importance of canonical Wnt signaling during embryonic tissue development[57], its roles in the postnatal brain are not fully defined. In the perinatal period (E18~P0), canonical Wnt signaling

pathway has been shown to play a role in the transition of multipolar neurons to bipolar migrating neurons in the CTX[106]. Further, between P1-P6, the canonical Wnt signaling pathway is reported to function in subsequent laminar positioning of cortical neurons[59]. We first defined the normal pattern of canonical Wnt signaling *in vivo* by examining eGFP reporter expression in P7, P11, and P28 cortices of *Rosa26 Tcf/Lef H2B-eGFP* WT mice. We observed robust nuclear eGFP expression in neurons and Olig2+ cells at P7 and P11 (Fig 6.4.A). In contrast, little to no neuronal GFP expression is detected at P28 when developmental myelination is almost complete (Fig 6.4.A. and Fig 6.4.B). However, GFP continues to be expressed in approximately 20% of Olig2+ cells (Fig 6.4.A. and Fig 6.4.B). These observations reveal that canonical Wnt signaling is dynamic in the first month of life and they are consistent with potential roles for canonical Wnt signaling in OL maturation. Importantly, Wnt activation in WT neurons overlaps with GDE2 neuronal expression and the temporal profile of GDE2 requirement in OL maturation. These observations raise the possibility that Wnt signaling activity might mediate GDE2-dependent control of OL maturation. To test this hypothesis, I introduced the *Rosa26 Tcf/Lef H2B-eGFP* reporter into *Gde2-/-* animals. Total numbers of GFP+ cells were reduced in *Gde2-/-; Rosa26 Tcf/Lef H2B-eGFP* animals compared with WT controls, suggesting reduced Wnt pathway activation in absence of GDE2 (Fig 6.5.A). *Gde2-/-; Rosa26 Tcf/Lef H2B-eGFP* animals showed a marked 40% reduction in the number of eGFP expressing neurons (NeuN+) compared with WT littermates. No change in the number of neurons was detected between genotypes (Fig 6.5.B and Fig 6.5.C). This observation suggests that GDE2 is required to maintain canonical Wnt signaling in neurons at the time of OL maturation. Interestingly, *Gde2-/-; Rosa26 Tcf/Lef H2B-eGFP*

cortices at P11 also show 25% and 40% reduced eGFP expression in oligodendroglia (Olig2+ cells) in CC and adjacent CTX, respectively (Fig 6.5.D and Fig 6.5.E). Numbers of oligodendroglia were equivalent in both WT *Rosa26 Tcf/Lef H2B-eGFP* and *Gde2-/-; Rosa26 Tcf/Lef H2B-eGFP* animals at P11 (Fig 6.5.E). Among oligodendroglia, NG2+ OPCs show robust GFP expression while immature (TCF4+ CC1-) and mature (TCF4- CC1+) OLs show minimal eGFP expression, suggesting that Wnt activity is restricted to OPCs (Fig 6.6.A and Fig 6.6.B). These observations indicate that GDE2 maintains canonical Wnt activity in neurons and OPCs at the time of OL maturation in the developing postnatal cortex.

6.3 Summary

We utilized RNA-seq analysis to identify canonical Wnt signaling as a candidate mediator of GDE2-dependent control of OL maturation in the developing postnatal cortex. Using a reporter mouse for canonical Wnt signaling, we discovered that WT cortices show dynamic temporal profiles of Wnt activation with peak reporter gene expression during the time of OL maturation and little to no expression when OL development is complete. Loss of GDE2 results in marked reduction of Wnt activity in both neurons and OPCs. Because GDE2 is not expressed in OPCs, reduced Wnt activity in *Gde2-/-* OPCs is likely due to non-cell autonomous effects. Collectively, these observations indicate that GDE2 is required to maintain canonical Wnt signaling activity in the postnatal cortex.

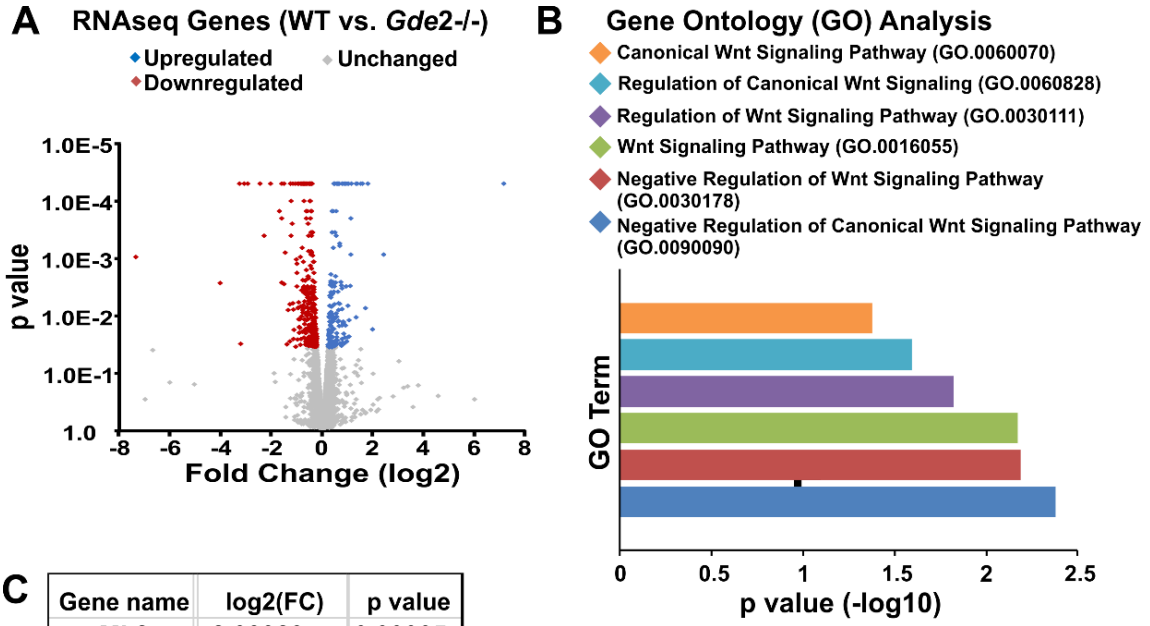

C

Gene name	log2(FC)	p value
Mitf	-2.03989	0.00005
Pttg1	-0.685154	0.00005
Sox9	-0.440899	0.00005
Vegfc	-0.678135	0.00245
Islr	-0.387588	0.0037
Axin2	-0.353966	0.024
Cd44	-0.314482	0.0263

Figure 6.1. RNA-sequencing analysis shows altered Wnt signaling pathways in *Gde2-/-* spinal cord

(A) Volcano plot showing genes that are differentially expressed between WT and *Gde2-/-* spinal cord. Data points represent individual genes in the analysis. B) Gene ontology analysis using p-value (< 0.05) highlights disrupted Wnt signaling pathways in absence of GDE2. (C) List of known canonical Wnt target genes that are altered in *Gde2-/-* condition. All show downregulation in absence of GDE2.

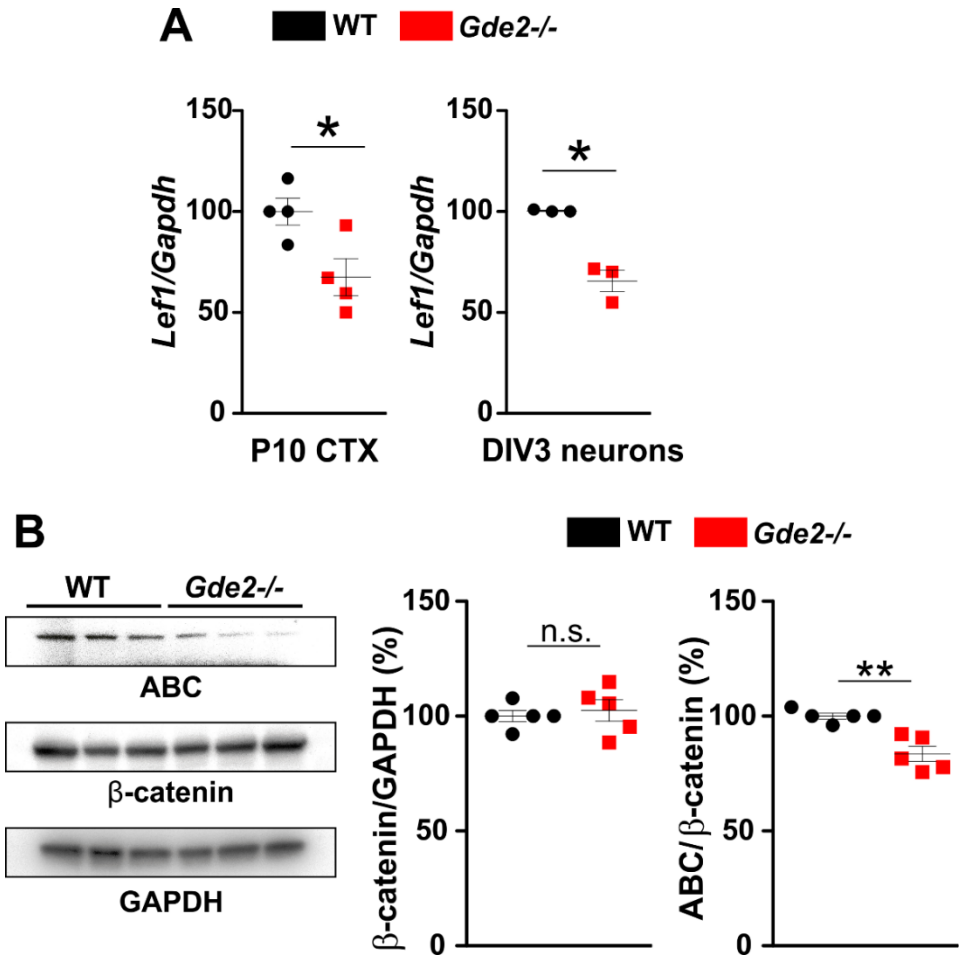

Figure 6.2. Reduced canonical Wnt signaling pathway in *Gde2-/-* neurons

(A) Graph showing quantitative measurement of transcript expression of *Lef1*, a downstream target gene of canonical Wnt signaling pathway via qPCR. *Lef1* transcripts normalized to *Gapdh* mRNAs show a significant reduction in *Gde2-/-* P10 cortex (CTX) (*p = 0.0231; n = 4 WT, 4 *Gde2-/-*) and cultured DIV3 cortical neurons (*p = 0.0362; n = 3 WT, 3 *Gde2-/-*). (B) Western blot of DIV3 WT and *Gde2-/-* cortical neuronal lysates. Active β-catenin (ABC) is decreased but no change in β-catenin ise observed in *Gde2-/-* neurons (n.s. p = 0.6465, **p = 0.0018 n = 5 WT, 5 *Gde2-/-*). Mean ± sem, two-tailed unpaired Students t-test.

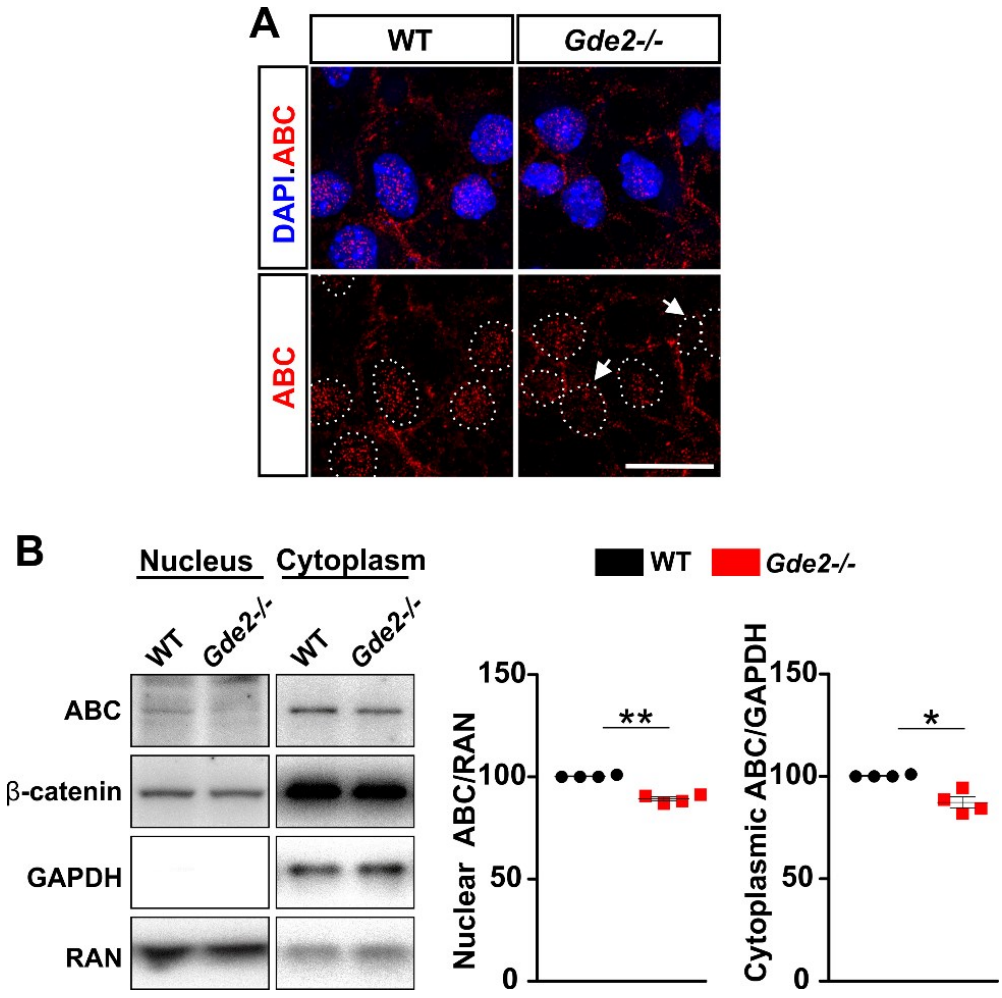

Figure 6.3. Reduced active β-catenin in *Gde2-/-* neurons

(A) Immunocytochemistry of ABC shows reduced staining in *Gde2-/-* cortical neurons (arrows). Nuclei are marked by dashed lines (B) Western blot of fractionated DIV3 cortical neurons shows reduction in nuclear and cytosolic ABC levels normalized to RAN and GAPDH respectively in absence of GDE2 (nuclear **p = 0.0019, cytoplasmic *p = 0.0186 n = 4 WT, 4 *Gde2-/-*). Mean ± sem, two-tailed unpaired Students t-test. Scale bars: 5 μm

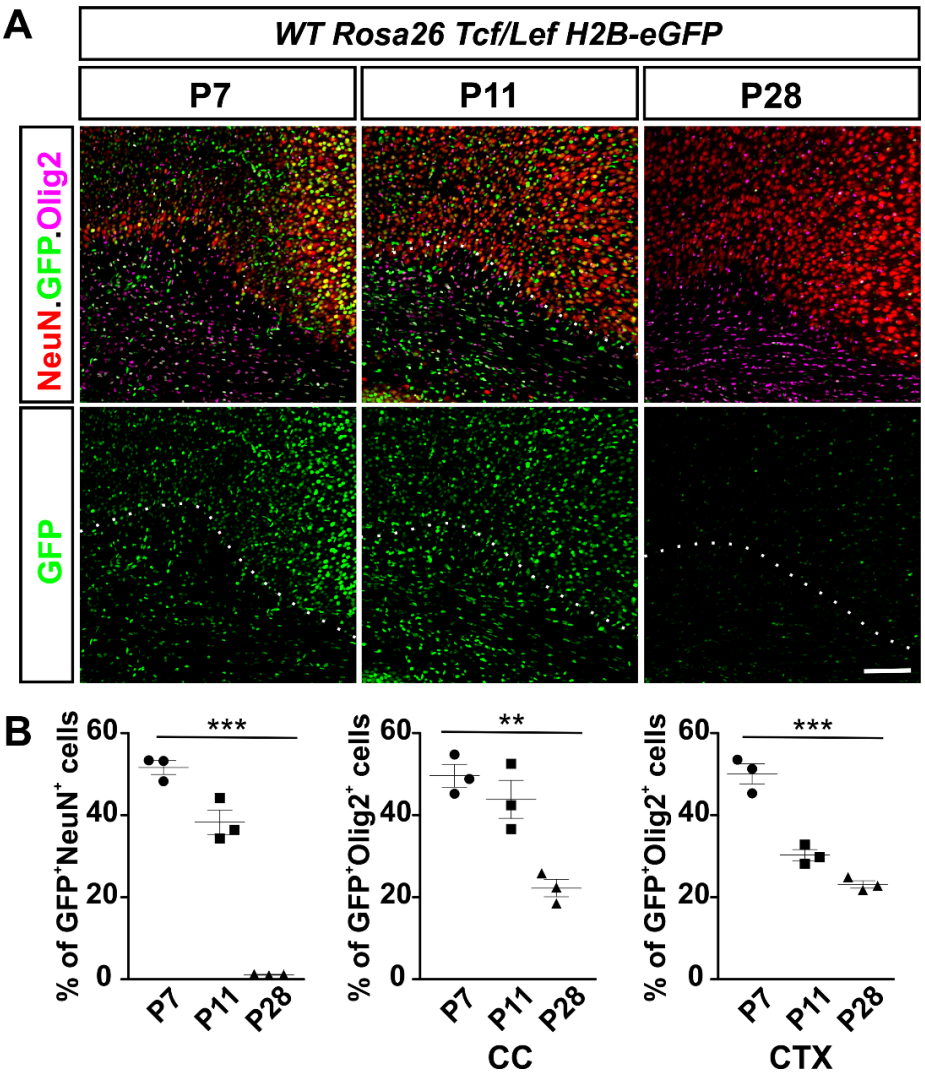

Figure 6.4. GDE2 loss decreases canonical Wnt signaling activity

(A) Coronal sections of P7, 11, and 28 mouse motor cortex (CTX) and corpus callosum (CC) of canonical Wnt-reporter animals (*Rosa26 Tcf/Lef H2B-eGFP*). Hatched lines delineate the border between the CTX and CC. (B) Graphs quantifying percentage of eGFP+ neurons (NeuN+) and oligodendroglia (Olig2+) in the CC and CTX. eGFP expression in neurons and oligodendroglia progressively decreases over the observed time period. GFP+NeuN+ ***$p < 0.0001$, GFP+Olig2+ CC **$p = 0.0027$, GFP+Olig2+ CTX **$p < 0.0001$. n = 3 P7, 3 P11, 3 P28, 1-way ANOVA. Mean ± sem. Scale bar: 100 μm

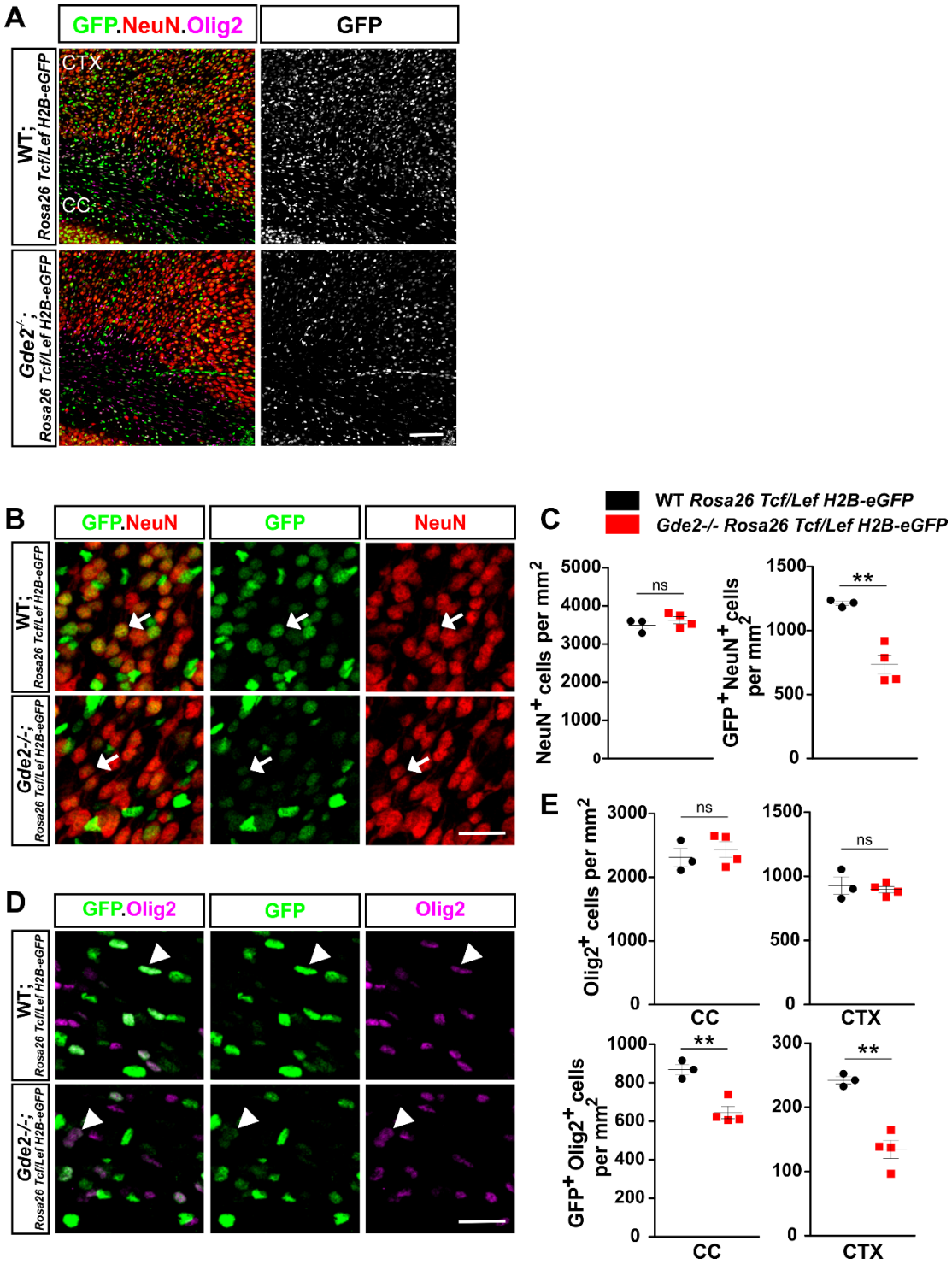
A
GFP.NeuN.Olig2
GFP
CTX
CC
WT; Rosa26 Tcf/Lef H2B-eGFP
Gde2-/-; Rosa26 Tcf/Lef H2B-eGFP
B
GFP.NeuN
GFP
NeuN
C
WT Rosa26 Tcf/Lef H2B-eGFP
Gde2-/- Rosa26 Tcf/Lef H2B-eGFP
NeuN+ cells per mm2
GFP+NeuN+cells per mm2
ns
**
D
GFP.Olig2
GFP
Olig2
E
Olig2+ cells per mm2
GFP+ Olig2+ cells per mm2
CC
CTX

Figure 6.5. Canonial Wnt signaling is reduced in *Gde2-/-* neurons and oligodendroglia

(A) Coronal section of P11 WT and *Gde2-/-* mice carrying *Rosa26 Tcf/Lef H2B-eGFP*. Loss of GDE2 displays markedly low GFP expression compared to WT. (B) An enlarged area of CTX in (A) showing GFP expression in neurons. Arrows mark NeuN+ neurons with GFP expression in WT animals carrying the *Rosa26 Tcf/LefH2B-eGFP* Wnt-reporter transgene; in *Gde2-/-; Rosa26 Tcf/LefH2B-eGFP* animals, arrows highlight NeuN+ neurons with reduced GFP expression. (C) Graphs show equivalent numbers of NeuN+ neurons in WT *Rosa26 Tcf/LefH2B-eGFP* and *Gde2-/-; Rosa26 Tcf/LefH2B-eGFP* P11 animals (ns, p = 0.3936); however, numbers of GFP+ neurons are reduced in *Gde2-/-; Rosa26 Tcf/LefH2B-eGFP* animals (**p = 0.0078). (D) An enlarged area of CC in (A) showing GFP expression in oligodendroglia. Arrowheads mark Olig2+ oligodendroglia with GFP expression in WT animals carrying the *Rosa26 Tcf/LefH2B-eGFP* Wnt-reporter transgene; in *Gde2-/-; Rosa26 Tcf/LefH2B-eGFP* animals, arrowheads highlight Olig2+ oligodendroglia with reduced GFP expression. (E) Graphs show that Olig2+ cells are equivalent in WT *Rosa26 Tcf/LefH2B-eGFP* and *Gde2-/-; Rosa26 Tcf/LefH2B-eGFP* P11 animals in CC (ns, p = 0.557) and CTX (ns, p = 0.7089); numbers of GFP expressing Olig2+ cells are reduced in *Gde2-/-; Rosa26 Tcf/LefH2B-eGFP* CC (**p = 0.006) and CTX (**p = 0.0057). n = 3 WT *Rosa 26 Tcf/LefH2B-eGFP*, 4 *Gde2-/-; Rosa26 Tcf/LefH2B-eGFP.* All graphs: Mean ± sem, two-tailed unpaired Students t-test. Scale bars: (A) 100 μm, (B, D) 20 μm.

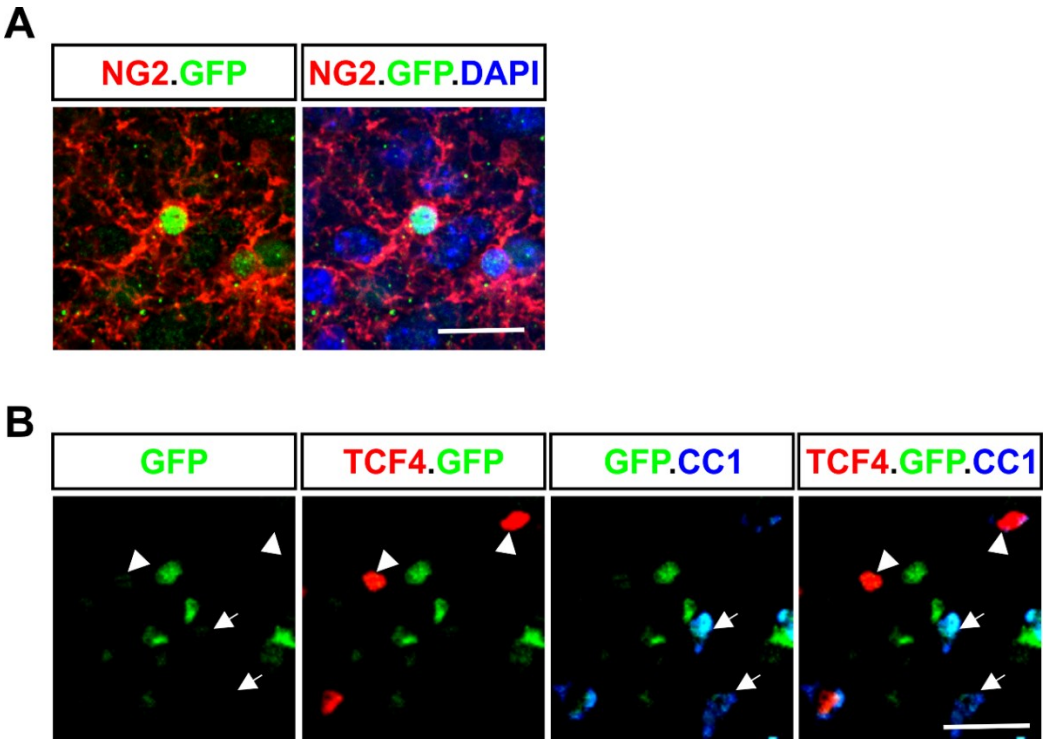

Figure 6.6. Wnt-reporter is expressed in OPCs but not at later stages of OL development

(A) Representative images of an NG2+ cell showing eGFP Wnt-reporter gene expression in sections of P11 mouse brain. (B) Representative images showing eGFP Wnt-reporter -gene expression at later OL developmental stages. eGFP Wnt-reporter expression is absent in immature OLs (TCF4+ CC1-, arrowheads) and mature OLs (CC1+, arrows) in P11 Wnt-reporter animals (*Rosa26 Tcf/Lef H2B-eGFP*). Scale bars: 20 μm.

Table 6.1. RNA-sequencing genes that were differentially expressed and annotated in *Gde2-/-* spinal cord tissue.

Number of affected genes: 454

Gene ID	Gene	Locus	*Gde2* KO	*Gde2* WT	Fold Change (log2)	p value
XLOC_037454	Trim30d	chr7:104470013-104507849	0.07	0.64	-3.2743	0.00005
XLOC_037320	Myo7a	chr7:98050844-98119524	0.33	2.84	-3.0877	0.00005
XLOC_036015	Rdh13	chr7:4424769-4445667	5.22	40.43	-2.9521	0.00005
XLOC_035489	Gdpd5	chr7:99381344-99461816	1.19	6.59	-2.4709	0.00005
XLOC_032939	Mitf	chr6:97807051-98021349	4.12	16.93	-2.0399	0.00005
XLOC_001500	Gm7068	chr1:177808549-177962233	0.17	0.53	-1.6087	0.00005
XLOC_006533	Bahcc1	chr11:120232745-120292296	2.67	7.68	-1.5221	0.00005
XLOC_013754	Tuba1c	chr15:99029890-99038105	1.12	2.72	-1.2755	0.00005
XLOC_012591	Opn4	chr14:34590617-34600142	0.34	0.80	-1.2617	0.00005
XLOC_045344	Erdr1	chrY:90777786-90816464	3.98	9.00	-1.1769	0.00005
XLOC_008935	Gm6969	chr12:24638668-24639010	22.33	47.48	-1.0885	0.00005
XLOC_003579	Moxd1	chr10:24223469-24302790	0.92	1.83	-0.9931	0.00005
XLOC_037423	Hbb-bt	chr7:103812523-103813996	5.71	11.04	-0.9518	0.00005
XLOC_016143	Pi16	chr17:29318876-29329413	1.26	2.31	-0.8668	0.00005
XLOC_040328	Aldh1a2	chr9:71215788-71296243	1.50	2.72	-0.8514	0.00005
XLOC_033215	Apold1	chr6:134982000-134986836	1.57	2.78	-0.8224	0.00005
XLOC_033068	Slc6a13	chr6:121300226-121337733	1.95	3.38	-0.7965	0.00005
XLOC_002719	Btg2	chr1:134075169-134079120	2.01	3.46	-0.7869	0.00005

XLOC_024653	Adh1	chr3:138260990-138307022	2.97	5.04	-0.7628	0.00005
XLOC_009056	Clec14a	chr12:58264719-58269258	1.03	1.74	-0.7600	0.00005
XLOC_005382	Hba-a2	chr11:32296488-32297298	11.53	19.12	-0.7303	0.00005
XLOC_019409	Rbp4	chr19:38116619-38125321	5.01	8.18	-0.7059	0.00005
XLOC_035470	Ndufc2	chr7:97400002-97407802	113.15	184.34	-0.7041	0.00005
XLOC_006867	Pttg1	chr11:43420249-43426503	27.76	44.63	-0.6852	0.00005
XLOC_032575	Creb5	chr6:53573256-53700361	2.02	3.23	-0.6723	0.00005
XLOC_005380	Hba-a1	chr11:32283510-32284465	17.59	27.36	-0.6376	0.00005
XLOC_004626	Col6a2	chr10:76595761-76623630	4.33	6.66	-0.6226	0.00005
XLOC_031272	Kdr	chr5:75932826-75978458	3.07	4.73	-0.6201	0.00005
XLOC_036479	Zfp36	chr7:28376783-28379255	3.80	5.72	-0.5876	0.00005
XLOC_031826	Eln	chr5:134702599-134747382	8.04	11.73	-0.5451	0.00005
XLOC_036781	Kcnj11	chr7:46097165-46100226	7.73	11.10	-0.5227	0.00005
XLOC_009037	Nfkbia	chr12:55489410-55492647	18.83	27.00	-0.5205	0.00005
XLOC_037814	Ifitm3	chr7:141009585-141010770	25.27	35.90	-0.5067	0.00005
XLOC_040114	Bcl9l	chr9:44482413-44556391	4.82	6.81	-0.4989	0.00005
XLOC_038336	D8Ertd82e	chr8:36094656-36147787	7.49	10.37	-0.4695	0.00005
XLOC_003244	C130074G19Rik	chr1:184871925-184883218	5.59	7.73	-0.4670	0.00005
XLOC_037334	Serpinh1	chr7:99345374-99353230	13.38	18.48	-0.4655	0.00005
XLOC_006413	Sox9	chr11:112782223-112787760	5.90	8.00	-0.4409	0.00005
XLOC_004529	Ddit4	chr10:59949674-59951770	32.70	43.89	-0.4246	0.00005
XLOC_014231	Tob2	chr15:81848269-81858326	8.06	10.65	-0.4011	0.00005
XLOC_001516	Sccpdh	chr1:179668209-179687193	123.63	91.34	0.4368	0.00005
XLOC_033631	Nt5c3	chr6:56882399-56923932	32.19	23.15	0.4755	0.00005
XLOC_033821	Mat2a	chr6:72414307-72439558	62.45	44.76	0.4804	0.00005

XLOC_035382	Sh3gl3	chr7:82173839-82311244	49.94	33.85	0.5610	0.00005
XLOC_032906	Klf15	chr6:90462553-90479686	15.97	10.64	0.5863	0.00005
XLOC_035043	Rhpn2	chr7:35334169-35396817	8.24	5.47	0.5903	0.00005
XLOC_005699	Ubb	chr11:62551170-62553213	200.72	129.47	0.6325	0.00005
XLOC_034082	Adipor2	chr6:119353147-119417704	58.16	37.03	0.6512	0.00005
XLOC_021164	Id1	chr2:152736250-152737410	16.95	10.77	0.6539	0.00005
XLOC_020939	Mertk	chr2:128698386-128802942	7.37	4.67	0.6565	0.00005
XLOC_031752	Ubc	chr5:125385964-125390554	45.19	26.45	0.7727	0.00005
XLOC_039268	Arrdc2	chr8:70835131-70839802	12.83	7.38	0.7984	0.00005
XLOC_021268	Fam83d	chr2:158768092-158786637	7.74	4.26	0.8605	0.00005
XLOC_036279	Hif3a	chr7:17031365-17062427	2.38	1.29	0.8810	0.00005
XLOC_016930	Fkbp5	chr17:28399029-28517524	19.89	10.43	0.9320	0.00005
XLOC_013395	Cthrc1	chr15:39076931-39087121	8.76	4.50	0.9628	0.00005
XLOC_015416	Nrros	chr16:32142784-32165594	4.48	2.20	1.0224	0.00005
XLOC_035644	Olfml1	chr7:107567445-107591094	29.83	13.49	1.1455	0.00005
XLOC_035509	Coa4	chr7:100537099-100540395	7.69	3.07	1.3218	0.00005
XLOC_037269	Folh1	chr7:86719351-86775864	20.48	7.97	1.3624	0.00005
XLOC_039831	Maml2	chr9:13619984-13710174	7.83	2.75	1.5085	0.00005
XLOC_041198	Zbtb16	chr9:48651846-48836356	8.25	2.79	1.5628	0.00005
XLOC_017771	Gm3550	chr18:34732973-34751573	0.72	0.21	1.7759	0.00005
XLOC_044663	Kdm5d	chrY:897625-956786	1.17	0.01	7.1425	0.00005
XLOC_035984	Mrgprf	chr7:145300827-145309557	0.21	0.49	-1.2352	0.0001
XLOC_022598	Bmf	chr2:118528756-118549687	2.08	3.48	-0.7431	0.0001
XLOC_012051	Mmp14	chr14:54431368-54442305	7.98	11.36	-0.5091	0.0001
XLOC_017776	Egr1	chr18:34859822-34864984	6.04	8.49	-0.4915	0.0001

XLOC_013830	Hoxc12	chr15:102936756-102940930	0.09	0.30	-1.6926	0.00015
XLOC_024358	Fam212b	chr3:105704598-105720902	1.75	2.72	-0.6413	0.00015
XLOC_041284	Loxl1	chr9:58287722-58313212	1.76	2.64	-0.5873	0.00015
XLOC_001082	Fmod	chr1:134037253-134048277	9.14	12.59	-0.4620	0.00015
XLOC_017947	Pdgfrb	chr18:61045116-61085061	4.84	6.50	-0.4269	0.00015
XLOC_014349	Slc38a2	chr15:96687393-96699698	66.70	51.16	0.3825	0.00015
XLOC_028648	Mfsd2a	chr4:122946847-122963475	57.97	43.58	0.4115	0.00015
XLOC_003786	Rtkn2	chr10:67979569-68059969	6.26	4.31	0.5379	0.00015
XLOC_005683	Aldh3a1	chr11:61207536-61218421	0.20	0.61	-1.6110	0.0002
XLOC_015568	Col8a1	chr16:57624257-57754737	0.72	1.12	-0.6433	0.0002
XLOC_039288	Fcho1	chr8:71707035-71725718	11.94	16.73	-0.4870	0.0002
XLOC_017651	Rpl27-ps3	chr18:6332589-6333064	3.45	1.60	1.1088	0.0002
XLOC_031054	Fgfbp1	chr5:43978857-43981779	0.29	0.67	-1.1993	0.00025
XLOC_037339	Slco2b1	chr7:99657803-99711340	4.00	5.93	-0.5685	0.00025
XLOC_006125	Col1a1	chr11:94936223-94953042	12.929	16.96	-0.3912	0.00035
XLOC_006293	Arl4d	chr11:101665540-101667832	14.557	19.7	-0.4363	0.00035
XLOC_013079	Rgcc	chr14:79288755-79301645	16.837	12.02	0.4860	0.00035
XLOC_020108	Eng	chr2:32646543-32704145	8.957	12.35	-0.4631	0.00035
XLOC_037106	Klf13	chr7:63886346-63938915	26.536	20.38	0.3807	0.00035
XLOC_008215	Osr1	chr12:9574441-9581499	0.052	0.256	-2.3005	0.0004
XLOC_012414	Gm3411	chr14:6259746-6287250	0.1624	0.381	-1.2323	0.0004
XLOC_023271	Sox18	chr2:181669835-181671640	6.8919	4.765	0.5324	0.0004
XLOC_024240	Txnip	chr3:96555764-96566801	13.621	18.43	-0.4359	0.0004
XLOC_025663	Bcl9	chr3:97203661-97298003	4.4014	6.454	-0.5522	0.0004
XLOC_017418	Srd5a2	chr17:74016574-74047916	2.1477	1.342	0.6787	0.00055

XLOC_013649	Pnpla3	chr15:84167815-84189512	0.8235	0.515	0.6774	0.0006
XLOC_009242	Dio2	chr12:90724553-90750693	5.1719	3.888	0.4116	0.00065
XLOC_028911	Crocc	chr4:141016636-141060731	1.2545	2.2	-0.8107	0.00065
XLOC_031916	Micall2	chr5:139706692-139736336	1.3109	1.908	-0.5416	0.00075
XLOC_038526	Klf2	chr8:72319032-72321656	6.4018	8.78	-0.4558	0.00075
XLOC_007549	Sgca	chr11:94962790-94976327	0.3733	1.035	-1.4714	0.0008
XLOC_022166	Serping1	chr2:84765367-84775444	11.629	15.78	-0.4401	0.0008
XLOC_025713	Cd101	chr3:100993528-101029556	0.2139	0.098	1.1207	0.00085
XLOC_033133	Vwf	chr6:125546773-125686679	5.1602	7.096	-0.4597	0.00085
XLOC_033158	Clec2h	chr6:128662384-128677374	0.2409	0.045	2.4077	0.00085
XLOC_040098	Pvrl1	chr9:43744575-43807454	6.0375	7.858	-0.3802	0.0009
XLOC_037449	Trim12a	chr7:104244456-104353526	0.0065	1.052	-7.3496	0.00095
XLOC_037863	Th	chr7:142892751-142931128	0.4066	0.745	-0.8742	0.00095
XLOC_011580	1700112E06Rik	chr14:22019711-23094571	1.007	2.069	-1.0390	0.00105
XLOC_005958	Vtn	chr11:78499090-78502324	34.736	44.13	-0.3454	0.00115
XLOC_009900	Sfrp4	chr13:19623174-19632821	0.6398	1.077	-0.7518	0.00115
XLOC_041336	Plekho2	chr9:65554385-65580040	9.3723	12.12	-0.3715	0.00115
XLOC_019448	Pyroxd2	chr19:42725804-42752775	0.1855	0.372	-1.0037	0.00125
XLOC_013796	Nr4a1	chr15:101254211-101274792	2.0734	2.894	-0.4811	0.00135
XLOC_012900	Gjb2	chr14:57098599-57104702	3.7324	5.05	-0.4361	0.0015
XLOC_017315	Lrg1	chr17:56119679-56121946	1.7382	2.713	-0.6420	0.0016
XLOC_013555	Apol6	chr15:77015488-77057107	0.3432	0.693	-1.0135	0.0018
XLOC_014026	Fbxo32	chr15:58175878-58324169	5.8918	7.494	-0.3471	0.0018
XLOC_044383	Tsc22d3	chrX:140539527-140600659	134.9	106.9	0.3354	0.0019
XLOC_019506	Obfc1	chr19:47501032-47537507	5.6154	3.959	0.5041	0.00205

XLOC_042089	Slc38a5	chrX:8271132-8280179	3.7933	5.676	-0.5815	0.00205
XLOC_010503	Depdc1b	chr13:108316331-108408664	1.2144	1.793	-0.5625	0.0022
XLOC_018602	Cd248	chr19:5068077-5070637	1.2401	1.806	-0.5426	0.0022
XLOC_037356	P2ry2	chr7:100994438-101012084	0.3393	0.584	-0.7846	0.0024
XLOC_018325	Zfp608	chr18:54888044-55079414	2.4862	3.255	-0.3888	0.00245
XLOC_038401	Vegfc	chr8:54077531-54186454	0.8241	1.319	-0.6781	0.00245
XLOC_037605	Pik3c2a	chr7:116336160-116444316	7.5306	5.999	0.3281	0.0025
XLOC_004292	Cnksr3	chr10:7119062-7212237	8.2557	6.44	0.3584	0.0026
XLOC_013572	Cdc42ep1	chr15:78842646-78855529	30.22	37.73	-0.3201	0.0026
XLOC_018344	Smim3	chr18:60474192-60501983	7.4219	5.553	0.4184	0.0026
XLOC_033863	Mthfd2	chr6:83305690-83317606	16.209	12.7	0.3519	0.00255
XLOC_039222	Tma16	chr8:65617899-66486551	10.785	6.58	0.7130	0.0026
XLOC_025951	Usp53	chr3:122929713-122984514	17.147	12.07	0.5063	0.00265
XLOC_032869	Gp9	chr6:87778135-87779762	0.1935	0.591	-1.6113	0.00265
XLOC_004583	Zfp365	chr10:67886102-67912662	41.594	32.93	0.3368	0.0027
XLOC_013999	Gm10020	chr15:52477613-52478228	0.1289	2.107	-4.0306	0.0027
XLOC_003846	Tspear	chr10:77829466-77887021	0.1597	0.459	-1.5220	0.0028
XLOC_035278	Ndn	chr7:62348276-62349928	142.95	115.6	0.3069	0.0029
XLOC_004405	Cenpw	chr10:30196010-30200540	0.5727	0.27	1.0872	0.003
XLOC_011009	Ctla2b	chr13:60895350-60897447	0.9509	0.497	0.9374	0.0031
XLOC_011675	Mmrn2	chr14:34375503-34404287	1.6593	2.249	-0.4388	0.00305
XLOC_013566	Ncf4	chr15:78244772-78262580	0.3764	0.754	-1.0032	0.0031
XLOC_015748	Prdm15	chr16:97791355-97852087	2.1073	1.263	0.7386	0.00295
XLOC_016695	Tagap1	chr17:6954964-6961156	3.254	2.359	0.4637	0.0031
XLOC_017936	Iigp1	chr18:60376028-60392627	0.3385	0.563	-0.7335	0.0031

XLOC_018380	Atp8b1	chr18:64528978-64661061	0.3491	0.53	-0.6022	0.00305
XLOC_021477	Phactr3	chr2:178118974-178338492	56.16	41.88	0.4231	0.003
XLOC_030993	Mxd4	chr5:34173855-34187720	26.703	20.67	0.3695	0.0031
XLOC_015369	Sst	chr16:23889580-23890844	68.359	86.2	-0.3346	0.00315
XLOC_011537	Il3ra	chr14:14346326-14355491	0.6171	1.038	-0.7495	0.00325
XLOC_005839	Xaf1	chr11:72301593-72313733	10.453	15.15	-0.5358	0.0033
XLOC_017979	Grp	chr18:65872819-65886579	2.0962	1.241	0.7565	0.00335
XLOC_027118	Trabd2b	chr4:114406235-114615098	0.1487	0.243	-0.7096	0.00335
XLOC_035468	Kctd21	chr7:97332326-97350213	9.2592	11.71	-0.3385	0.00345
XLOC_002661	Cxcr4	chr1:128588198-128592334	1.3359	2.108	-0.6581	0.0036
XLOC_023558	Tnfsf10	chr3:27317027-27342427	0.4709	0.829	-0.8156	0.0036
XLOC_041281	Islr	chr9:58156264-58159221	6.4809	8.478	-0.3876	0.0037
XLOC_025821	Gstm2	chr3:107981701-107986453	1.3928	2.172	-0.6413	0.00375
XLOC_000771	Mlph	chr1:90915084-90951142	0.6864	0.451	0.6066	0.0038
XLOC_012173	Chrna2	chr14:66140959-66152948	2.4327	1.788	0.4442	0.0038
XLOC_013812	Igfbp6	chr15:102144361-102149511	3.9066	5.489	-0.4905	0.00385
XLOC_030230	Dao	chr5:114003702-114025682	14.391	18.28	-0.3454	0.00385
XLOC_027510	Mfap2	chr4:141010417-141015984	1.7881	2.961	-0.7275	0.00395
XLOC_036319	Apoc1	chr7:19689483-19692658	6.5657	9.878	-0.5893	0.00395
XLOC_036774	Kcnj14	chr7:45816460-45824756	19.469	15.62	0.3176	0.0039
XLOC_000054	Sgk3	chr1:9798106-9900845	7.8919	5.967	0.4034	0.0041
XLOC_035482	Lrrc32	chr7:98489918-98501831	0.7114	1.038	-0.5445	0.00415
XLOC_033480	Slc13a4	chr6:35267956-35308131	0.6493	1.012	-0.6402	0.00425
XLOC_022677	Fbn1	chr2:125300593-125507993	0.7978	1.061	-0.4114	0.0043
XLOC_017374	Rab31	chr17:65651725-65772752	60.976	50.01	0.2860	0.0044

XLOC_022858	Cd93	chr2:148436639-148443563	2.1006	2.712	-0.3686	0.00445
XLOC_040374	Fam214a	chr9:74952883-75032468	9.7943	7.819	0.3250	0.00445
XLOC_030242	Fam222a	chr5:114568015-114613220	5.4029	6.897	-0.3523	0.00465
XLOC_007559	Ngfr	chr11:95568817-95587735	0.5413	0.817	-0.5941	0.00475
XLOC_016643	Cript	chr17:87025549-87035810	41.126	32.8	0.3262	0.00475
XLOC_001440	Tagln2	chr1:172500046-172507381	16.388	20.82	-0.3455	0.00485
XLOC_030434	Fzd10	chr5:128600843-128604093	1.1094	1.57	-0.5008	0.0049
XLOC_037226	Arnt2	chr7:84246277-84410441	37.024	45.07	-0.2836	0.00495
XLOC_029021	Ptchd2	chr4:148236768-148287965	4.0897	5.488	-0.4242	0.005
XLOC_002717	Prelp	chr1:133897198-133921414	10.571	13.56	-0.3597	0.0052
XLOC_042752	Efnb1	chrX:99136129-99149023	1.554	2.199	-0.5010	0.00525
XLOC_019323	Mamdc2	chr19:23302608-23448322	0.7479	1.092	-0.5455	0.00545
XLOC_005435	C1qtnf2	chr11:43474275-43491525	0.7389	1.206	-0.7064	0.0056
XLOC_024001	Crabp2	chr3:87948665-87953376	0.3282	0.63	-0.9417	0.0058
XLOC_004430	Amd2	chr10:35708690-35711891	0.6824	0.44	0.6348	0.0061
XLOC_012490	Kcnk5	chr14:20140057-20181782	0.8421	1.194	-0.5042	0.006
XLOC_016221	H2-Ab1	chr17:34263208-34269418	1.5691	2.348	-0.5813	0.00615
XLOC_033069	Slc6a12	chr6:121342585-121365950	0.1197	0.269	-1.1697	0.0061
XLOC_039299	Calr3	chr8:72424175-72443870	4.1001	5.561	-0.4398	0.00605
XLOC_040105	Ccdc153	chr9:44240676-44247306	2.4952	3.598	-0.5282	0.0061
XLOC_040497	Ctsh	chr9:90054151-90076089	11.013	14.04	-0.3503	0.00615
XLOC_030141	Pde6b	chr5:108388390-108432397	0.5718	0.357	0.6812	0.0062
XLOC_018938	Ankrd2	chr19:42036037-42045110	0.1302	0.319	-1.2937	0.0063
XLOC_031862	Sh2b2	chr5:136218146-136246595	3.0584	2.199	0.4758	0.0063
XLOC_002800	Cfh	chr1:140084707-140183764	7.022	8.762	-0.3194	0.00645

XLOC_016274	H2-Q6	chr17:35424849-35430055	0.332	0.56	-0.7533	0.00655
XLOC_038676	Mt2	chr8:94172276-94173640	610.81	502.3	0.2821	0.0066
XLOC_044588	Tmsb4x	chrX:167207092-167209315	763.13	628.8	0.2793	0.0066
XLOC_044590	Tlr7	chrX:167304688-167330558	1.401	0.699	1.0024	0.0066
XLOC_009305	Serpina1b	chr12:103728155-103830373	0.3407	0.611	-0.8433	0.0068
XLOC_002567	Cdh19	chr1:110888325-110977758	7.244	5.672	0.3529	0.0069
XLOC_018455	Nfatc1	chr18:80606204-80713089	1.771	2.304	-0.3795	0.0069
XLOC_040650	Poc1a	chr9:106280945-106351762	2.7335	4.219	-0.6262	0.007
XLOC_013835	Hoxc11	chr15:102954426-102957788	3.5383	4.746	-0.4236	0.00705
XLOC_037367	Folr1	chr7:101858330-101870788	0.381	0.739	-0.9567	0.00715
XLOC_013342	Myo10	chr15:25622524-25813674	6.4295	8.382	-0.3825	0.0072
XLOC_002686	Ikbke	chr1:131254342-131279606	0.1783	0.349	-0.9678	0.0074
XLOC_016968	Sik1	chr17:31844247-31855792	2.5101	3.207	-0.3533	0.00735
XLOC_040761	Ltf	chr9:111019270-111042767	0.2936	0.091	1.6973	0.0074
XLOC_003476	Myct1	chr10:5593727-5606787	0.2341	0.398	-0.7655	0.00755
XLOC_039281	Plvap	chr8:71487788-71511769	4.9815	7.345	-0.5602	0.00755
XLOC_027398	Map3k6	chr4:133240817-133252929	1.6147	0.954	0.7585	0.00765
XLOC_020025	Gbgt1	chr2:28496890-28505415	0.2353	0.518	-1.1390	0.00775
XLOC_003623	Lama4	chr10:38965259-39112055	1.4488	1.884	-0.3791	0.0078
XLOC_007436	Ccl3	chr11:83647843-83649355	0.1967	0.503	-1.3552	0.0079
XLOC_019313	Anxa1	chr19:20373427-20390944	0.5548	0.96	-0.7912	0.00785
XLOC_041208	Rpl10-ps3	chr9:50344239-50344981	2.9964	1.926	0.6379	0.0079
XLOC_032918	Slc6a6	chr6:91684066-91759063	18.841	22.76	-0.2726	0.008
XLOC_004627	Col6a1	chr10:76708689-76726168	2.7711	3.549	-0.3570	0.00835
XLOC_024670	Gbp5	chr3:142493977-142522344	0.7949	1.189	-0.5804	0.00835

XLOC_042562	Bgn	chrX:73483601-73495933	29.784	39.14	-0.3942	0.0083
XLOC_003898	Efna2	chr10:80179481-80190010	4.0348	5.222	-0.3722	0.0084
XLOC_032802	Eva1a	chr6:82041042-82093099	12.359	9.811	0.3331	0.00855
XLOC_033061	Cecr2	chr6:120666368-120771190	0.8225	1.412	-0.7799	0.0088
XLOC_021763	Fam163b	chr2:27110379-27142491	13.164	16.07	-0.2878	0.0089
XLOC_025104	Slc7a11	chr3:49892525-50443614	1.4723	2.252	-0.6135	0.00885
XLOC_016058	Tekt4	chr17:25471589-25476594	2.0113	1.389	0.5346	0.009
XLOC_037228	Fah	chr7:84585158-84606722	33.916	27.83	0.2855	0.00905
XLOC_036772	Sult2b1	chr7:45729982-45759612	1.5752	2.554	-0.6974	0.0091
XLOC_002711	Snrpe	chr1:133603870-133610291	37.921	29.58	0.3582	0.0092
XLOC_037595	Calca	chr7:114631479-114636357	66.595	54.66	0.2849	0.0093
XLOC_023493	Car3	chr3:14863511-14872523	2.5416	3.533	-0.4754	0.0095
XLOC_014386	Tuba1b	chr15:98931424-98934565	172.25	136	0.3411	0.00955
XLOC_035275	Atp10a	chr7:58658117-58830765	3.4281	2.723	0.3323	0.0096
XLOC_043602	Rpl39	chrX:37082519-37085402	78.565	63.95	0.2970	0.01
XLOC_018827	Tmem252	chr19:24673922-24862243	1.9904	3.072	-0.6259	0.01005
XLOC_003757	Tacr2	chr10:62252437-62265990	0.151	0.269	-0.8355	0.0101
XLOC_004656	Pdxk	chr10:78436743-78464985	37.674	31.55	0.2562	0.01025
XLOC_004973	Nxph4	chr10:127525472-127534559	30.211	36.63	-0.2781	0.0107
XLOC_005348	Efemp1	chr11:28853203-28926743	2.324	3.14	-0.4343	0.0107
XLOC_006790	Rps27a	chr11:29545844-29578367	179.97	149.5	0.2678	0.01065
XLOC_011025	Zfp935	chr13:62453166-62466830	1.6557	1.119	0.5658	0.0104
XLOC_012972	Scara3	chr14:65919394-65953744	1.3575	1.801	-0.4081	0.01055
XLOC_014193	Sox10	chr15:79151937-79256674	55.452	67.66	-0.2870	0.01035
XLOC_027459	Wnt4	chr4:137277488-137299726	1.0808	1.443	-0.4170	0.01045

XLOC_031242	Nfxl1	chr5:72513300-72559691	1.7118	1.235	0.4706	0.01055
XLOC_036783	Ush1c	chr7:46195349-46238503	0.274	0.109	1.3290	0.01055
XLOC_042173	Kdm6a	chrX:18162574-18279936	4.1738	5.159	-0.3059	0.0106
XLOC_004221	Stat2	chr10:128270575-128292849	3.8185	4.764	-0.3192	0.01115
XLOC_004417	Nkain2	chr10:31689309-32891456	41.346	30.13	0.4564	0.0113
XLOC_015383	Uts2b	chr16:27353321-27370239	12.542	9.565	0.3909	0.0113
XLOC_003110	Slamf8	chr1:172581757-172590568	0.1469	0.281	-0.9347	0.01135
XLOC_000678	Sp100	chr1:85600377-85709998	1.5998	2.382	-0.5740	0.0115
XLOC_007224	Alox12	chr11:70241456-70255353	0.191	0.314	-0.7169	0.01155
XLOC_010109	Ppp1r3g	chr13:35958838-35970388	2.5058	1.864	0.4269	0.01155
XLOC_043222	Usp51	chrX:153006452-153011451	0.1397	0.262	-0.9065	0.01145
XLOC_002443	Iqca	chr1:90042131-90153401	0.3109	0.507	-0.7053	0.01165
XLOC_017416	Xdh	chr17:73883907-73950182	1.1127	0.829	0.4244	0.01165
XLOC_004908	Lyz2	chr10:117277333-117282274	8.0137	10.23	-0.3521	0.0119
XLOC_037890	Ano1	chr7:144588548-144751974	1.1389	1.788	-0.6504	0.0119
XLOC_035826	Itgad	chr7:128154375-128223816	2.3565	1.135	1.0538	0.0119
XLOC_022938	Nol4l	chr2:153407387-153530266	5.3727	6.907	-0.3624	0.012
XLOC_041306	Paqr5	chr9:61953480-62026856	2.8163	1.838	0.6160	0.0121
XLOC_033033	Cxcl12	chr6:117168534-117181367	12.242	15.64	-0.3537	0.0122
XLOC_018262	Pcdh1	chr18:38185603-38229145	11.439	14.29	-0.3213	0.01235
XLOC_010112	Ly86	chr13:37345344-37419036	9.8847	12.62	-0.3521	0.0125
XLOC_011026	Zfp934	chr13:62517499-62520544	0.5215	0.299	0.8029	0.0125
XLOC_024411	Taf13	chr3:108571697-108583222	31.749	25.01	0.3441	0.0125
XLOC_012726	Gmfb	chr14:46808148-46822242	39.715	32.94	0.2700	0.01255
XLOC_011189	Crhbp	chr13:95431370-95444831	4.1961	3.186	0.3973	0.0126

XLOC_001696	Sox17	chr1:4490930-4499558	3.379	2.221	0.6057	0.0127
XLOC_001962	Sema4c	chr1:36548638-36683183	4.4254	5.883	-0.4107	0.01325
XLOC_034741	Ceacam20	chr7:19965411-19991113	0.2777	0.158	0.8147	0.01325
XLOC_040164	Gm7293	chr9:51621424-51624874	0.2617	0.149	0.8095	0.0132
XLOC_021873	Stom	chr2:35313985-35336976	4.6994	5.889	-0.3255	0.0133
XLOC_023244	Hrh3	chr2:180099464-180104488	6.9194	8.559	-0.3067	0.01355
XLOC_033107	C1rl	chr6:124493112-124510643	0.1852	0.303	-0.7114	0.0139
XLOC_035171	Shank1	chr7:44310252-44358644	19.978	24.46	-0.2918	0.0141
XLOC_016128	Brpf3	chr17:28800914-28838546	2.8453	4.185	-0.5568	0.0143
XLOC_014285	Celsr1	chr15:85897906-86034122	0.3355	0.446	-0.4093	0.0144
XLOC_020130	Hspa5	chr2:34771969-34800187	127.25	103.7	0.2951	0.0145
XLOC_015917	Zfp97	chr17:17121414-17146831	0.2948	0.175	0.7560	0.01465
XLOC_027203	Lao1	chr4:118961577-118968912	0.2487	0.132	0.9093	0.01485
XLOC_010626	Sugct	chr13:16857854-17694732	1.2866	0.817	0.6545	0.0151
XLOC_033336	Slc25a13	chr6:6041217-6217173	4.3111	3.43	0.3300	0.0151
XLOC_018960	Pax2	chr19:44756044-44837871	5.5422	6.847	-0.3050	0.0152
XLOC_024674	Gbp2	chr3:142620601-142638008	1.7623	2.397	-0.4438	0.01525
XLOC_023569	Rpl22l1	chr3:28805435-28813985	37.466	29.52	0.3440	0.01555
XLOC_005799	Asgr1	chr11:70054084-70057894	0.21	0.397	-0.9200	0.0157
XLOC_036531	Kmt2b	chr7:30568787-30589343	5.9773	8.813	-0.5602	0.0158
XLOC_004050	Lum	chr10:97565500-97572703	2.0155	2.687	-0.4149	0.0159
XLOC_019203	Best1	chr19:9985173-10001633	0.2599	0.487	-0.9065	0.0161
XLOC_033989	Frmd4b	chr6:97286866-97617541	9.8257	12.12	-0.3025	0.01675
XLOC_008358	Coch	chr12:51593340-51605773	0.3574	0.555	-0.6342	0.01685
XLOC_002270	Igfbp5	chr1:72857931-72875085	16.476	19.55	-0.2470	0.01695

XLOC_006326	Rprml	chr11:103649569-103650579	4.4738	3.272	0.4512	0.01695
XLOC_013884	Rxfp3	chr15:11033716-11037991	0.1422	0.226	-0.6664	0.017
XLOC_017872	Kcnn2	chr18:45268859-45896509	12.783	9.623	0.4097	0.01725
XLOC_035161	Klk1b22	chr7:44112672-44116922	0.3086	0.079	1.9716	0.0173
XLOC_027745	Mxra8	chr4:155839491-155844088	3.8953	6.275	-0.6880	0.01735
XLOC_027207	Slc2a1	chr4:119108710-119138801	107.34	90.73	0.2425	0.01745
XLOC_017944	Camk2a	chr18:60925597-60988152	6.773	8.263	-0.2868	0.01755
XLOC_038472	Tm6sf2	chr8:70072923-70080120	0.1678	0.365	-1.1204	0.0176
XLOC_027295	Csf3r	chr4:126024549-126044440	0.8871	1.287	-0.5363	0.01765
XLOC_003280	Prox1	chr1:190118022-190217276	5.9603	7.872	-0.4014	0.01775
XLOC_006998	Lyrm7	chr11:54826865-54860916	4.0059	5.966	-0.5747	0.018
XLOC_031036	Hs3st1	chr5:39613934-39755475	16.88	20.45	-0.2771	0.01835
XLOC_007962	Lgals3bp	chr11:118392749-118403903	13.608	17.63	-0.3736	0.0186
XLOC_009296	Ifi27l2a	chr12:103442166-103443680	1.0778	1.874	-0.7983	0.01875
XLOC_015655	Adamts1	chr16:85793826-85803113	5.291	6.653	-0.3304	0.01875
XLOC_029439	Lrrc17	chr5:21483846-21645634	1.4839	2.05	-0.4664	0.01875
XLOC_032220	Tac1	chr6:7554878-7565834	3.9288	5.416	-0.4632	0.0186
XLOC_005315	Xpo1	chr11:23255606-23298262	10.817	8.827	0.2932	0.01885
XLOC_007181	Gucy2e	chr11:69218116-69237036	0.427	0.579	-0.4401	0.01895
XLOC_038313	Gsr	chr8:33652522-33698163	19.904	15.7	0.3424	0.0193
XLOC_037191	Man2a2	chr7:80343011-80371375	31.745	26.57	0.2566	0.0194
XLOC_040555	Rbp1	chr9:98422960-98446575	2.6912	3.414	-0.3432	0.0195
XLOC_000655	Daw1	chr1:83159751-83210574	0.1439	0.272	-0.9202	0.0196
XLOC_017942	Cd74	chr18:60803838-60812646	4.4157	5.727	-0.3752	0.01985
XLOC_032976	Lmcd1	chr6:112273757-112330425	1.5562	2.101	-0.4328	0.0198

XLOC_036262	Gltscr1	chr7:15970690-16048066	2.6088	3.189	-0.2898	0.01985
XLOC_034289	Gucy2c	chr6:136697284-136781765	0.1419	0.225	-0.6635	0.02015
XLOC_027542	Lrrc38	chr4:143349756-143371032	0.6684	0.451	0.5681	0.0202
XLOC_013935	Rpl30	chr15:34440504-34443640	200.41	166.9	0.2642	0.02035
XLOC_036550	Fxyd1	chr7:31051680-31055664	117.35	139.5	-0.2497	0.02035
XLOC_030486	Stx1a	chr5:135023481-135051220	2.4067	3.118	-0.3734	0.0204
XLOC_019354	Insl6	chr19:29321343-29325356	0.8009	0.451	0.8287	0.0206
XLOC_041411	Unc13c	chr9:73479421-73968966	9.0711	10.82	-0.2550	0.0206
XLOC_004049	Dcn	chr10:97479499-97518162	22.631	27.14	-0.2620	0.02125
XLOC_023947	Ctso	chr3:81932600-81956725	16.963	14.26	0.2507	0.0216
XLOC_018894	Btaf1	chr19:36926078-37014130	4.3033	3.546	0.2792	0.02175
XLOC_042276	Slc25a5	chrX:36795650-36798900	224.84	191.3	0.2331	0.0217
XLOC_037424	Hbb-bs	chr7:103826530-103828096	69.837	84.73	-0.2788	0.02195
XLOC_022396	Creb3l1	chr2:91982327-92024502	1.1702	1.546	-0.4019	0.02205
XLOC_035265	Tubgcp5	chr7:55793951-55831447	11.025	9.181	0.2641	0.0222
XLOC_040985	Rgl3	chr9:21971424-21989453	1.1903	1.579	-0.4073	0.0221
XLOC_035445	Sytl2	chr7:90302224-90410439	13.141	15.64	-0.2514	0.0226
XLOC_008230	Rpl36-ps3	chr12:12911985-12912369	1.4171	0.69	1.0375	0.0231
XLOC_012166	Zfp395	chr14:65358675-65398930	2.5832	3.183	-0.3011	0.02285
XLOC_012802	Sall2	chr14:52311171-52328762	22.152	25.99	-0.2307	0.02305
XLOC_015665	Grik1	chr16:87895893-88290426	3.3495	4.158	-0.3120	0.023
XLOC_018966	Lzts2	chr19:45015175-45046614	24.53	20.58	0.2530	0.02285
XLOC_019317	Gda	chr19:21391306-21473445	0.4337	0.622	-0.5196	0.02295
XLOC_001121	Kif21b	chr1:136131384-136177998	6.7134	8.068	-0.2651	0.02325
XLOC_037450	Trim12c	chr7:104244456-104353526	1.0719	0.54	0.9889	0.02325

XLOC_010314	Rsl1	chr13:67173130-67183474	1.0972	0.75	0.5480	0.02355
XLOC_015529	Gm4737	chr16:46152996-46155077	2.6966	2.062	0.3868	0.0235
XLOC_027933	Slc35a1	chr4:34663256-34687438	6.7891	5.266	0.3665	0.02345
XLOC_006394	Axin2	chr11:108920348-108950783	2.0861	2.666	-0.3540	0.024
XLOC_009143	Plek2	chr12:78888690-78906964	0.2288	0.124	0.8839	0.0239
XLOC_014898	Gpr156	chr16:37916456-38007527	0.2744	0.409	-0.5753	0.0237
XLOC_030686	Mtus2	chr5:147957319-148316065	8.3245	10.95	-0.3953	0.0239
XLOC_038844	Dynlrb2	chr8:116505014-116515896	3.335	4.801	-0.5256	0.02395
XLOC_038906	Fcer2a	chr8:3681736-3694174	0.1512	0.254	-0.7456	0.02395
XLOC_011192	F2r	chr13:95601803-95618459	5.0015	6.093	-0.2848	0.02425
XLOC_015193	AU021092	chr16:5211827-5222299	2.0964	2.786	-0.4101	0.02425
XLOC_004615	Mmp11	chr10:75923221-75932502	0.6405	0.925	-0.5301	0.0245
XLOC_012457	Gm3839	chr14:11280734-11356726	74.672	87.57	-0.2299	0.02465
XLOC_015250	Myh11	chr16:14194526-14291408	3.13	2.58	0.2785	0.02465
XLOC_001390	Olfml2b	chr1:170644531-170682789	2.7706	3.444	-0.3140	0.02475
XLOC_026146	Cyr61	chr3:145646975-145649981	2.1066	2.743	-0.3806	0.0248
XLOC_008666	Bdkrb2	chr12:105563104-105595223	1.591	2.006	-0.3345	0.0253
XLOC_015866	1700010I14Rik	chr17:8988332-9008319	0.246	0.144	0.7772	0.0252
XLOC_017786	Cxxc5	chr18:35828275-35861823	32.128	38.14	-0.2476	0.02525
XLOC_019407	Myof	chr19:37899035-38043739	0.7717	0.984	-0.3509	0.02505
XLOC_020290	Dapl1	chr2:59484652-59505020	0.2018	0.449	-1.1552	0.0253
XLOC_036526	Arhgap33	chr7:30522214-30535209	3.3728	4.097	-0.2805	0.02535
XLOC_040754	Prss50	chr9:110857966-110864629	0.1993	0.362	-0.8596	0.0254
XLOC_011125	Rfesd	chr13:76000372-76018712	4.7869	5.915	-0.3054	0.0259
XLOC_021266	Ppp1r16b	chr2:158665397-158766334	31.892	27.28	0.2251	0.02575

XLOC_029848	Spata18	chr5:73651379-73679484	0.2619	0.408	-0.6397	0.026
XLOC_035336	Agbl1	chr7:76318071-76766608	0.162	0.322	-0.9890	0.02575
XLOC_022450	Cd44	chr2:102811140-102901665	4.2318	5.262	-0.3145	0.0263
XLOC_010943	Msx2	chr13:53466883-53473074	0.3133	0.475	-0.6012	0.02685
XLOC_017307	Zfp119b	chr17:55938380-55949500	0.6561	0.438	0.5837	0.0268
XLOC_028585	Tie1	chr4:118471190-118490061	3.2723	3.986	-0.2846	0.0269
XLOC_029620	Cytl1	chr5:37735518-37739820	2.1205	1.488	0.5114	0.027
XLOC_030072	Ptpn13	chr5:103425163-103598303	3.6524	4.369	-0.2584	0.0267
XLOC_031026	Msx1	chr5:37820484-37824583	1.546	2.045	-0.4036	0.02695
XLOC_038408	Hpgd	chr8:56294551-56321046	8.2168	6.641	0.3072	0.0268
XLOC_018346	Synpo	chr18:60593872-60660142	3.8753	4.77	-0.2996	0.0272
XLOC_034808	Gm9844	chr7:24862212-24862697	4.2253	5.86	-0.4719	0.0272
XLOC_004692	Mex3d	chr10:80380354-80387661	4.3749	5.515	-0.3342	0.02745
XLOC_011004	Gas1	chr13:60174404-60177365	2.3157	2.923	-0.3359	0.02775
XLOC_017352	Pdzph1	chr17:58878807-58991375	0.7625	0.398	0.9397	0.02785
XLOC_021618	St8sia6	chr2:13651020-13794064	0.6801	1.076	-0.6613	0.0276
XLOC_030248	Oasl2	chr5:114896935-114912239	1.4769	1.927	-0.3838	0.02795
XLOC_033867	Actg2	chr6:83512904-83536265	0.0786	0.191	-1.2842	0.02795
XLOC_037157	St8sia2	chr7:73939118-74013690	0.7366	0.95	-0.3672	0.0273
XLOC_039421	Sall1	chr8:89027236-89071418	8.7845	10.44	-0.2489	0.0279
XLOC_040860	Clec3b	chr9:123150945-123157430	14.542	11.78	0.3040	0.0277
XLOC_002460	Per2	chr1:91415259-91459324	2.1007	1.557	0.4322	0.0284
XLOC_014811	Hes1	chr16:30063104-30067796	5.2422	3.73	0.4911	0.02835
XLOC_037859	Igf2	chr7:142650765-142670356	24.077	30.42	-0.3373	0.0284
XLOC_040776	Susd5	chr9:114057353-114098733	2.9795	2.416	0.3027	0.0284

XLOC_042508	Fmr1	chrX:68678484-68717963	12.212	9.154	0.4158	0.02835
XLOC_011175	Cmya5	chr13:93040712-93144724	0.2839	0.213	0.4110	0.029
XLOC_026049	Tet2	chr3:133463678-133585053	1.2593	1.732	-0.4597	0.02885
XLOC_035788	Gdpd3	chr7:126765998-126776818	0.2817	0.162	0.7987	0.0289
XLOC_036614	Kctd15	chr7:34637025-34660416	10.167	12.25	-0.2689	0.0288
XLOC_043893	Irak1	chrX:74013913-74023936	13.302	17.33	-0.3820	0.029
XLOC_013018	Sorbs3	chr14:70180423-70217659	20.706	24.47	-0.2411	0.02925
XLOC_010651	Zkscan3	chr13:21387007-21402801	4.651	3.745	0.3126	0.02965
XLOC_002045	Slc40a1	chr1:45908067-45926523	3.6031	4.743	-0.3964	0.03005
XLOC_008376	Srp54b	chr12:55155103-55189213	6.1378	5.064	0.2774	0.0301
XLOC_017883	Eno1b	chr18:48045334-48048378	11.588	9.281	0.3203	0.0299
XLOC_019383	Ch25h	chr19:34473785-34481546	0.0631	0.589	-3.2205	0.03045
XLOC_026617	Glipr2	chr4:43957400-43979118	3.2809	4.114	-0.3265	0.0303
XLOC_028804	Arid1a	chr4:133679003-133757929	13.761	16.46	-0.2588	0.02975
XLOC_033838	Gm9008	chr6:76496356-76497631	0.9939	0.61	0.7036	0.03035
XLOC_035643	Syt9	chr7:107370348-107548761	3.7946	4.693	-0.3065	0.0304
XLOC_040241	Gramd2	chr9:59680143-59718874	0.4998	0.783	-0.6483	0.0298
XLOC_040742	Ngp	chr9:110419746-110423012	0.3502	0.195	0.8473	0.03025
XLOC_031883	Mospd3	chr5:137596644-137601058	14.733	17.88	-0.2789	0.03055
XLOC_014276	Phf21b	chr15:84785302-84856135	0.9234	1.293	-0.4852	0.0308
XLOC_007594	Gpr179	chr11:97332108-97352442	0.8867	1.337	-0.5926	0.03105
XLOC_013654	Prr5	chr15:84663206-84706535	8.0568	6.486	0.3129	0.0311
XLOC_013779	Mettl7a3	chr15:100334928-100340341	0.3471	0.538	-0.6314	0.0311
XLOC_015979	Zfp51	chr17:21450301-21465591	1.4834	1.129	0.3945	0.0311
XLOC_031441	Plac8	chr5:100553724-100572245	0.0864	0.229	-1.4042	0.03105

XLOC_034209	Clec7a	chr6:129461590-129472825	0.3444	0.55	-0.6740	0.0313
XLOC_013367	Pop1	chr15:34495303-34531057	1.5246	1.031	0.5646	0.03155
XLOC_009666	Itgb8	chr12:119158021-119238802	22.487	19.29	0.2212	0.03165
XLOC_001397	Fcgr4	chr1:171018919-171029761	0.1613	0.293	-0.8629	0.0321
XLOC_002393	Sp110	chr1:85575675-85598817	0.2818	0.45	-0.6758	0.0321
XLOC_022983	2900097C17Rik	chr2:156391830-156392979	47.012	55.2	-0.2316	0.0321
XLOC_016097	Syngap1	chr17:26940257-26972434	4.2632	5.084	-0.2539	0.0323
XLOC_022393	Mdk	chr2:91929804-91932297	45.721	54.14	-0.2438	0.03225
XLOC_016240	Ehmt2	chr17:34850390-34914052	21.297	16.92	0.3323	0.03245
XLOC_023200	Gm4631	chr2:175318351-175338197	9.1411	7.747	0.2388	0.03265
XLOC_018964	Sema4g	chr19:44989096-45003397	4.689	5.596	-0.2551	0.0328
XLOC_035755	Chp2	chr7:122219495-122222824	0.7162	1.058	-0.5625	0.0328
XLOC_008375	Fam177a	chr12:55124527-55142078	10.592	8.961	0.2412	0.0344
XLOC_010119	Bmp6	chr13:38345715-38499728	2.8058	3.495	-0.3170	0.03445
XLOC_010940	Nfil3	chr13:52967208-52981073	3.76	4.65	-0.3064	0.03435
XLOC_013286	Dab2	chr15:6299787-6440712	4.5653	5.935	-0.3785	0.03385
XLOC_013982	Eif3e	chr15:43250039-43282736	35.011	29.84	0.2307	0.03375
XLOC_016975	Brd4	chr17:32195114-32298689	14.99	17.75	-0.2437	0.03435
XLOC_020019	Col5a1	chr2:27882924-28039514	0.7824	1.005	-0.3605	0.0335
XLOC_026966	Tek	chr4:94739128-94874976	4.6483	5.579	-0.2632	0.03345
XLOC_027256	Heyl	chr4:123233555-123249875	4.5976	5.676	-0.3041	0.03395
XLOC_028071	Tbc1d2	chr4:46604389-46650209	0.3611	0.499	-0.4661	0.03325
XLOC_030170	Pole	chr5:110286305-110337633	0.4581	0.273	0.7458	0.0331
XLOC_030203	Crybb1	chr5:112255814-112269585	2.7829	2.02	0.4624	0.03385
XLOC_033495	Klrg2	chr6:38618851-38637735	1.6778	1.29	0.3790	0.0333

XLOC_034142	Ptpn6	chr6:124720706-124738714	1.5183	2.183	-0.5236	0.0333
XLOC_034190	BC048546	chr6:128539821-128581606	1.5763	1.945	-0.3030	0.0341
XLOC_035645	Ppfibp2	chr7:107595050-107758076	5.3114	6.375	-0.2634	0.0339
XLOC_036742	Rcn3	chr7:45082912-45092312	6.3369	7.984	-0.3333	0.034
XLOC_037284	Ccdc81	chr7:89866147-89903629	0.2928	0.43	-0.5552	0.03315
XLOC_037378	Trim21	chr7:102557921-102565469	1.1573	0.868	0.4143	0.0335
XLOC_038722	Cdh5	chr8:104101624-104144502	5.5978	6.654	-0.2494	0.0333
XLOC_017386	Arhgap28	chr17:67842708-68004120	0.1205	0.25	-1.0550	0.0347
XLOC_043787	Cdr1	chrX:61183245-61185558	7.627	6.317	0.2719	0.03465
XLOC_016090	Atp6v0e	chr17:26676395-26699644	40.765	34.18	0.2542	0.03485
XLOC_035860	Edrf1	chr7:133637542-133672971	5.5365	4.287	0.3689	0.03495

Chapter 7
Neuronal Wnt activity underlies GDE2-mediated OL maturation

7.1 Introduction

Genetic ablation of GDE2 results in a reduction of canonical Wnt activity in the postnatal brain (chapter 6). The reduction of Wnt activity in neurons and OPCs is coincident with OL maturation deficits in *Gde2-/-* animals. This raises the possibility that GDE2 regulates OL maturation through activation of canonical Wnt signaling. If this is true, then activation of Wnt signaling should rescue the impaired OL maturation observed in *Gde2-/-* animals. To test this hypothesis, we utilized a mouse line that carries the *Ctnnb1flex3* allele to genetically stabilize β-catenin *in vivo*. *Ctnnb1flex3* mice harbor lox-P sites flanking exon 3 of β-catenin, which contains phosphorylation sites for GSK3β that target β-catenin for degradation[107]. Cre-dependent excision of exon 3 prevents GSK3β phosphorylation of β-catenin, thus stabilizing β-catenin and increasing canonical Wnt signaling. To distinguish the cellular sites of Wnt activation relevant to GDE2-dependent regulation of OL maturation, we activated Wnt signaling in neurons or OPCs. To stabilize β-catenin in neurons, we generated *Gde2-/-* mice that carry the *Ctnnb1flex3* allele and the *Nex-Cre* transgene, which expresses Cre recombinase in excitatory neurons[92]. Similarly, stabilization of β-catenin in OPCs was achieved by generating *Ctnnb1flex3; Gde2-/-* animals that carry *PDGFαR-CreER,* which expresses Cre recombinase in OPCs when 4-HT is administered. OL maturation in WT, *Gde2-/-* and *Gde2-/-* animals with stabilized β catenin was assessed by IHC and FISH of OL maturation markers. Findings from these *in vivo* studies were further investigated in *in vitro* culture settings. Outcomes from these studies suggest that neuronal Wnt activity mediates GDE2-dependent regulation of OL maturation by potentiating the release of soluble factors from neurons.

7.2 Results

7.2.1 Increasing neuronal Wnt activity in *Gde2-/-* neurons rescues OL maturation

Reduced canonical Wnt activity was observed in *Gde2-/-* neurons at the time of impaired OL maturation in *Gde2-/-* animals (Fig 6.5.C). To test the hypothesis that reduced Wnt activity in neurons mediates OL maturation deficits in *Gde2-/-* animals, we utilized a genetic approach to genetically activate canonical Wnt signaling in *Gde2-/-* neurons in vivo. We generated *Gde2-/-* animals that contain a single copy of the *Ctnnb1flex3* allele and that express Cre recombinase under the control of regulatory sequences from the promoter of the NEX transcription factor (*Nex-Cre)*. Western blots from cortical extracts of P14 mice carrying *Nex-Cre* alleles (lane 3 and 4) display a band of the expected size for a modified β-catenin protein deleted for exon 3 (black arrowhead), in addition to WT β-catenin (white arrowhead). This observation confirms effective Cre-dependent generation of mutant β-catenin protein lacking exon 3 in *Gde2-/-; Ctnnb1flex3/+*; *Nex-Cre* animals but not in *WT; Ctnnb1flex3/+* and *Gde2-/-; Ctnnb1flex3/+* controls (Fig 7.1).

IHC analysis of cortical sections revealed that there were equivalent numbers of Olig2+ cells among the 3 genotypes, suggesting that β-catenin stabilization in neurons had minimal effect on the number of OL lineage cells in CC and CTX (Fig 7.2.B). However, analysis of mature OLs, marked by CC1 and Olig2 coexpression, showed a substantial increase of CC1+ Olig2+ OLs in *Gde2-/-; Ctnnb1flex3/+*; *Nex-Cre* cortices compared to *Gde2-/-; Ctnnb1flex3/+* controls, restoring the number of mature CC1+ OLs to WT levels (Fig 7.2.C) in CC. However, the number of CC1+ Olig2+ OLs in *Gde2-/-; Ctnnb1flex3/+*; *Nex-Cre* animals was partially rescued in CTX (Fig 7.2.C). *Gde2-/-; Ctnnb1flex3/+*; *Nex-*

Cre cortices also showed recovery of *Mbp*+ Olig2+ OLs compared with *Gde2-/-; Ctnnb1flex3/*+ cortices (Fig 7.3.A and Fig 7.3.B). These observations suggest that GDE2 mediates OL maturation through stimulation of canonical Wnt signaling in neurons.

7.2.2 Increasing Wnt activity in *Gde2-/-* OPCs worsens OL maturation deficits

Gde2-/- animals display reduced Wnt signaling in OPCs (Fig 6.5.E), raising the possibility that GDE2-dependent activation of Wnt signaling in OPCs may also contribute to OL maturation. To determine if this is the case, we generated *Gde2-/-; Ctnnb1flex3/*+; *PDGFαR-CreER* animals, where administration of 4-HT induces the expression of Cre recombinase under the control of *PDGFα* receptor regulatory sequences to target Cre expression in OPCs[93]. We administered 4-HT to *Gde2-/-; Ctnnb1flex3/*+; *PDGFαR-CreER* mice and to *WT; Ctnnb1flex3/*+ and *Gde2-/-; Ctnnb1flex3/*+ controls at P7 and examined OL maturation at P11. Of note, administration of 4-HT to pups carrying both *Ctnnb1flex3/*+ and *PDGFαR-CreER* alleles before P6 caused lethality. β-catenin stabilization in OPCs in *Gde2-/-; Ctnnb1flex3/*+; *PDGFαR-CreER* mice resulted in a significant reduction in the number of Olig2+ oligodendroglia in CC compared with controls, whereas Olig2+ cells in CTX were equivalent between genotypes (Fig 7.4.A and Fig 7.4.B). In addition, OL maturation was further retarded in both CC and CTX in *Gde2-/-; Ctnnb1flex3/*+; *PDGFαR-CreER* cortex (Fig S7C-S7E). Because OL maturation phenotypes are not rescued in *Gde2-/-; Ctnnb1flex3/*+ *PDGFαR-CreER* animals, we conclude that GDE2 regulation of Wnt signaling in OPCs does not promote OL maturation. Nevertheless, this observation suggests that tight regulation of Wnt signaling in OPCs is critical for appropriate OL development.

7.2.3 Wnt activation in neurons stimulates the release of promaturation factors

Our studies described above suggest that GDE2 normally functions to promote Wnt signaling in neurons, and that this process leads to the release of soluble factors that promote OL maturation. Accordingly, CM prepared from *Gde2-/-* neurons with stabilized β-catenin should rescue the delay in OL maturation observed in our *in vitro* assays. We thus collected CM from DIV3 *Gde2-/-; Ctnnb1flex3/+* and *Gde2-/-; Ctnnb1flex3/+*; *Nex-Cre* neurons (Fig 7.6.A) and applied these CM to WT OPCs for 3 days. Cell lysates were then subjected to biochemical analysis and cells were fixed to examine OL maturation by morphology, MBP expression and phalloidin labeling (Fig 7.6.A). Strikingly, a robust 70% increase in MBP protein was observed in lysates from OPCs cultured with CM from β-catenin stabilized *Gde2-/-* neurons (*Gde2-/-; Ctnnb1flex3/+*; *Nex-Cre*) by Western blot (Fig 7.6.B). Similarly, I observed an increase in mature OLs with CM from neurons with stabilized β-catenin (Fig 7.7.A). OPCs cultured in CM from *Gde2-/-* neurons with stabilized β-catenin (*Gde2-/-; Ctnnb1flex3/+*; *Nex-Cre*) showed an approximately 60% increase in the number of MBP+ OLs compared with CM from *Gde2-/-* neurons (*Gde2-/-; Ctnnb1flex3/+*) (Fig 7.7.B). In addition, we observed a 60% increase in the number of Stage 1, Stage 2 and Stage 3 MBP+ OLs in CM from *Gde2-/-; Ctnnb1flex3/+*; *Nex-Cre* neurons compared with CM from *Gde2-/-; Ctnnb1flex3/+* condition (Fig 7.7.B). Thus, stabilizing β-catenin in *Gde2-/-* neurons stimulates the release of factors that enhance OL maturation. This observation is consistent with the model that GDE2 maintains canonical Wnt signaling in neurons, and that this pathway potentiates the release of neuronally-derived factors to promote OL maturation. CM from β-catenin stabilized *Gde2-/-* neurons

was more potent in enhancing OL maturation because the number of Stage 1 OLs was increased with CM from β-catenin stabilized *Gde2-/-* neurons but not with CM from WT neurons. This can be attributed to the robust and continuous release of OL maturation factors when β-catenin is constitutively stabilized in neurons.

7.3 Summary

To determine if reduced canonical Wnt activity underlies the delay in OL maturation in *Gde2-/-* animals, we genetically stabilized β-catenin in *Gde2-/-* neurons or OPCs *in vivo*. This approach determined that activating canonical Wnt signaling in *Gde2-/-* neurons restored *Gde2-/-* OL maturation deficits, thus indicating that GDE2-dependent activation of Wnt signaling is important for regulating OL maturation. This observation was confirmed by our in vitro experiments using neuronal CM, which further supports our observations that GDE2-dependent regulation of Wnt activation in neurons promotes the release of soluble factors that promote OL maturation. Interestingly, increasing Wnt activity in *Gde2-/-* OPCs resulted in a profound inhibition of OL maturation, suggesting that this pathway does not mediate GDE2-dependent function in OL maturation. Collectively, these observations support the model that GDE2 promotes OL maturation by stimulating canonical Wnt activity in neurons in the postnatal cortex.

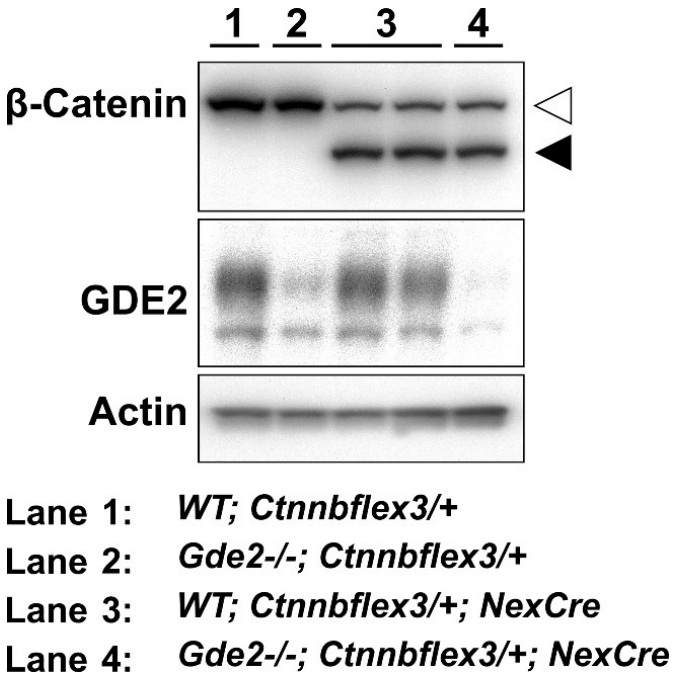

Figure 7.1. Genetic stabilization of β-catenin in neurons

Western blot of P14 cortical extracts from 4 mouse groups. Stabilized β-catenin is detected in mice carrying *Nex-Cre*. White arrowhead indicates wild type β-catenin. Black arrowhead marks the stabilized mutant β-catenin deleted for exon 3. Actin is used as a loading control.

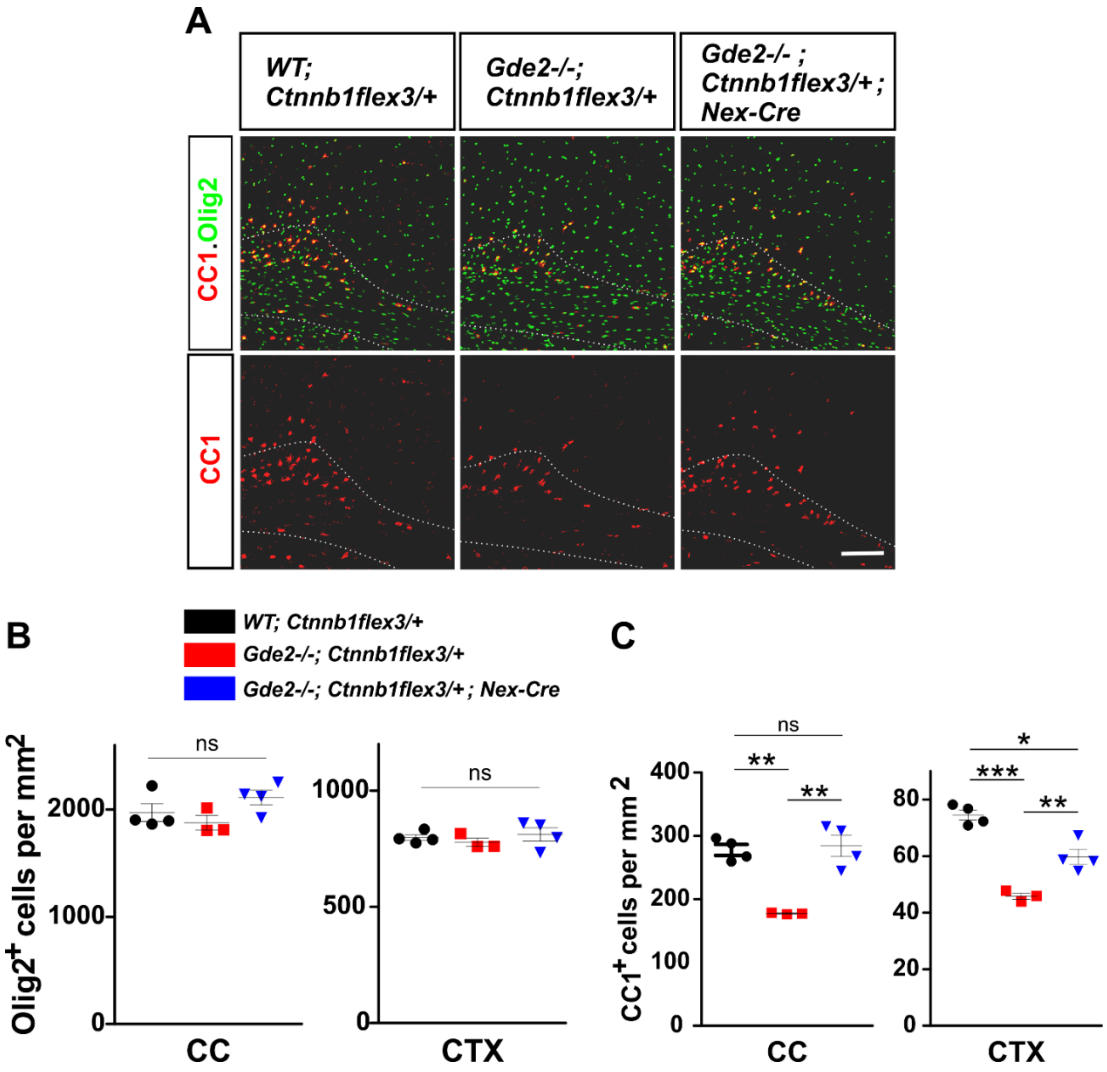
A
WT; Ctnnb1flex3/+
Gde2-/-; Ctnnb1flex3/+
Gde2-/- ; Ctnnb1flex3/+ ; Nex-Cre
CC1.Olig2
CC1
B
WT; Ctnnb1flex3/+
Gde2-/-; Ctnnb1flex3/+
Gde2-/-; Ctnnb1flex3/+ ; Nex-Cre
Olig2+ cells per mm2
ns
ns
2000
1000
0
1000
500
0
CC
CTX
C
CC1+ cells per mm 2
ns
**
**
*
***
**
400
300
200
100
0
80
60
40
20
0
CC
CTX

Figure 7.2. Stabilizing β-catenin in neurons rescues *Gde2-/-* CC1+ mature OLs

(A) Coronal section of P11 mouse motor cortex (CTX) and corpus callosum (CC). Hatched lines mark the CC. (B) Graph quantifying number of Olig2+ cells shows no change upon genetic stabilization of β-catenin in neurons in CC and CTX. ns CC p = 0.1608, ns CTX p = 0.6109. n = 4 *WT; Ctnnb1flex3/+*, 3 *Gde2-/-; Ctnnb1flex3/+*; 4 *Gde2-/-; Ctnnb1flex3/+; Nex-Cre.* Mean ± sem, 1-way ANOVA/Bonferroni's multiple comparison test. (C) Graph quantifying numbers of CC1+ OLs shows that stabilization of β-catenin in neurons of *Gde2-/-* animals increases the number of mature OLs in CC and CTX (*Gde2-/-; Ctnnb1flex3/+* vs *Gde2-/-; Ctnnb1flex3/+; Nex-Cre*; **p CC = 0.0078, **p CTX = 0.0098) and restores numbers to WT condition in CC (compare WT*; Ctnnb1flex3/+* vs *Gde2-/-; Ctnnb1flex3/+* **p = 0.0014 to WT*; Ctnnb1flex3/+* vs *Gde2-/-; Ctnnb1flex3/+; Nex-Cre;* ns = 0.7592) but partially rescues in CTX (compare WT*; Ctnnb1flex3/+* vs *Gde2-/-; Ctnnb1flex3/+* ***p = 0.0006 to WT*; Ctnnb1flex3/+* vs *Gde2-/-; Ctnnb1flex3/+; Nex-Cre;* *p = 0.0156). n = 4 WT*; Ctnnb1flex3/+*, 3 *Gde2-/-; Ctnnb1flex3/+*, 4 *Gde2-/-; Ctnnb1flex3/+; Nex-Cre*. Scale bar: 100 μm

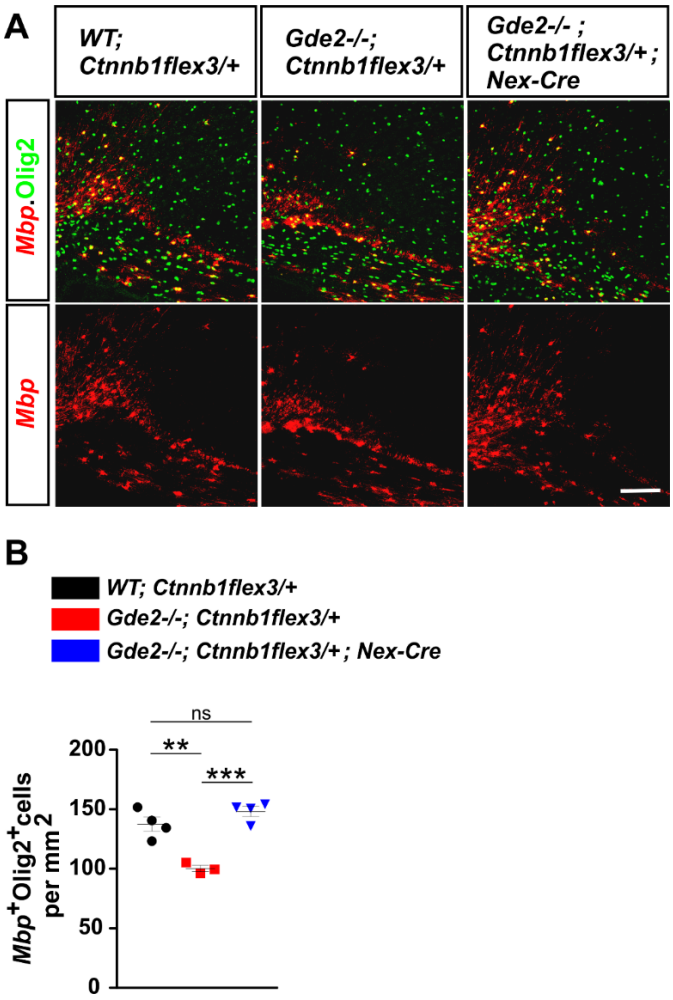

Figure 7.3. Stabilizing β-catenin in neurons rescues *Gde2-/- Mbp*+ OLs

(A) Coronal section of P11 mouse motor cortex (CTX) and corpus callosum (CC). FISH visualizing *Mbp* transcript is coupled with IHC to mark Olig2+ cells. (B) Graph quantifying Olig2+ cells expressing *Mbp* transcripts shows that stabilization of β-catenin in *Gde2-/-* neurons increases number of *Mbp* + OLs (*Gde2-/-; Ctnnb1flex3/+* vs *Gde2-/-; Ctnnb1flex3/+; Nex-Cre*; ***p = 0.0006) and restores numbers to WT condition (compare WT*; Ctnnb1flex3/+* vs *Gde2-/-; Ctnnb1flex3/+* **p = 0.0047 to WT*; Ctnnb1flex3/+* vs *Gde2-/-; Ctnnb1flex3/+; Nex-Cre;* ns = 0.204). Mean ± sem, two-tailed unpaired Students t-test. Scale bar: 100 μm

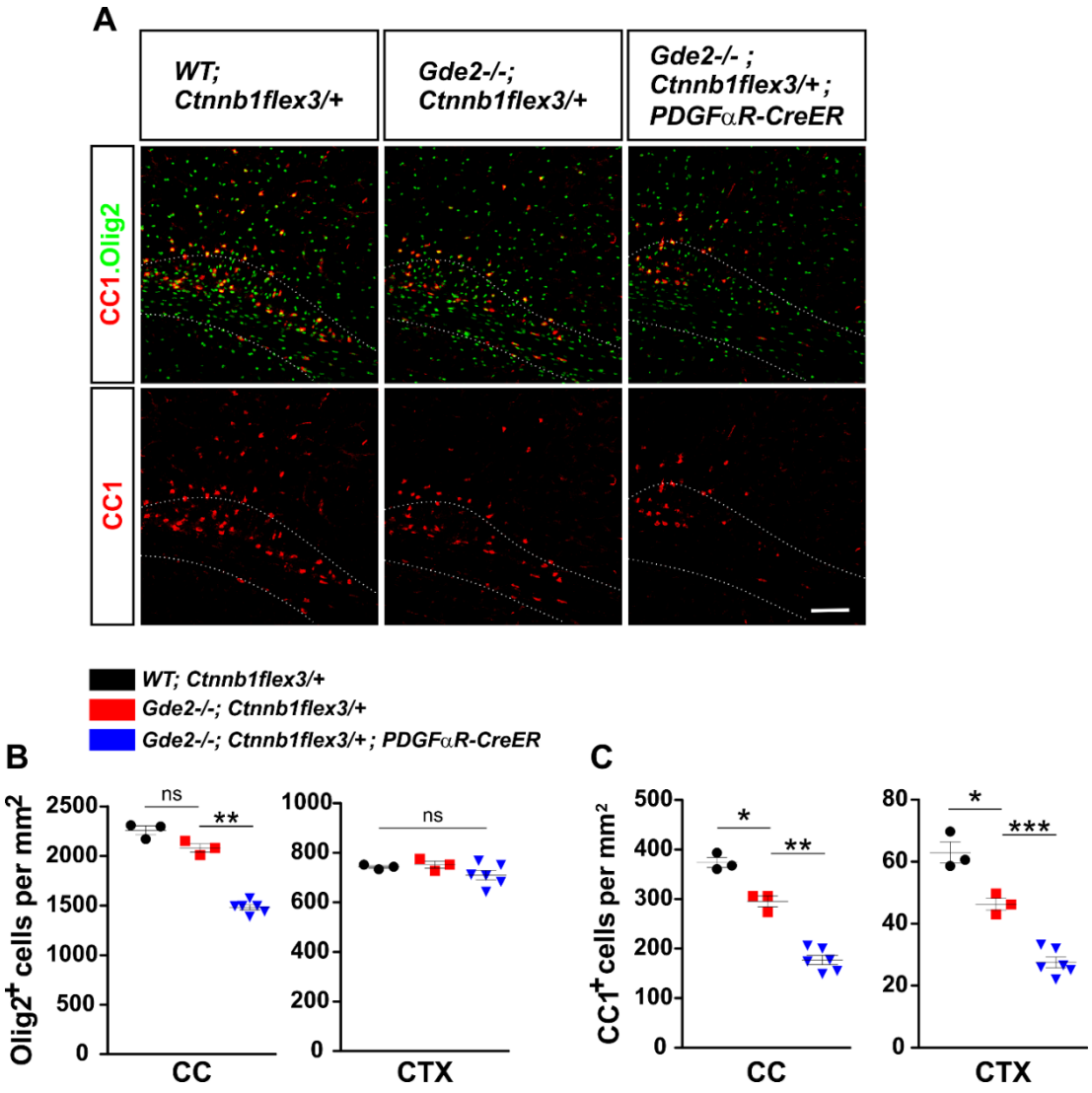
A
WT; Ctnnb1flex3/+
Gde2-/-; Ctnnb1flex3/+
Gde2-/- ; Ctnnb1flex3/+ ; PDGFαR-CreER
CC1.Olig2
CC1
WT; Ctnnb1flex3/+
Gde2-/-; Ctnnb1flex3/+
Gde2-/-; Ctnnb1flex3/+ ; PDGFαR-CreER
B
Olig2+ cells per mm2
ns
**
ns
2500
2000
1500
1000
500
0
1000
800
600
400
200
0
CC
CTX
C
CC1+ cells per mm2
*
**
*
***
500
400
300
200
100
0
80
60
40
20
0
CC
CTX

Figure 7.4. Stabilizing β-catenin in *Gde2-/-* OPCs farther reduced CC1+ OLs

(A) Coronal section of P11 mouse motor cortex (CTX) and corpus callosum (CC). Hatched lines mark the CC. (B) Graphs quantifying the number of Olig2+ cells in corpus callosum (CC) and cortex (CTX). No change in Olig2+ cell numbers are observed between *WT; Ctnnb1flex3/+* and *Gde2-/-; Ctnnb1flex3/+* in CC (p = 0.0601, two-tailed unpaired t- test). Stabilization of β-catenin in OPCs in *Gde2-/-; Ctnnb1flex3/+; PDGFαR-CreER* results in reduction of Olig2+ cells in CC (**p = 0.0011, two-tailed unpaired t- test, *Gde2-/-; Ctnnb1flex3/+* vs *Gde2-/-; Ctnnb1flex3/+; PDGFαR-CreER*) but not CTX (ns p = 0.1235, 1-way ANOVA Bonferroni's multiple comparison test, all 3 genotypes). n = 3 *WT; Ctnnb1flex3/+*, 3 *Gde2-/-; Ctnnb1flex3/+*, 6 *Gde2-/-; Ctnnb1flex3/+; PDGFαR-CreER*. (C) Graphs quantifying number of CC1+ OLs. (*WT; Ctnnb1flex3/+* vs *Gde2-/-; Ctnnb1flex3/+* *p CC = 0.0132 *p CTX = 0.0242; *Gde2-/-; Ctnnb1flex3/+* vs *Gde2-/-; Ctnnb1flex3/+; PDGFαR-CreER* **p CC = 0.0012 ***p CTX = 0.0008, n = 3 *Gde2-/-; Ctnnb1flex3/+*, 6 *Gde2-/-; Ctnnb1flex3/+; PDGFαR-CreER*). Two tailed unpaired Student's t-test. All graphs: Mean ± sem. Scale bars: 100 μm

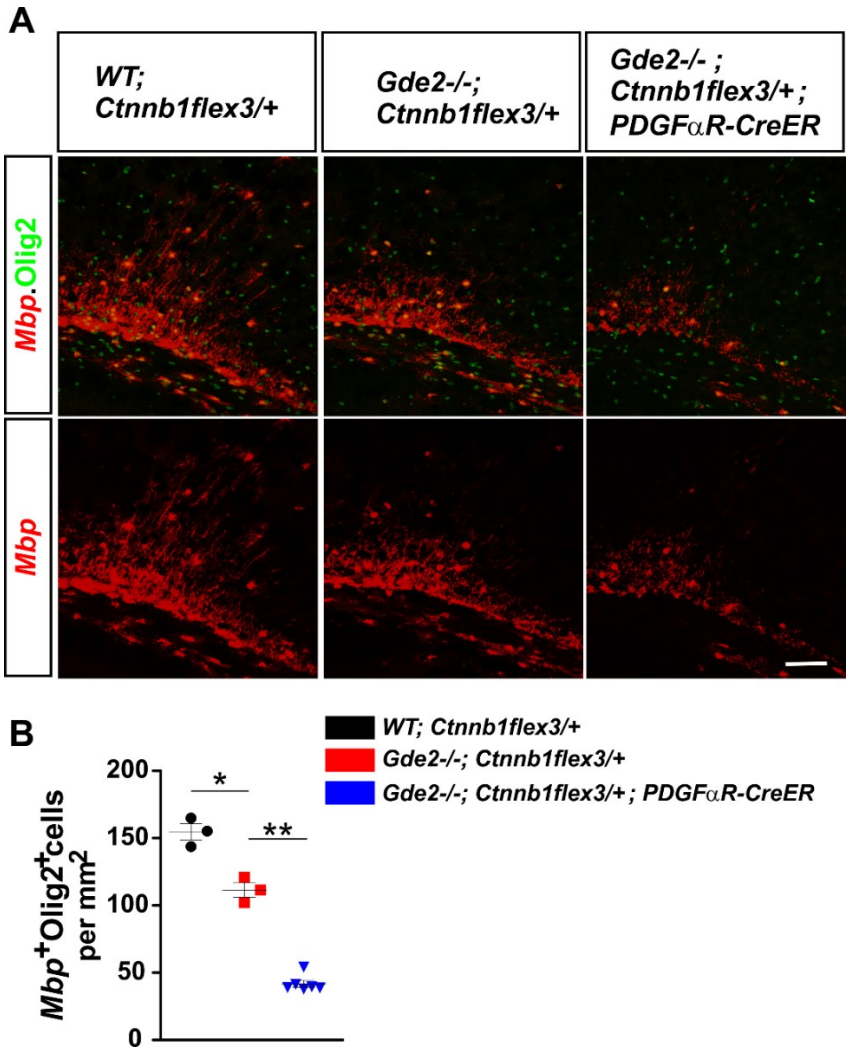

Figure 7.5. Stabilizing β-catenin in *Gde2-/-* OPCs farther reduced *Mbp*+ OLs

(A) Coronal section of P11 mouse motor cortex (CTX) and corpus callosum (CC). FISH visualizing *Mbp* transcript is coupled with IHC to mark Olig2+ cells. (B) Graph quantifying the number of MBP+Olig2+ cells, shows further reduction of mature OLs when β-catenin is stabilized in OPCs (*WT; Ctnnb1flex3/+* vs *Gde2-/-; Ctnnb1flex3/+* *p = 0.0132; *Gde2-/-; Ctnnb1flex3/+* vs *Gde2-/-; Ctnnb1flex3/+; PDGFαR-CreER* **p = 0.0073, n = 3 *Gde2-/-; Ctnnb1flex3/+*, 6 *Gde2-/-; Ctnnb1flex3/+; PDGFαR-CreER*) Two tailed unpaired Student's t-test. Mean ± sem. Scale bar: 100 μm

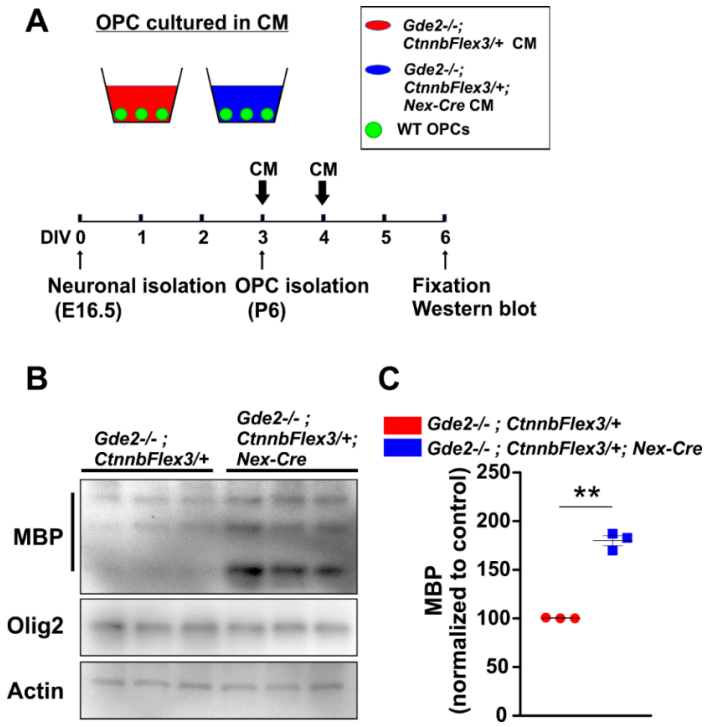

Figure 7.6. WT OPCs cultured with β-catenin stabilized *Gde2-/-* neuronal CM increases MBP expression

(A) Schematic illustrating OPCs cultured in CM from *Gde2-/-* neurons with or without β-catenin stabilization. CM prepared from DIV3 and DIV4 neurons were added to OPCs purified from P6 pups. OPCs were cultured in CM for 3 days before analysis. (B) Western blot of WT cell lysates shows increased MBP protein expression in OPCs cultured with CM from *Gde2-/-* neurons expressing stabilized β-catenin (*Gde2-/-; CtnnbFlex3/+; Nex-Cre*) compared with control (*Gde2-/-; CtnnFlex3/+*). (C) Graph quantifying intensity of MBP protein in Western blots of OPCs cultured with CM from *Gde2-/-; CtnnbFlex3/+; Nex-Cre* neurons compared with CM from *Gde2-/-; CtnnFlex3/+* controls (**p = 0.0043, n = 3 CM *Gde2-/-; CtnnFlex3/+*, 3 CM *Gde2-/-; CtnnbFlex3/+; Nex-Cre*). Actin is used as loading control. Mean ± sem, two-tailed unpaired Students t-test.

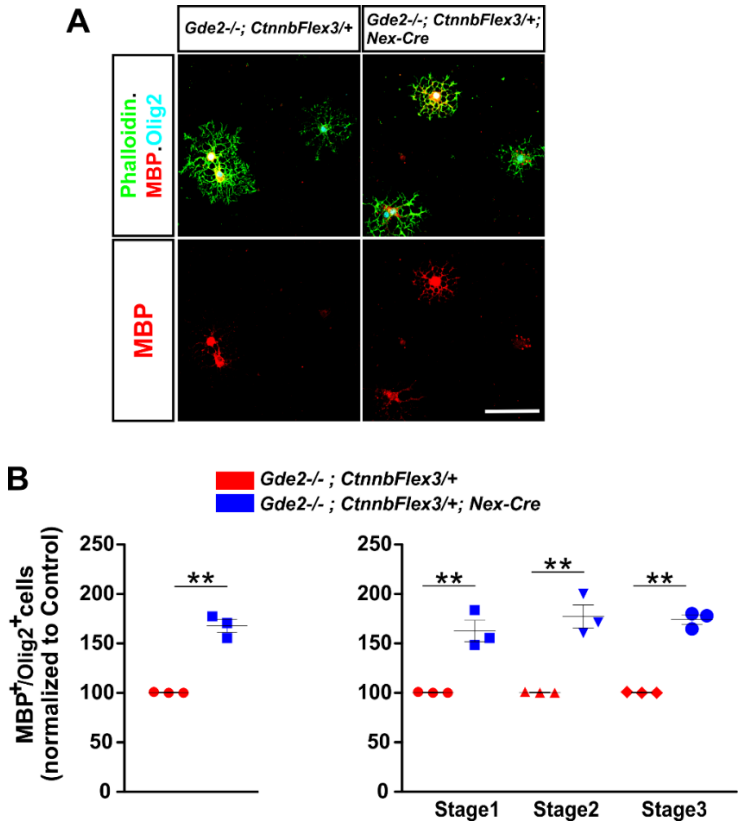

Figure 7.7. β-catenin stabilized *Gde2-/-* neuronal CM enhanced OL maturation

(A) Immunocytochemical detection of OPCs cultured in CM. (B) Graphs quantifying the percentage of MBP+Olig2+ cells show increase in OPCs cultured with CM from *Gde2-/-; CtnnbFlex3/+; Nex-Cre* neurons (**p = 0.009). These increases span all 3 stages of OL maturation: 2 way Anova ***p<0.0001 (Bonferroni correction Stage 1 **p<0.001, Stage 2 **p <0.001, Stage 3 **p<0.001) n = 3 CM *Gde2-/-; CtnnFlex3/+* (936 Olig2+cells, 108 MBP+ cells, Stage 1= 65 MBP+, Stage 2 = 26 MBP+, Stage 3 = 17 MBP+), 3 CM *Gde2-/-; CtnnbFlex3/+; Nex-Cre* (894 Olig2+cells, 171 MBP+ cells, Stage 1= 100 MBP+, Stage 2 = 43 MBP+, Stage 3 = 28 MBP+). Mean ± sem, two-tailed unpaired Students t-test. Scale bar: 20 μm

Chapter 8
GDE2–regulation of Wnt activity increases the release of OL promaturation factors

8.1 Introduction

Our genetic *in vivo* and *in vitro* studies so far suggest that GDE2 control of Wnt activity in neurons potentiates the release of soluble factors that promote OL maturation from neurons. To identify candidate factors whose release is dependent on GDE2 functions, CM from WT and from *Gde2-/-* neurons were subjected to proteomic profiling. One candidate protein, phosphacan, was further assessed for its ability to mediate GDE2- dependent OL maturation. Outcomes from these studies suggest that phosphacan is one of several factors released by GDE2/Wnt pathways in neurons that help promote OL maturation.

8.2 Results

8.2.1 Candidate factors released by GDE2-Wnt activity in neurons

To identify OL maturation factors released by GDE2 neuronal function, we collected CM from DIV3 WT and *Gde2-/-* neurons and profiled proteins that were differentially expressed between the two conditions using mass spectrometry (Fig 8.1.A). 149 proteins were identified that were expressed at 40% or higher levels in *Gde2-/-* neuronal CM compared to WT CM (Table 2). GDE2 promotes the release of GPI-anchored proteins from the plasma membrane. While several GPI-anchored proteins were identified in CM, none of them were differentially expressed in CM from WT and *Gde2-/-* neurons (Fig 8.1.B). This suggests that neuronal GPI-anchored substrates of GDE2 are unlikely candidates for the promaturation factors released by GDE2-mediated

pathways. This observation is consistent with our hypothesis that the release of neuronal factors that promote OL maturation are downstream of activated Wnt signaling.

Our proteomic analysis identified 11 secreted or extracellular matrix (ECM) associated proteins that were differentially expressed in WT and *Gde2-/-* neuronal CM, with 10 proteins showing decreased expression in *Gde2-/-* CM samples (Fig 8.1.C). Of these 10 proteins, soluble Receptor-type tyrosine-protein phosphatase zeta (RPTPzeta), the secreted splice variant of the full-length transmembrane RPTPzeta, also called phosphacan, can promote OL maturation through interaction with Contactin-1 in OPCs; however, the cellular source of phosphacan is not well defined[108]. Phosphacan is one of the most abundant proteoglycans in the postnatal brain[109] and is expressed in neurons, astrocytes and oligodendroglia[86,110]; accordingly, released phosphacan from neurons is a promising candidate for mediating GDE2-dependent regulation of OL maturation. Neuronally derived phosphacan can be distinguished from glial phosphacan using antibodies that recognize cell-type specific O-mannosyl glycans [110]. Using the neuronal phosphacan-specific antibodies, Western blot analysis of CM from WT and *Gde2-/-* neurons shows that levels of neuronal phosphacan are reduced in CM from *Gde2-/-* neurons compared to WT (Fig 8.2.A and Fig 8.2.B). In contrast, levels of the GPI-anchored protein TAG1 are equivalent between conditions (Fig 8.2.A and Fig 8.2.B). These observations confirm the proteomic analysis of phosphacan and Tag1 expression in *Gde2-/-* and WT neuronal CM (Fig 8.1.B and Fig 8.1.C), and they highlight neuronal phosphacan as one candidate for mediating GDE2-dependent OL maturation.

If neuronal phosphacan stimulates OL maturation, then OPCs cultured with phosphacan-depleted WT neuronal CM should display deficits in OL maturation. To test

this hypothesis, we depleted phosphacan from WT neuronal CM by incubation with antibodies to neuronal phosphacan-conjugated to protein L (Fig 8.3.A). Strikingly, OPCs grown in CM depleted of phosphacan showed profound deficits in OL maturation that largely recapitulate deficits elicited by *Gde2-/-* CM; specifically, the number of MBP+ cells was markedly decreased, with concomitant reductions in Stage 1, Stage 2 and Stage 3 MBP+ OLs (Fig 8.3.B). The degree of OL maturation was not changed in WT neuronal CM incubated with protein L alone, suggesting that the observed deficits are due to depletion of neuronal phosphacan (Fig 8.3.C).

In our model, GDE2 activation of Wnt signaling stimulates the release of soluble factors that promote OL maturation. If neuronal phosphacan mediates GDE2-dependent regulation of OL maturation, then levels of released phosphacan would be increased in CM from *Gde2-/-* neurons with enhanced Wnt activity. We thus performed Western blot analysis on CM prepared from *Gde2-/-; Ctnnb1flex3/+*; *Nex-Cre* and *Gde2-/-; Ctnnb1flex3/+* neuronal cultures. Levels of soluble neuronally-derived phosphacan were markedly increased in neuronal CM from *Gde2-/-; Ctnnb1flex3/+*; *Nex-Cre* cortical cultures compared with control *Gde2-/-; Ctnnb1flex3/+* CM (Fig 8.4.A and Fig 8.4.B). These observations are consistent with our working model that GDE2 stimulation of Wnt signaling in neurons releases soluble factors such as phosphacan, that promote OL maturation (Fig 8.5).

8.3 Summary

Proteomic analysis of *Gde2-/-* neuronal CM using mass spectrometry identified several candidate factors that mediate GDE2-dependent regulation of OL maturation.

Several candidates were reduced in *Gde2-/-* neuronal CM, one of which was neuronal phosphacan. Our studies revealed that neuronally-derived phosphacan is required to promote OL maturation and that phosphacan release is elevated by increasing Wnt activity in *Gde2-/-* neurons. Collectively, these studies suggest that GDE2 stimulates canonical Wnt activity in neurons, which releases potent promaturation factors, such as phosphacan, to promote timely OL maturation in the postnatal brain.

A

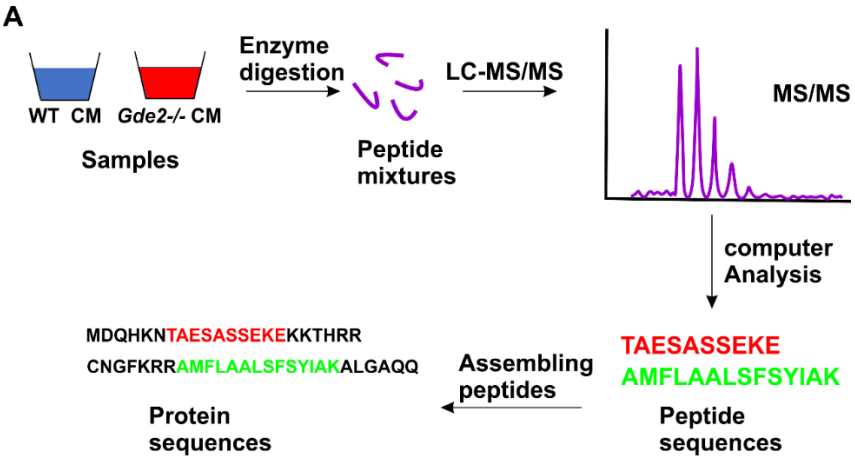

B

Protein name	Gene name	KO/WT ratio
Glypican-1;Secreted glypican-1	*Gpc1*	0.82
Glypican-2;Secreted glypican-2	*Gpc2*	0.91
Semaphorin-7A	*Sema7a*	0.94
Cadherin-13	*Cdh13*	0.95
Contactin-2 (a.k.a. TAG-1)	*Cntn2*	1.05
Neural cell adhesion molecule 1	*Ncam1*	1.11
RGM domain family member B	*Rgmb*	1.22
Lipoprotein lipase	*Lpl*	1.23
Repulsive guidance molecule A	*Rgma*	1.25
Contactin-1	*Cntn1*	1.25
Neural cell adhesion molecule 2	*Ncam2*	1.40

C

Protein name	*Gene name*	KO/WT ratio
Carboxypeptidase B2	*Cpb2*	0.33
Phosphatidylethanolamine-binding protein 1	*Pebp1*	0.43
Receptor-type tyrosine-protein phosphatase zeta	*Ptprz1*	0.44
Gamma-glutamyl hydrolase	*Ggh*	0.47
Follistatin-related protein 5	*Fstl5*	0.50
Glucose-6-phosphate isomerase	*Gpi*	0.51
ProSAAS	*Pcsk1n*	0.53
Noelin	*Olfm1*	0.53
Glia-derived nexin	*Serpine2*	0.54
Complement C5	*C5*	0.57
Collagen alpha-1(I) chain	*Col1a1*	3.98

Figure 8.1. Identification of candidates mediating GDE2-regulated OL maturation

(A) Schematic detailing proteomic analysis workflow of WT and *Gde2-/-* CM. (B) Table of GPI-anchored proteins identified in WT and *Gde2-/-* CM by mass spectrometry. (C) Table of secreted and extracellular matrix proteins identified in WT and *Gde2-/-* CM by mass spectrometry. RPTPzeta (phosphacan) is highlighted in red.

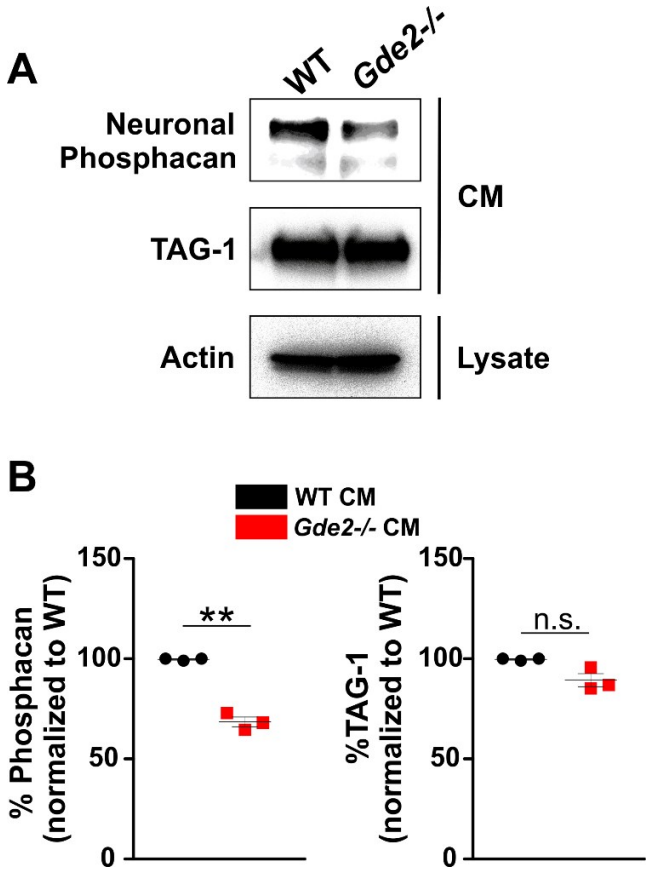

Figure 8.2. Phosphacan is reduced in *Gde2-/-* CM

(A) Western blot of WT and *Gde2-/-* neuronal CM. (B) Graphs quantifying Western blots show decrease in phosphacan levels in *Gde2-/-* neuronal CM (**p = 0.0062) but no change in TAG-1 (ns p = 0.0864). n = 3 WT CM, 3 *Gde2-/-* CM. +). Mean ± sem, two-tailed unpaired Students t-test.

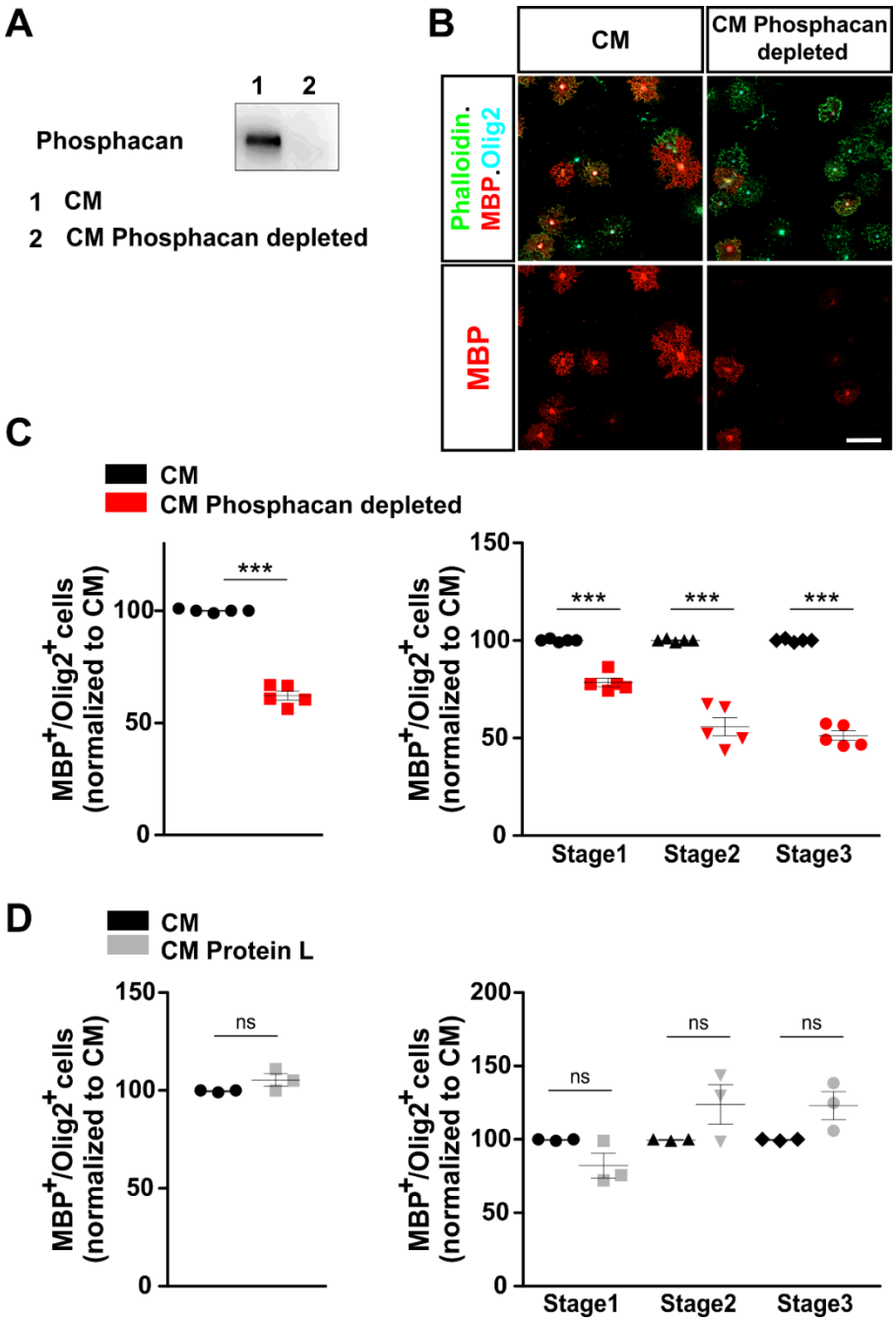
A
1 2
Phosphacan
1 CM
2 CM Phosphacan depleted
B
CM
CM Phosphacan depleted
Phalloidin.
MBP.Olig2
MBP
C
CM
CM Phosphacan depleted
MBP+/Olig2+cells (normalized to CM)
***
Stage1
Stage2
Stage3
D
CM
CM Protein L
ns

Figure 8.3. Phosphacan deletion causes deficits in OL maturation

(A) Western blot of phosphacan showing effective depletion of phosphacan using neuronal phosphacan antibodies conjugated to protein-L. Lane 1: WT CM, lane 2: WT CM with phosphacan depleted using CAT-315 pre-bound protein L beads. (B) Representative images of WT OPCs cultured with WT neuronal CM and WT neuronal CM depleted for phosphocan. (C) Left; Graph quantifying the percentage of MBP+Olig2+ OLs (normalized to WT CM) in WT OPC cultures grown with WT neuronal CM or phosphacan depleted WT neuronal CM. Phosphacan depleted WT neuronal CM results in delayed maturation of WT OPCs (***p<0.0001, n = 5 WT CM [2189 Olig2+ cells; 856 MBP+ cells], 5 Phosphacan depleted CM [2815 Olig2+ cells; 722 MBP+ cells], two tailed unpaired t-test). Right; All 3 stages of OL maturation are also affected (2-way ANOVA ***p < 0.0001; Bonferroni correction Stage 1 ***p <0.001; Stage 2 ***p <0.001; Stage 3 ***p <0.001; n = 5 WT CM, 5 Phosphacan depleted CM; WT MBP+ Stage 1 = 290, Stage 2 = 377, Stage 3 = 189; Phosphacan depleted CM MBP+ Stage 1 = 306, Stage 2 = 278, Stage 3 = 138). (D) Left; No change in OPC maturation is observed between WT neuronal CM or WT neuronal CM preincubated with protein L alone (ns p = 0.1456, n = 3 WT CM [1007 Olig2+ cells; 325 MBP+ cells], 3 Protein L incubated CM [869 Olig2+ cells; 304 MBP+ cells], two tailed unpaired t-test). Right; stages of OL maturation were equivalent between WT neuronal CM and WT neuronal CM preincubated with protein L (2-way ANOVA ns p = 0.1262; Bonferroni correction Stage 1 ns p >0.05; Stage 2 ns p >0.05; Stage 3 ns p >0.05; n = 5 WT CM, 5 Phosphacan depleted CM; WT CM MBP+ Stage 1 = 132, Stage 2 = 132, Stage 3 = 61; Phosphacan depleted CM MBP+ Stage 1 = 97, Stage 2 = 140, Stage 3 = 67). All graphs: Mean $\pm$ sem. Scale bars: 100 μm

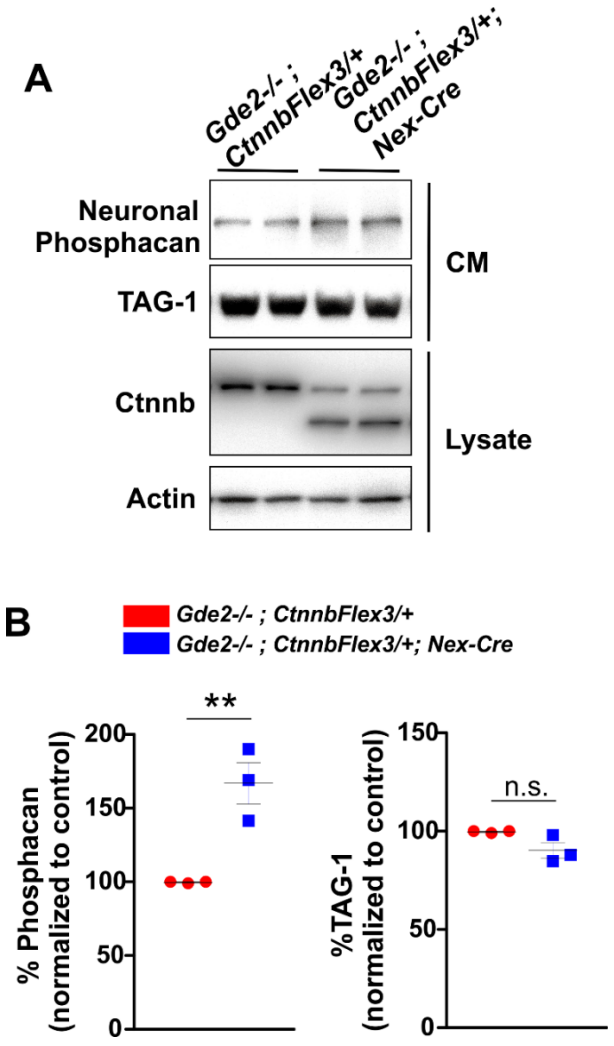

Figure 8.4. Phosphacan is increased in β-catenin stabilized *Gde2-/-* CM

(A) Western blots of *Gde2-/-* CM with or without β-catenin stabilization. (B) Western blot of *Gde2-/-; CtnnFlex3/+* and *Gde2-/-; CtnnbFlex3/+; Nex-Cre* neuronal CM. Graphs quantifying Western blots show robust increase in phosphacan levels in *Gde2-/-; CtnnbFlex3/+; Nex-Cre* neuronal CM (**p = 0.009) but no change in TAG-1 (ns p = 0.0781). n = 3 *Gde2-/-; CtnnbFlex3/+* CM, 3 *Gde2-/-; CtnnbFlex3/+; Nex-Cre* CM. All graphs: Mean ± sem, two-tailed unpaired Students t-test.

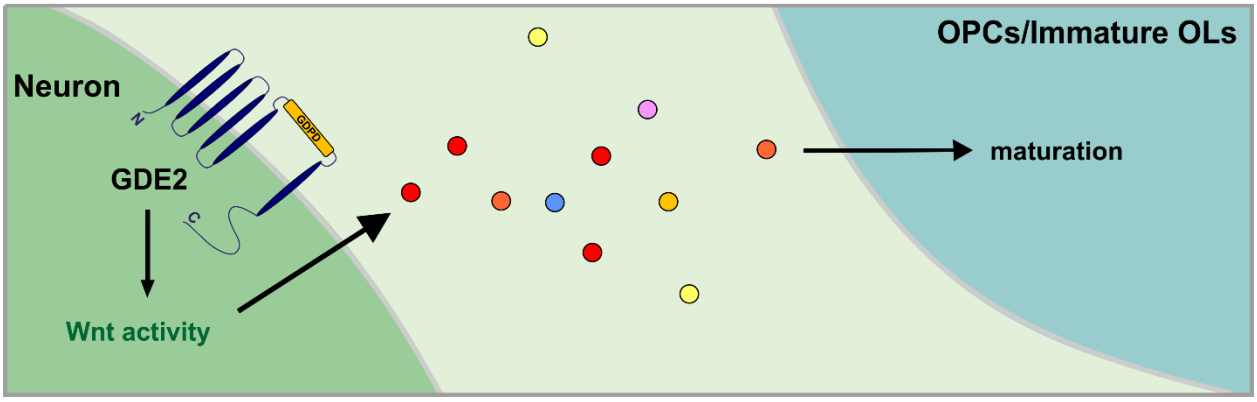

Figure 8.5. A model for GDE2 regulation of OL maturation

GDE2 is primarily expressed in neurons in the postnatal cortex. GDE2 in neurons stimulates canonical Wnt signaling. Wnt activation leads to release of neuronally-derived factors such as phosphacan, which act on neighboring OPCs or immature OLs to promote their maturation into myelinating oligodendrocytes.

Table 8.1. Mass spectrometry proteins that were differentially enriched in *Gde2-/-* CM.

Number of altered protein expression: 149

Protein IDs	Protein names	Gene names	Sequence coverage KO [%]	Sequence coverage WT [%]	LFQ intensity KO	LFQ intensity WT	Ratio (KO/WT)
A8DUK4	beta-globin	Hbbt1	60.9	58.2	3.67E+06	3.93E+08	0.0093
Q80ZV4	Cadherin-4	Cdh4	3.6	3.6	3.59E+05	6.73E+06	0.0533
P35979	60S ribosomal protein L12	Olfm1	9.7	9.7	3.50E+05	3.35E+06	0.1047
Q3TLP8	Ras-related C3 botulinum toxin substrate 1	Rac1	9.45	12.3	1.22E+06	1.16E+07	0.1056
P58283	E3 ubiquitin-protein ligase RNF216	Rnf216	0.8	0.8	7.20E+05	5.81E+06	0.1241
Q6ZWQ9	Myosin regulatory light chain 12B	Myl12a	17.4	9.3	2.92E+06	2.11E+07	0.1385
P48678	Prelamin-A/C	Lmna	1.8	0.75	7.71E+04	3.94E+05	0.1956
F6VYE2	Zinc finger MYM-type protein 4	Zmym4	0.7	0.7	3.81E+07	1.28E+08	0.2985
G5E866	Splicing factor 3B subunit 1	Sf3b1	0.35	1.1	6.29E+05	2.08E+06	0.3018
Q99JI6	Ras-related protein Rap-1b	Rap1b	11.15	11.15	2.20E+06	7.24E+06	0.3041
P62897	Cytochrome c, somatic	Cycs	17.15	17.15	1.47E+06	4.78E+06	0.3074
P32233	Developmentally-regulated GTP-binding protein 1	Drg1	4.4	4.4	4.55E+05	1.37E+06	0.3316
Q2KIG3	Carboxypeptidase B2	Cpb2	2.6	2.15	2.81E+05	8.34E+05	0.3367
P19253	60S ribosomal protein L13a	Rpl13a	8.1	8.1	1.20E+06	3.52E+06	0.3410
P97350	Plakophilin-1	Pkp1	2.25	2.25	2.43E+06	6.66E+06	0.3647
P62242	40S ribosomal protein S8	Rps8	8.9	7.2	7.11E+05	1.75E+06	0.4059
Q3UHN9	Bifunctional heparan sulfate N-deacetylase	Ndst1	0.8	1.6	9.53E+05	2.35E+06	0.4064
A0A087WPL5	ATP-dependent RNA helicase A	Dhx9	0.6	0.85	4.55E+05	1.11E+06	0.4094
Q8QZY9	Splicing factor 3B subunit 4	Sf3b4	1.65	3.3	2.16E+06	5.03E+06	0.4288

P70296	Phosphatidylethanolamine-binding protein 1	Pebp1	32.6	29.15	4.56E+07	1.05E+08	0.4363
Q62189	U1 small nuclear ribonucleoprotein A	Snrpa	9.55	9.55	7.22E+06	1.64E+07	0.4395
B9EKR1	Receptor-type tyrosine-protein phosphatase zeta	Ptprz1	7.05	6.8	1.08E+08	2.43E+08	0.4454
Q9DBG3	AP-2 complex subunit beta;AP complex subunit beta	Ap2b1	2	1.3	2.06E+06	4.55E+06	0.4524
Q60648	Ganglioside GM2 activator	Gm2a	8.8	4.4	1.39E+06	2.98E+06	0.4667
Q9CXV9	DCN1-like protein 5	Dcun1d5	6.3	6.3	3.76E+07	8.06E+07	0.4668
Q9Z0L8	Gamma-glutamyl hydrolase	Ggh	12.9	12.9	6.49E+06	1.37E+07	0.4751
P80317	T-complex protein 1 subunit zeta	Cct6a	4.35	2.85	1.13E+06	2.35E+06	0.4792
B1AX58	Plastin-3	Pls3	0.7	1.4	8.46E+05	1.76E+06	0.4812
Q9R1P3	Proteasome subunit beta type-2	Psmb2	6.2	9.95	8.15E+06	1.65E+07	0.4937
Q8R093	Uridine phosphorylase	Upp2	4.2	2.1	5.18E+07	1.03E+08	0.5007
Q8BFR2	Follistatin-related protein 5	Fstl5	8	9.8	1.04E+07	2.08E+07	0.5017
Q9EST1	Gasdermin-A	Gsdma	1	2.6	1.80E+06	3.50E+06	0.5149
Q91V64	Isochorismatase domain-containing protein 1	Isoc1	5.2	10.4	1.33E+06	2.58E+06	0.5164
P06745	Glucose-6-phosphate isomerase	Gpi	5.2	5.2	9.57E+05	1.84E+06	0.5188
Q9CQU0	Thioredoxin domain-containing protein 12	Txndc12	6.45	4.4	1.93E+06	3.68E+06	0.5235
Q08331	Calretinin	Calb2	11.8	11.8	3.97E+06	7.51E+06	0.5290
Q9QXV0	ProSAAS	Pcsk1n	12.2	10.5	9.84E+06	1.85E+07	0.5323
A3KGE4	Noelin	Olfm1	4.3	4.3	7.73E+05	1.44E+06	0.5357
Q3TKX1	V-type proton ATPase subunit S1	Atp6ap1	14.2	14.2	1.28E+07	2.37E+07	0.5404
Q9DAY9	Nucleophosmin	Npm1	4.1	14	1.17E+07	2.15E+07	0.5427
Q07235	Glia-derived nexin	Serpine2	13.35	13.35	5.49E+06	1.00E+07	0.5480

Q9JJU8	SH3 domain-binding glutamic acid-rich-like protein	Sh3bgrl	25	18	7.48E+06	1.36E+07	0.5488
P61164	Alpha-centractin	Actr1a	2.95	7.85	1.46E+06	2.65E+06	0.5501
P61358	60S ribosomal protein L27	Rpl27	7.35	10.65	2.31E+06	4.20E+06	0.5504
O09061	Proteasome subunit beta type-1	Psmb1	14.15	18.3	1.62E+07	2.92E+07	0.5535
Q5RKN9	F-actin-capping protein subunit alpha-1	Capza1	13.6	13.6	4.36E+06	7.85E+06	0.5549
E9PYH2	Cytosolic acyl coenzyme A thioester hydrolase	Acot7	8.3	6.75	6.44E+06	1.15E+07	0.5594
P24369	Peptidyl-prolyl cis-trans isomerase B	Ppib	18.05	16	2.04E+07	3.62E+07	0.5644
Q9D1C8	Vacuolar protein sorting-associated protein 28 homolog	Vps28	2.75	5.5	7.42E+05	1.31E+06	0.5653
Q3TX55	Actin-related protein 2/3 complex subunit 4	Arpc4	20.25	17.9	1.39E+07	2.44E+07	0.5691
P62702	40S ribosomal protein S4	Gm15013	5.1	8.1	7.23E+06	1.27E+07	0.5698
S4R1N6	40S ribosomal protein S18	Rps18	22.9	18.7	1.08E+07	1.88E+07	0.5730
P06684	Complement C5	C5	1.05	1.05	2.07E+06	3.60E+06	0.5753
D3Z6E4	Enolase;Gamma-enolase	Eno2	6.35	7.9	4.46E+05	7.64E+05	0.5834
P50247	Adenosylhomocysteinase	Ahcy	9	9	5.44E+06	9.19E+06	0.5925
P20029	78 kDa glucose-regulated protein	Hspa5	7.25	9.4	2.20E+06	3.68E+06	0.5991
P55821	Stathmin-2	Stmn2	14.5	14.5	2.67E+07	1.91E+07	1.4007
O35136	Neural cell adhesion molecule 2	Ncam2	3.5	3.5	2.09E+06	1.49E+06	1.4047
Q60994	Adiponectin	Adipoq	10.75	10.75	7.19E+07	5.10E+07	1.4090
Q60864	Stress-induced-phosphoprotein 1	Stip1	2.9	2.9	5.38E+06	3.81E+06	1.4108
D3YYE1	Acidic leucine-rich nuclear phosphoprotein 32 family member A	Anp32a	13.9	17.2	1.19E+07	8.38E+06	1.4150

Q8BGQ7	Alanine--tRNA ligase, cytoplasmic	Aars	0.9	0.9	1.01E+06	7.09E+05	1.4222
Q93092	Transaldolase	Taldo1	14	11.5	1.43E+08	9.97E+07	1.4303
Q99J36	THUMP domain-containing protein 1	Thumpd1	8.45	7.3	2.46E+06	1.72E+06	1.4344
Q99PT1	Rho GDP-dissociation inhibitor 1	Arhgdia	29.9	30.15	8.03E+07	5.58E+07	1.4393
Q61598	Rab GDP dissociation inhibitor beta	Gdi2	17.75	16.95	5.91E+07	4.07E+07	1.4504
A2A4I8	Amine oxidase	Aoc3	1.9	1.9	1.04E+08	7.17E+07	1.4506
P08030	Adenine phosphoribosyltransferase	Aprt	10	7.2	4.33E+06	2.98E+06	1.4561
P21460	Cystatin-C	Cst3	27.5	27.5	5.77E+08	3.93E+08	1.4677
P35441	Thrombospondin-1	Thbs1	4.8	5	6.15E+06	4.14E+06	1.4860
P04444	Hemoglobin subunit beta-H1	Hbb-bh1	21.1	21.1	7.56E+06	5.08E+06	1.4896
P02104	Hemoglobin subunit epsilon-Y2	Hbb-y	40.15	39.15	2.39E+08	1.60E+08	1.4902
Q8CBG6	6-phosphogluconolactonase	Pgls	7.2	10.9	4.86E+06	3.26E+06	1.4919
P63158	High mobility group protein B1	Hmgb1	24.3	24	5.03E+07	3.37E+07	1.4921
Q564E2	L-lactate dehydrogenase	Ldha	32.5	32.5	1.43E+08	9.51E+07	1.5027
P34022	Ran-specific GTPase-activating protein	Ranbp1	8.1	10.8	5.39E+06	3.58E+06	1.5047
P62869	Transcription elongation factor B polypeptide 2	Tceb2	26.25	22	7.90E+06	5.24E+06	1.5071
O70251	Elongation factor 1-beta	Eef1b2	11.7	15.2	6.12E+06	4.03E+06	1.5189
Q9WU60	Attractin	Atrn	0.55	0.55	2.72E+06	1.78E+06	1.5250
A2AI62	Hephaestin	Heph	0.9	0.9	6.04E+07	3.94E+07	1.5320
Q5XJF6	Ribosomal protein	Rpl10a	12.4	12.4	1.26E+07	8.16E+06	1.5469
Q9WTP6	Adenylate kinase 2	Ak2	6.9	4.2	6.54E+05	4.19E+05	1.5606
P21619	Lamin-B2	Lmnb2	2.3	1.15	8.17E+05	5.23E+05	1.5622
P10126	Elongation factor 1-alpha 1	Eef1a1	15.35	12.75	2.10E+09	1.33E+09	1.5713
Q5SXR6	Clathrin heavy chain;Clathrin heavy chain 1	Cltc	10.55	10.15	6.69E+07	4.26E+07	1.5720

Q9CQI6	Coactosin-like protein	Cotl1	14.45	16.55	1.03E+08	6.50E+07	1.5812
Q6P1J1	Dihydropyrimidinase-related protein 1	Crmp1	6.15	6.15	5.37E+06	3.38E+06	1.5861
B2M1R7	Poly(rC)-binding protein 2	Pcbp2	14.25	13.85	1.76E+07	1.11E+07	1.5871
Q9DCD0	6-phosphogluconate dehydrogenase, decarboxylating	Pgd	5.8	5.8	1.23E+07	7.69E+06	1.6019
Q8BHZ0	Protein FAM49A	Fam49a	8.5	6.5	7.84E+05	4.87E+05	1.6099
P35585	AP-1 complex subunit mu-1	Ap1m1	5.8	4.05	1.90E+06	1.17E+06	1.6273
Q61171	Peroxiredoxin-2	Prdx2	25	25	5.06E+08	3.10E+08	1.6326
F6ZBL2	E3 ubiquitin-protein ligase MIB1	Mib1	2.5	2.5	1.95E+09	1.18E+09	1.6437
Q3U3V1	Coagulation factor X	F10	1.8	1.8	3.78E+06	2.28E+06	1.6583
Q8BTU6	Eukaryotic initiation factor 4A-II	Eif4a2	24.2	21.65	9.47E+06	5.57E+06	1.6981
P43277	Histone H1.3	Hist1h1d	18.55	18.55	2.84E+08	1.67E+08	1.6982
Q91WU0	Carboxylic ester hydrolase	Ces1f	2.1	2.1	6.60E+07	3.84E+07	1.7195
E0CZ27	Histone H3	H3f3a	15.55	19.3	5.70E+08	3.30E+08	1.7249
E9Q6B6	C-Jun-amino-terminal kinase-interacting protein 3	Mapk8ip3	1.4	1.4	3.23E+07	1.86E+07	1.7333
Q8BIZ0	Protocadherin-20	Pcdh20	0.7	0.7	6.59E+05	3.79E+05	1.7369
P29788	Vitronectin	Vtn	3.8	3.8	2.38E+06	1.35E+06	1.7573
Q9CQV8	14-3-3 protein beta/alpha	Ywhab	20.9	23.15	4.20E+07	2.38E+07	1.7636
P17897	Lysozyme C-1	Lyz1	8.1	8.1	3.90E+06	2.19E+06	1.7755
P97333	Neuropilin-1	Nrp1	2.3	3.1	3.55E+06	1.99E+06	1.7818
G3X9I4	Aly/REF export factor 2	Alyref2	5	5	1.75E+07	9.73E+06	1.8023
P63260	Actin	Actg1	47.6	44.65	3.53E+06	1.94E+06	1.8262
P62082	40S ribosomal protein S7	Rps7	2.1	2.1	7.19E+06	3.94E+06	1.8267
H7BX52	Cullin-2	Cul2	17.8	17.8	5.21E+06	2.85E+06	1.8277
Q9R1P1	Proteasome subunit beta type-3	Psmb3	6.8	3.4	6.64E+06	3.63E+06	1.8285

F6W8R9	Nesprin-2	Syne2	1.1	0.55	7.38E+06	4.00E+06	1.8434
Q8VEK3	Heterogeneous nuclear ribonucleoprotein U	Hnrnpu	4.65	4.65	5.36E+06	2.89E+06	1.8557
A2A813	Protein deglycase DJ-1	Park7	9.1	7.7	7.71E+06	4.15E+06	1.8573
G3UZR0	N(G),N(G)-dimethylarginine dimethylaminohydrolase 2	Ddah2	16.55	19.7	3.48E+06	1.87E+06	1.8595
P2604	Moesin	Msn	4.75	4.75	3.57E+06	1.91E+06	1.8642
Q9JMG7	Hepatoma-derived growth factor-related protein 3	Hdgfrp3	8.2	8.2	2.53E+06	1.34E+06	1.8808
D3Z7E6	Platelet-activating factor acetylhydrolase IB subunit gamma	Pafah1b3	13.9	16.4	8.71E+06	4.61E+06	1.8873
Q5SW88	Ras-related protein Rab-1A	Rab1	8.9	12.4	1.80E+07	9.38E+06	1.9215
Q61233	Plastin-2	Lcp1	9	6.45	1.52E+07	7.75E+06	1.9644
D3Z315	Coatomer subunit epsilon	Cope	7.3	9.9	1.54E+06	7.76E+05	1.9872
P26645	Myristoylated alanine-rich C-kinase substrate	Marcks	16.2	8.1	5.31E+06	2.52E+06	2.1103
Q62084	Protein phosphatase 1 regulatory subunit 14B	Ppp1r14b	17	17.35	8.34E+06	3.89E+06	2.1448
G3UY42	Polyadenylate-binding protein 2	Pabpn1	8.5	8.5	2.45E+06	1.12E+06	2.1813
B7FAV1	Filamin-A	Flna	1	0.3	2.64E+06	1.19E+06	2.2174
Q9CQI3	Glia maturation factor beta	Gmfb	14.6	14.6	1.14E+07	5.01E+06	2.2675
H7BXC3	Triosephosphate isomerase	Tpi1	12.9	12.6	4.71E+06	2.07E+06	2.2688
Q60865	Caprin-1	Caprin1	3.3	3.3	2.74E+07	1.20E+07	2.2891
F6Q2E3	26S protease regulatory subunit 6A	Psmc3	7.9	3.95	6.35E+05	2.72E+05	2.3319
F6VRI6	Ubiquitin-like modifier-activating enzyme 5	Uba5	16.2	8.1	5.56E+05	2.33E+05	2.3832
P60867	40S ribosomal protein S20	Rps20	14.25	9.65	1.46E+07	6.10E+06	2.3875

Q14AA6	GTP-binding nuclear protein Ran	Ran	9.7	14.8	5.11E+07	2.13E+07	2.3990
P68134	Actin, alpha skeletal muscle	Acta1	26.4	23.45	8.55E+07	3.55E+07	2.4109
P35700	Peroxiredoxin-1	Prdx1	17.75	20.15	6.77E+07	2.75E+07	2.4658
P02089	Hemoglobin subunit beta-2	Hbb-b2	46.9	46.6	1.84E+08	7.40E+07	2.4912
Q04750	DNA topoisomerase 1	Top1	2.1	2.1	1.98E+06	7.37E+05	2.6874
Q543K9	Purine nucleoside phosphorylase	Pnp;Pnp2	6.6	3.3	7.72E+05	2.84E+05	2.7204
Q8CGP4	Histone H2A	Hist1h2aa	21.4	21.4	4.88E+08	1.74E+08	2.8048
P83917	Chromobox protein homolog 1	Cbx1	9.2	7.55	1.22E+06	4.26E+05	2.8538
O35864	COP9 signalosome complex subunit 5	Cops5	14.3	14.3	4.69E+06	1.63E+06	2.8805
Q9CR00	26S proteasome non-ATPase regulatory subunit 9	Psmd9	5.1	2.55	4.20E+06	1.36E+06	3.0805
P00015	Cytochrome c, testis-specific	Cyct	24.3	17.65	1.89E+07	5.88E+06	3.2052
P28658	Ataxin-10	Atxn10	1.45	1.45	8.12E+05	2.29E+05	3.5437
P20357	Microtubule-associated protein 2	Map2	1.75	1.4	4.00E+06	1.13E+06	3.5490
P61750	ADP-ribosylation factor 4	Arf4	11.7	11.7	9.87E+06	2.49E+06	3.9554
P11087	Collagen alpha-1(I) chain	Col1a1	6.15	3.95	1.68E+07	4.21E+06	3.9850
P97379	Ras GTPase-activating protein-binding protein 2	G3bp2	12	12	3.87E+06	9.04E+05	4.2785
D3Z7K0	Ubiquitin thioesterase OTUB1	Otub1	18.65	14.9	2.72E+07	5.13E+06	5.3105
P27048	Small nuclear ribonucleoprotein-associated protein B	Snrpb	8.25	3.25	1.68E+06	2.01E+05	8.3721
P35396	Peroxisome proliferator-activated receptor delta	Ppard	1.6	1.6	1.39E+08	1.00E+07	13.8777
P07309	Transthyretin	Ttr	11.9	5.1	7.35E+07	1.55E+06	47.4083

Chapter 9
Summary and Future Directions

9.1 Summary

Our studies identify GDE2 as part of a novel signaling pathway in neurons that is required to promote OL maturation in the developing postnatal cortex. In previous studies, GDE2 has been shown to regulate the timing of neuronal differentiation in the cortex and the spinal cord during embryonic development[77,78]. These functions are achieved by regulating activities of GPI-anchored proteins through cleavage of the GPI-anchor and release from the plasma membrane[71]. Here, FISH of *Gde2* transcripts showed that *Gde2* continues to be expressed in the postnatal cortex. *Gde2* transcripts are predominantly expressed in neurons, with lower levels of expression in a subset of OLs. The temporal pattern of *Gde2* expression in the cortex is highly dynamic and, intriguingly, resembles the pattern of OL maturation during developmental myelination. Specifically, *Gde2* transcripts initially appear in deep cortical layers (P11) but later extend to more superficial layers (P28). Because deficits in neurogenesis from the loss of embryonic GDE2 expression do not persist postnatally, these observations raise the possibility that GDE2 has a role in OL development.

To determine if GDE2 plays roles in OL development in the postnatal brain, we genetically ablated GDE2 expression in mouse models (*Gde2-/-*). *Gde2-/-* animals showed equivalent levels of OPCs as observed in WT littermates; however, they displayed a marked decrease in the number of mature OLs marked by either CC1+ or ASPA+ expression, and they showed robust reductions in the levels of myelin proteins such as MBP and MOG. Consistent with impaired OL maturation, *Gde2-/-* animals exhibited hypomyelination during the peak period of developmental myelination. Specifically, TEM analysis of myelin sheath ultrastructure revealed that *Gde2-/-* animals

had lower numbers of myelinated axons, and axons that were myelinated had thinner myelin sheaths with no change in axon diameter. Interestingly, levels of myelin-associated proteins largely recover by P28, when developmental myelination is complete; however, *Gde2-/-* animals at 2 months of age still show a decrease in the number of myelinated axons whose diameter is larger than 2 μm. Thus, GDE2-dependent mechanisms of OL maturation are important for the timing of OL maturation during development and to ensure appropriate axonal myelination.

GDE2 is expressed in neurons and OLs, raising the question as to the cellular requirements for GDE2 in regulating OL maturation. Genetic deletion of GDE2 in neurons resulted in impaired OL maturation with normal OPC proliferation and differentiation, which phenocopies global GDE2 deletion. These observations suggest that GDE2 function in neurons is required to promote OL maturation. Interestingly, deletion of GDE2 in oligodendroglia showed enhanced OL maturation, hinting at a role for GDE2 in OLs to check their precocious maturation. Based on the known roles of GDE2 in regulating functions of GPI-anchored proteins on the cell surface and the expression of GDE2 in OLs but not OPCs, we propose a model where GDE2 in OLs regulates responsiveness to extracellular cues that arise from neighboring other cell types or local environment. As differentiating OLs undergo maturation, they upregulate the expression of genes and proteins that drive maturation in response to cell-extrinsic cues. Binding of such signaling molecules to their cognate receptors or receptor complexes expressed on the OL plasma membrane is the first step to induce signal transduction to initiate OL maturation. Thus, the expression, localization, and organization of these receptors or receptor complexs are expected to be subjects for

the fine tuning of OL maturation. Notably, GPI-anchored proteins exhibit diverse and dynamic localization and contribute to clustering and formation of multimeric receptor complexes at the cell surface thus modulating signal transduction[111,112]. In this regard, GDE2 could regulate the surface expression of GPI-anchored proteins that are involved in the control of OL maturation. It is conceivable that when GDE2 function is disrupted, the accumulation of GPI-anchored proteins on the cell surface could increase response to extrinsic cues, thus resulting in precocious OL maturation. Proteomic screening that probes the amount of surface GPI-anchored proteins on WT and *Gde2-/-* OLs will provide a stringent test of this model.

To better understand how neuronal GDE2 promotes OL maturation, we utilized *in vitro* primary culture systems that are more amenable to rapid manipulation. Cocultures of *Gde2-/-* neurons and WT OPCs recapitulated *in vivo* phenotypes in that there was a marked delay of OL maturation manifest by decreased numbers of mature MBP+ OLs and a marked reduction in myelinated axonal segments in contrast to cocultures of WT neurons with WT OPCs. Importantly, OPCs cultured in CM from *Gde2-/-* neurons phenocopied these OL maturation deficits. These observations suggest that GDE2 promotes OL maturation via the release of soluble factors rather than contact-mediated signals. Neuronal activity has been shown to positively regulate OL development via the release of neurotransmitters, such as glutamate and ATP[37,38]. To test the possibility that GDE2 regulates neuronal activity to promote OL maturation, calcium transients ($\Delta F/F0$) were monitored in living neurons from WT and *Gde2-/-* animals. However, no detectable calcium transients were observed in neurons of both genotypes at DIV3, a time point

when neuronal GDE2 promotes OL maturation. This observation suggests that GDE2-mediated OL maturation occurs independently of neuronal activity.

Our studies indicate that known neuronal factors that regulate OL maturation such as contact-mediated signals, axon diameter, and neuronal activity do not mediate GDE2-dependent OL maturation, thus suggesting that GDE2 regulates OL maturation via a novel pathway. To gain insights into the mechanisms involved, we analyzed RNA-seq data that compared transcriptional changes between WT and *Gde2-/-* nervous system tissue. This analysis revealed that Wnt signaling pathways are disrupted in the absence of GDE2. Known canonical Wnt signaling target genes identified in the analysis were downregulated, implying that GDE2 normally potentiates canonical Wnt signaling. To validate the relationship between GDE2 and canonical Wnt signaling, we assessed components of the Wnt signaling pathway by various methods. We discovered that *Gde2-/-* neurons showed a significant reduction in ABC using immunocytochemistry and Western blot. Nuclear ABC regulates the transcription of Wnt target genes by interacting with specific transcription factors. Consistent with reduced neuronal Wnt signaling in the absence of GDE2, there was a concomitant reduction in the expression of *Lef1*, a known downstream target gene, in *Gde2-/-* cortex and cultured neurons. Further, analysis of *Rosa26 Tcf/Lef H2B-eGFP* Wnt reporter mice confirmed a decrease in canonical Wnt signaling activity in neurons and OPCs in *Gde2-/-* cortices at the time of OL maturation. These studies suggest that GDE2 stimulates canonical Wnt activity during the period of OL maturation in the developing cortex.

To test if GDE2 activates neuronal Wnt signaling to stimulate OL maturation, we genetically activated Wnt pathways in *Gde2-/-* animals by stabilizing β-catenin

expression in neurons and in OPCs. Stabilization of β-catenin in *Gde2-/-* neurons rescued OL maturation deficits, suggesting that neuronal Wnt activity mediates GDE2-regulated OL maturation. In contrast, stabilization of β-catenin in *Gde2-/-* OPCs resulted in further impairment of OL maturation. In line with neuronal Wnt signaling mediating GDE2-dependent regulation of OL maturation, OPCs cultured with CM from β-catenin stabilized *Gde2-/-* neurons showed a robust enhancement in OL maturation.

To identify promaturation factors whose release is dependent on GDE2 functions, we performed an unbiased proteomic analysis of CM from WT and *Gde2-/-* neurons. Among the identified candidate factors, levels of phosphacan were significantly reduced in CM from *Gde2-/-* neurons. Strikingly, OPCs cultured in phosphacan-depleted CM from WT neurons recapitulated OL maturation deficits elicited by *Gde2-/-* neuronal CM, suggesting that phosphacan is one of the promaturation factors released from neurons by GDE2. Notably, CM from *Gde2-/-* neurons with stabilized β-catenin showed increased release of phosphacan compared to CM from *Gde2-/-* neurons.

The collective outcomes from my thesis work suggest that GDE2 stimulation of Wnt signaling in neurons releases soluble factors such as phosphacan that promote OL maturation.

9.2 Discussion and Future Directions

9.2.1 Neuronal GDE2 and OL maturation

Known factors in neurons that regulate OL development include contact-dependent signals between axons and oligodendroglia, axon caliber and neuronal activity [27,32,34]. Here we show that GDE2 activity in neurons stimulates OL maturation through a novel pathway that appears independent of these mechanisms. Analysis of OL maturation using WT OPCs cultured with WT and *Gde2-/-* neuronal CM indicates that the ability of neuronal GDE2 to regulate OL maturation does not rely on contact-mediated signals between axons and OPCs but is instead transmitted through soluble promaturation factors. Notably, neuronal CM in these studies was derived from neurons grown for DIV3. These neurons are immature and lack obvious neuronal activity as assayed by calcium imaging, thus ruling out possible contributions of activity-dependent mechanisms. In addition, measurements of axonal diameters in our TEM studies indicate that axonal caliber is unaffected by disruption of GDE2 function. Taken together, these studies provide support for a previously unappreciated mechanism driven by GDE2 whereby neurons release soluble factors that promote nearby OPCs to differentiate and initiate the myelination program. This idea is consistent with the expression of GDE2 in the developing cortex, which matches the pattern of OL maturation and myelination that initiates in deep layers and broadens to the superficial laminae[10].

We note that GDE2 loss leads to a delay in OL maturation; by P28, the numbers of myelinating OLs and the levels of myelin associated proteins in *Gde2-/-* animals are equivalent to WT. This recovery is likely due to the robust compensatory mechanisms known to occur when OL development is disrupted. However, the increased incidence of unmyelinated large-diameter axons in *Gde2-/-* adult animals suggests that the timing of

OL maturation regulated by GDE2-dependent mechanisms is important to ensure appropriate axonal myelination. GDE2 is vertebrate-specific[113]. We speculate that GDE2 could constitute one of several regulatory pathways that have evolved in vertebrates to myelinate axons in order to facilitate complex neural circuit function.

9.2.2 GDE2 regulation of canonical Wnt signaling and OL maturation

Canonical Wnt signaling has been previously observed in the developing cortex and roles for Wnt activation in progenitor proliferation, differentiation, and neuronal migration have been established [59,114,115]. My analysis of *Rosa26 Tcf/Lef H2B-eGFP* mice that report canonical Wnt signaling *in vivo* confirms Wnt signaling in the developing cortex and reveals that Wnt signaling is prevalent in neurons and OPCs during the period of developmental myelination. However, at P28, when developmental myelination is almost complete, there is remarkably little evidence of Wnt activation in neurons although subpopulations of oligodendroglial cells exhibit substantial reporter gene expression.

We show here that Wnt activation in neurons and OPCs is dependent in part on GDE2 function. Activation of canonical Wnt signaling in OPCs in *Gde2-/-* animals worsens OL maturation phenotypes and is consistent with previous studies showing that elevating Wnt signaling delays OL maturation and negatively regulates terminal OL differentiation [60,61]. In contrast, genetic stabilization of β-catenin in neurons of *Gde2-/-* animals rescues the OL maturation phenotypes in these animals, supporting the model that GDE2-dependent maintenance of Wnt signaling in neurons is important for appropriate OL development. This observation identifies new roles for neuronal canonical Wnt signaling in the crosstalk between neurons and oligodendroglia that operates to coordinate the

timing of OL maturation. Interestingly, while Wnt activation in neurons declines from P28, GDE2 continues to be expressed in neurons. This observation raises two main questions; how does GDE2 promote Wnt activation during developmental myelination, and how is this pathway switched off after P28? Greater insight into these questions will be gleaned from further investigation into the mechanisms by which GDE2 regulates canonical Wnt signaling. GDE2 is a membrane-bound enzyme that functions at the cell surface to regulate GPI-anchored protein function by cleavage of the GPI-anchor and release of the protein from the cell surface[70,71]. GPI-anchor cleavage can both activate or inhibit GPI-anchored proteins, and this occurs according to cellular context [116]. Accordingly, a plausible mechanism for GDE2 regulation of Wnt signaling is through regulation of GPI-anchored protein function. RECK and the heparan sulfate proteoglycans GPC6 and GPC4 are established substrates of GDE2[70,71]. RECK can bind Wnt7a/Wnt7b and can interact in a multiprotein complex with Gpr124 and Frizzled4 to stimulate Wnt signaling[112,117]. GPC6 and GPC4 are known to regulate Wnt pathway activation and can function as activators or inhibitors of Wnt signaling[118-120]. Notably, Wnt2b, 5a, 7b and Frizzled1, 2, 3, 9, and 10 are expressed in specified regions and lamallae in the postnatal CTX[47]. The known contributions of RECK, GPC6 and GPC4 in regulating Wnt signaling warrant further investigation into whether they mediate GDE2-dependent control of OL maturation.

9.2.3 Neuronal Wnt activity releases OL maturation factors

This study suggests that GDE2 function in neurons is required for the release of soluble factors that promote OL maturation. Strengthening the idea that GDE2 activation

of canonical Wnt signaling mediates this release is that CM from *Gde2-/-* neurons expressing stabilized β-catenin promotes OL maturation to an extent that is more potent than WT neuronal CM. Analysis of the proteins in WT and *Gde2-/-* CM identified a small number of secreted and ECM associated proteins that were reduced in CM from *Gde2-/-* neurons. We identified phosphacan within this cohort. Phosphacan is a splice variant of PTPRzeta encoded by the *Ptprz1* gene. It contains the extracellular domain of the full-length membrane-bound isoform of PTPRzeta that consists of an N-terminal carbonic anhydrase like domain, three fibronectin type III repeats, and attachment sites for chondroitin sulfate proteoglycan[121]. Loss of PTPRzeta results in increased OPC proliferation and impaired differentiation into OLs, and *in vitro* studies using cultured OPCs indicate that phosphacan regulates the rate of OL terminal maturation through interaction with Contactin 1 on OPCs[108,122]. PTPRzeta is widely expressed during the period of developmental myelination, but the relevant cellular source for phosphacan that regulates OL maturation has not been defined [109]. We show here that CM prepared from *Gde2-/-* neurons exhibit reduced levels of neuronal forms of phosphacan and that levels of phosphacan are restored in CM prepared from *Gde2-/-* neurons with stabilized β-catenin. Further, WT neuronal CM depleted for phosphacan mimics OL maturation deficits observed when OPCs are incubated with *Gde2-/-* neuronal CM. These collective observations are consistent with the model that phosphacan released by GDE2-dependent activation of Wnt signaling in neurons mediates OL maturation. While our study suggests that Wnt pathway activation is required for the release of phosphacan from neurons, how Wnt signaling promotes phosphacan release is not clear. Our bulk RNAseq data from *Gde2-/-* tissue showed no change in *Ptprz1* gene expression, which

encodes four different isoforms. Thus it is unclear whether the expression of phosphacan, the spliced isoform of the full-length transmembrane form, is affected in *Gde2-/-* neurons. Assessment of the expression of phosphacan transcript using qPCR would provide evidence whether the reduced phosphacan in *Gde2-/-* CM occurs via the transcriptional regulation of phosphcan expression or through secondary mechanisms that impact phosphacan protein production and secretion. In this study, we have focused on phosphacan because it is exemplar of a factor with known activities in promoting OL maturation. We note that CM contains a multitude of proteins and RNA species that, in part, could be contained in extracellular vesicles; it is thus possible that Wnt signaling pathways in neurons could promote the release of additional factors important for OL maturation.

In summary, we have identified GDE2 regulation of canonical Wnt signaling in neurons as a new pathway that controls the rate of OL maturation through the release of soluble promaturation factors that include phosphacan. This study provides new insight into the complex communication pathways between axons and oligodendroglia that collectively regulate developmental myelination.

Materials and Methods

Tissue processing and immunohistochemistry

Mice were deeply anesthetized with Avertin solution (1.3% 2,2,2-Tribromorethanol (Fluka 90710) and 0.7% 2-methyl-2-butanol (Sigma 240486) in Phosphate Buffered Saline (PBS) at 0.02 ml/g body weight and perfused transcardially with 0.1 M Phosphate Buffer (PB) followed by fixation solution (4% paraformaldehyde in 0.1 M PB). The brains were postfixed in the fixation solution overnight at 4°C and transferred to 30% sucrose solution and stored at 4°C for more than 48 hrs. The tissues were embedded in O.C.T. Compound (Tissue-Tek 62550–12), flash frozen, and coronally sectioned (50 μm for P7 brain tissues and 35 μm for the rest) with a cryostat (Thermo Fisher Scientific HM550). Immunofluorescence was performed on free-floating sections. Brain sections were boiled in sodium citrate buffer (10 mM sodium citrate with 0.05% Tween-20) at 95°C before blocking. Tissue sections were preincubated in blocking solution (1% normal goat serum, 0.3% Triton X-100 in PBS) for 2 hours at room temperature, then incubated in primary antibodies overnight at 4°C. Sections were mounted onto slides with mounting reagent (Polysciences 18606). Images were acquired using confocal microscopy (Zeiss LSM700) with 10 or 20x objective. A total of 4-5 sections were assessed per mouse and 3-5 mice were analyzed per group. For all studies, a region of interest (ROI) was chosen based on the anatomical structures of CC and CTX based on DAPI staining, subsequent to quantification (see section on Quantification and Statistical Analyses).

4-HT preparation and administration

4-hydroxytamoxifen (4-HT, sigma H7904) was prepared as described previously [123]. 0.2 mg of 4HT was injected to P7 pups intraperitoneally. Pups were sacrificed to collect tissue samples at P11.

Fluorescent in situ hybridization (FISH)

Embedded frozen tissues were sectioned at 16 μm. Sections were incubated in 3% hydrogen peroxide to block endogenous peroxidase activity and permeabilized with 0.3% Triton X-100 in PBS. Sections were acetylated in 0.3% acetic anhydride. After prehybridization, slides were hybridized with digoxigenin-labeled sense and antisense probes overnight at 65°C. To couple FISH with immunohistochemistry, sections were blocked in blocking solution (PerkinElmer FP1020) and incubated with sheep anti-digoxigenin-POD, 1:500 (Roche 11207733910) and relevant primary antibodies overnight at 4°C. After incubation with secondary antibodies (1 hour, room temperature), fluorescent signals were developed with TSA Plus Cy3 system (PerkinElmer NEL744001KT) according to the manufacturer's instructions. Images were acquired on a confocal microscope (Zeiss LSM700) with 20x objective and on Zeiss LSM800 with 10x objective for tiling (9x9).

Transmission Electron Microscopy (TEM)

Anesthetized mice were perfused intracardially with fixative containing 2% PFA (EM grade), 2% glutaraldehyde, 50 mM PO4, 5 mM MgCl2, in 50mM sodium cacodylate buffer, pH 7.4, for 30 min at a rate of 1 ml/min for P14 and 2min/ml for 10-week-old mice. Brains were post-fixed in the same fixative overnight at 4°C. CC and adjacent CTX

containing the ROI were carefully dissected out from 1000 μm coronally sectioned brain slices. For TEM imaging and analysis of the CC, the sagittal surface near the midline of the CC was sectioned further. All tissues were serially dehydrated, embedded, and sectioned by the JHU SOM Microscope Facility as previously described [124]. Images were acquired with a Hitachi 7600 TEM. Images (under 9700x and 65000x magnification) were obtained from the CC below the CTX at random with the operator blinded. ImageJ (National Institutes of Health) software was used to measure the number of myelinated axons and g-ratio per unit area. For g-ratio analysis, the diameters of axons and outer myelinated axons were calculated from the surface area derived from the circumference of each. For g-ratio analysis of P11 samples, selection of myelinated axons was unbiased. Specifically, a grid was first created, and axons located at grid line intersections were selected for g-ratio analysis. 100 myelinated axons were counted from 10~13 ROIs (under 9700x magnification) per animal and three animals were used per condition. For myelin sheath analysis of 10 week old samples, more than 500 axons with diameter greater than 0.5 μm were counted from 6~9 ROIs (under 9700x magnification) per animal with three animals per condition.

Cell culture

Mouse primary cortical neuronal cultures were prepared from embryonic day 16.5 (E16.5) fetuses from timed-pregnant mice using Neural Tissue Dissociation Kits (Miltenyi Biotec 130-092-628) according to the manufacturer's recommendations. Cortical preparations were plated at a density of 2.5 x 10^5 cells per cm^2 on plastic wells (6-well plate) or glass coverslips coated with poly-D-lysine (0.1 mg/ml in 0.1 M Trizma buffer pH 8.5) containing

1% laminin (Sigma-Aldrich L2020) and 1% PureCol Type I Bovine Collagen Solution (Advanced Biomatrix 5005-B). Cells were initially cultured in neurobasal medium (Gibco 21103-049) containing 5% fetal horse serum, 1% penicillin/streptomycin (Gibco 15140122), 1% Glutamax-I (Gibco 35050061), 1% sodium pyruvate (Gibco 11360070), 30 mM Glucose, and 2% SM1 supplement (STEMCELL Technologies 5711). The next day on DIV1, the medium was replaced with Neurobasal medium with 1% penicillin/streptomycin, 1% Glutamax-I, 1% sodium pyruvate, 30 mM Glucose, 2% SM1 supplement, and 1% N2B (STEMCELL Technologies 7156). OPCs were obtained from P6 cortices of WT pups using Neural Tissue Dissociation and Isolation kits (Miltenyi Biotec 130-090-312) with magnetic beads (Miltenyi Biotec 130-094-543) to positively select O4+ cells according to the manufacturer's recommendations. For neuron-OL cocultures, freshly isolated OPCs in coculture media (half DMEM:F12 and half Neural basal media containing 10 mM HEPES (Gibco 15630080), 2% SM1 supplement, 1% N2B, 0.5% penicillin/streptomycin, 5μg/mL N-Acetyl-Cysteine (Sigma A8199), 5 μM Forskolin (Calbiochem 344270), 10ng/mL CNTF (PeproTech 450-50) were added at a density of 30,000 cells on top of DIV3 neurons and cocultured for indicated time periods. Neuronally conditioned media (CM) were collected from neuronal cultures on DIV3 and spun at 3,000xg for 10 minutes at 4°C to remove cellular debris. Freshly isolated WT OPCs in DIV3 CM were plated at a density of 15,000 cells per cm^2 on plastic wells (24-well plate) or glass coverslips coated with poly-D-lysine (0.1 mg/ml in distilled water) containing 1% laminin. One day after plating, cells were replenished with CM collected from neurons on DIV4 and cultured for another 2 days prior to further analyses. For depletion of phosphacan from CM, CAT-315 antibodies recognizing neuronal phosphacan were bound to protein L magnetic beads

(Thermo Fisher Scientific 88849). Antibody-bound protein L magnetic beads were subsequently incubated with WT CM overnight at 4°C.

Immunocytochemistry

Cultured cells were fixed with 4% PFA solution for 10 minutes and permeabilized in PBS with 0.3% Tween-20 for 10 minutes followed by blocking with PBS containing 1% bovine serum albumin (BSA) and 0.15% Tween-20 for 1 hour at room temperature. The cells were incubated with primary antibodies diluted in PBS (1:500) overnight at 4°C. Primary antibodies used were as follows: Rat anti-MBP (Millipore MAB386), rabbit anti-Olig2 (Millipore AB9610), guinea pig anti-Olig2 (from B. Novitch), mouse anti-MBP (Covance SMI-99P-100), mouse anti-beta-Tubulin III (Sigma-Aldrich T8578), Rabbit anti-Neurofilament H (Millipore AB1989), rabbit anti-GFAP (Agilent Z0334), mouse anti-Active-β-Catenin (Anti-ABC) (Millipore 05-665). After incubation with appropriate secondary antibodies (1 hour room temperature), cells were counterstained with DAPI (Invitrogen R37606). To visualize F-actin network, cells were stained with Alexa Fluor 488-phalloidin (Invitrogen A12379) during secondary antibody incubation. Cells were mounted on slides with mounting reagent and imaged using confocal microscope (Zeiss LSM700) with 20x objective and on epifluorescence microscope (Keyence BZ-X710) with 10x objective for tiling (3x3).

Calcium transient imaging and analysis

Cortical neurons were loaded with the synthetic calcium indicator Fluo-4, AM (Thermo Scientific F14201) on DIV3. 4 mM Fluo-4 stock solution in DMSO (Sigma D8418) was

diluted in HEPES-buffered extracellular solution (143 mM NaCl, 5 mM KCl, 2 mM CaCl2, 1 mM MgCl2, 10 mM HEPES, 10 mM glucose, pH 7.2, osmolality 305-310 mOsm) to yield 2 μM working solution. At the end of image acquisition, 2 μM ionomycin (Tocris 1704) was added into each well as a positive control. Live recorded images of spontaneous calcium activity were acquired with epifluorescence microscope (Keyence BZ-X710) under 10X objective. Images were streamed at 3 Hz frame rate for 3.5 minutes. Each image frame was 680 x 480 pixels, which corresponded to 0.32 mm^2 rectangular area. F_0 (baseline) and F are the mean fluorescence intensities and fluorescence intensities at a given time in each ROI, respectively. A change in fluorescence (Δ F/F0) was considered as a Ca^{2+} rise if it was >10%. For peak analysis, F_0 for each ROI trace was manually adjusted to zero. Each data point represents mean value of Δ F/F_0 from at least 11 recordings per group at a given time.

mRNA-sequencing analysis

RNA-seq studies were performed using 5 week WT and *Gde2*-/- spinal cords. The ventral half of the lumbar spinal cord was freshly dissected from 3 WT and 3 *Gde2*-/- animals, and poly-adenylated mRNA was extracted using a Qiagen RNeasy Plus Mini Kit (Qiagen, 74134). cDNA libraries were prepared using the Illumina TruSeq Stranded mRNA Library Prep Kit (Illumina, RS-122-2101). Paired-end reads, 50 bp in length, were generated on an Illumina HiSeq 2500 system yielding between 50-61 million reads per sample. To analyze the RNA-seq data, reads were quality checked and trimmed using the programs fastqc [125] and fqtrim [126]. Reads were then mapped to the mouse genome mm10 using the spliced alignment program Tophat2 v2.1.1 [127] and assembled into transcripts using

Cufflinks v2.2.1 [128]. Mapping rates ranged from 91.7% to 95.2%, with 83-88% representing exonic reads, indicating very high-quality sequences. Transcript assemblies across all samples were merged with Cuffcompare v.2.2.1, using GENCODE v.M5 [129] as reference, to create a set of gene and transcript annotations that was later used in the differential analyses. Lastly, Cuffdiff v2.2.1 was run on each pairwise comparison to determine statistically significant differentially expressed genes (cutoffs: p-val<=0.05).

Mass spectrometry analysis

Neuronal CM samples were subjected to SDS-PAGE, followed by in-gel trypsin digestion (Shevchenko, et al, 2006). The extracted peptides were analyzed on an Orbitrap Fusion Lumos Tribrid Mass Spectrometer coupled with the UltiMate 3000 RSLCnano liquid chromatography system (Thermo Fisher Scientific). The peptides were loaded on Acclaim PepMap100 Nano-Trap Column (100 µm × 2 cm, Thermo Fisher Scientific). Peptides were resolved at 300-nl/min flow rate using a linear gradient of 10% to 35% solvent B (0.1% formic acid in 95% acetonitrile) over 95 minutes on an EASY-Spray column (50cm x 75 µm ID, Thermo Fisher Scientific). MaxQuant (v1.5.5.1) software was used for quantitation and identification of proteins from the mass spectrometry data using mouse UniProt database (released on May 2018) with common contaminant proteins (Cox et al., 2008). Search parameters included, a) trypsin as a proteolytic enzyme with up to 2 missed cleavages; b) first search peptide mass error tolerance of 20 ppm and the main search peptide mass error tolerance of 4 ppm; c) fragment mass error tolerance of 20 ppm; d) carbamidomethylation of cysteine (+57.02146 Da) as a fixed modification: e) oxidation of

methionine (+15.99492 Da) and protein acetyl (+42.01056 Da) on N-terminus as dynamic modifications. Peptides and proteins were filtered at 1 % false-discovery rate.

Immunoblotting

Samples were sonicated in lysis buffer (20 mM Tris-HCl pH 8.0, 130 mM NaCl, 2 mM EDTA, 0.5% TritonX-100, 0.5% NP-40, and 0.2% sodium deoxycholate) containing protease inhibitor cocktail (Sigma-Aldrich P8340), subjected to reducing SDS-PAGE, and transferred to PVDF membranes for immunoblotting. For detection of phosphacan in CM, CM samples were equilibrated at a final concentration of 3 mg/ml in chondroitinase buffer (50 mM Trizma, 60 mM sodium acetate, pH 8.0) and treated with chondroitinase ABC (0.25 U per 200 µg protein) from Proteus Vulgaris (Sigma-Aldrich, C3667) for 8 hours at 37°C. CM samples were then boiled in 1x gel loading buffer for electrophoresis and immunoblotting. Nuclear and cytosolic fractions were isolated by Nu-PER Nuclear and Cytoplasmic Extraction Reagents (Thermo Fisher Scientific 78833) according to the manufacturer's instructions. Transferred membranes were incubated with primary antibodies overnight at 4°C. Primary antibodies used were as follows: Rabbit anti-Olig2 (1:2,000 Millipore AB9610), Mouse anti-MBP (1:2,000 Covance SMI-99P-100), Mouse anti-MOG (1:3,000 Millipore MAB5680), Rabbit anti-Neurofilament H (1:10,000 Millipore AB1989), Rabbit anti-GDE2 (1:1000), Rabbit anti-PDGF receptor alpha (1:2,000 Cell Signaling Technology 3174), rabbit anti-Olig2 (Millipore AB9610), Mouse anti-ABC (1:1,000 Millipore 05-665), Ran (10,000 BD Biosciences 610341), Rabbit anti-β-Catenin (1:2,000 Cell Signaling Technology 8480), Goat anti-Contactin-2/TAG1 (1:1000 R and D Systems AF4439), Mouse anti-Chondroitin Sulfate Proteoglycan (CAT-315) (1:5000

Millipore MAB1581), Mouse anti-Phosphacan/protein tyrosinephosphatase-z/b (3F8) (1:1000 DSHB 3F8), Rabbit anti-GAPDH (1:1,000 Cell Signaling Technology 8884), Mouse anti-Actin (1:10,000 Millipore MAB1501). After incubation with appropriate HRP-conjugated secondary antibodies (1 hour room temperature), membranes were developed by film or by using a digital imaging system (KwikQuant, Kindle Biosciences).

Quantitative real-time PCR

Total RNA from *in vivo* or *in vitro* samples was extracted using Trizol (Thermo Fisher Scientific 15596018) and reverse transcription was carried out using SuperScript III (Thermo Fisher Scientific 18080051) according to the manufacturer's instructions. SYBR-green labeling (Thermo Fisher 4385612) was used for quantitative real-time PCR (Applied Biosystems). The Comparative CT ($\Delta\Delta$Ct) method was used to determine the relative quantities of mRNA.

Quantification and statistical analysis

3D Image quantification was performed using semi-automated Imaris (Bitplane). For quantification, 4-5 sections per animal and 3-5 animals per group were used. Littermate controls were utilized throughout the study. Images were obtained from brain regions of CC and CTX corresponding to retrosplenial and motor areas. After 3D image reconstruction, each ROI (CC and CTX) was created using the contour function in Imaris. Using spot and surface detection functions, parameters were set for size and fluorescent signal intensity threshold to create an object representing a nucleus or a cell body. After manual validation of parameter settings, the entire z-stack was subjected to automated

quantification using Imaris. Then, false-positive and false negative spots and surfaces were manually corrected. Number of cells was normalized to surface area of each ROI. All studies were blinded to the investigator. For quantifying intensity of *Gde2* transcript signal in FISH, mean signal intensity of *Gde2* channel (TSA-cy3) within each created 3D object (Olig2+ or NeuN+ cells) was obtained using Imaris. Percent cells expressing *Gde2* and mean intensity of *Gde2* signal per cell were analyzed. For quantifying GFP^+ nuclei in *Rosa26 Tcf/Lef H2B-eGFP* mice, spots were designated as GFP^+ when above a set threshold signal intensity. This threshold was applied across all analysis. The number of $NeuN^+$ GFP^+ and $Olig2^+$ GFP^+ cells in each ROI was analyzed using MATLAB modules in Imaris. For quantifying MBP^+ OLs at Stage1-Stage3 in culture, 3x3 tiled images with 10x objective (3.99 mm^2 area) were acquired from 2 wells per animal with at least three biological samples per experiment. The number of MBP^+ cells for each stage was divided by the number of Olig2+ cells in each group and then normalized to control. GraphPad Prism 5 software was used to generate plots and to conduct statistical analysis. The mean ± SEM are shown. Statistical significance was determined by a two-tailed, unpaired Student's t-test, 1-way or 2-way ANOVA test and is shown by * $p<0.05$, ** $p<0.01$, *** $p<0.001$. Power analysis (Sample Size Calculator, provided by UCSF Clinical & Translational Science Institute; http://www.sample-size.net/sample-size-means/) was conducted for all analyses. All samples sizes are sufficient to reach 80% power that detect estimated difference in means with a 5% significance level.

References

1 Sidoryk-Wegrzynowicz, M., Wegrzynowicz, M., Lee, E., Bowman, A. B. & Aschner, M. Role of astrocytes in brain function and disease. *Toxicologic pathology* **39**, 115-123, doi:10.1177/0192623310385254 (2011).
2 Araque, A., Parpura, V., Sanzgiri, R. P. & Haydon, P. G. Tripartite synapses: glia, the unacknowledged partner. *Trends in neurosciences* **22**, 208-215, doi:10.1016/s0166-2236(98)01349-6 (1999).
3 Paolicelli, R. C. *et al.* Synaptic pruning by microglia is necessary for normal brain development. *Science* **333**, 1456-1458, doi:10.1126/science.1202529 (2011).
4 Nave, K. A. Myelination and support of axonal integrity by glia. *Nature* **468**, 244-252, doi:10.1038/nature09614 (2010).
5 Kessaris, N. *et al.* Competing waves of oligodendrocytes in the forebrain and postnatal elimination of an embryonic lineage. *Nat Neurosci* **9**, 173-179, doi:10.1038/nn1620 (2006).
6 Tripathi, R. B. *et al.* Dorsally and ventrally derived oligodendrocytes have similar electrical properties but myelinate preferred tracts. *The Journal of neuroscience : the official journal of the Society for Neuroscience* **31**, 6809-6819, doi:10.1523/jneurosci.6474-10.2011 (2011).
7 Rowitch, D. H. & Kriegstein, A. R. Developmental genetics of vertebrate glial-cell specification. *Nature* **468**, 214-222, doi:10.1038/nature09611 (2010).
8 Pringle, N. P. & Richardson, W. D. A singularity of PDGF alpha-receptor expression in the dorsoventral axis of the neural tube may define the origin of the oligodendrocyte lineage. *Development (Cambridge, England)* **117**, 525-533 (1993).
9 Bergles, D. E. & Richardson, W. D. Oligodendrocyte Development and Plasticity. *Cold Spring Harbor perspectives in biology* **8**, a020453, doi:10.1101/cshperspect.a020453 (2015).
10 Tomassy, G. S. *et al.* Distinct profiles of myelin distribution along single axons of pyramidal neurons in the neocortex. *Science* **344**, 319-324, doi:10.1126/science.1249766 (2014).
11 Zhou, Q., Wang, S. & Anderson, D. J. Identification of a novel family of oligodendrocyte lineage-specific basic helix-loop-helix transcription factors. *Neuron* **25**, 331-343 (2000).
12 Kuhlbrodt, K., Herbarth, B., Sock, E., Hermans-Borgmeyer, I. & Wegner, M. Sox10, a novel transcriptional modulator in glial cells. *The Journal of neuroscience : the official journal of the Society for Neuroscience* **18**, 237-250 (1998).
13 Chang, A., Nishiyama, A., Peterson, J., Prineas, J. & Trapp, B. D. NG2-positive oligodendrocyte progenitor cells in adult human brain and multiple sclerosis lesions. *The Journal of neuroscience : the official journal of the Society for Neuroscience* **20**, 6404-6412 (2000).
14 Marques, S. *et al.* Oligodendrocyte heterogeneity in the mouse juvenile and adult central nervous system. *Science* **352**, 1326-1329, doi:10.1126/science.aaf6463 (2016).
15 Hammond, E. *et al.* The Wnt effector transcription factor 7-like 2 positively regulates oligodendrocyte differentiation in a manner independent of Wnt/beta-

catenin signaling. *The Journal of neuroscience : the official journal of the Society for Neuroscience* **35**, 5007-5022, doi:10.1523/jneurosci.4787-14.2015 (2015).
16 Bhat, R. V. *et al.* Expression of the APC tumor suppressor protein in oligodendroglia. *Glia* **17**, 169-174, doi:10.1002/(sici)1098-1136(199606)17:2<169::aid-glia8>3.0.co;2-y (1996).
17 Dugas, J. C., Tai, Y. C., Speed, T. P., Ngai, J. & Barres, B. A. Functional genomic analysis of oligodendrocyte differentiation. *The Journal of neuroscience : the official journal of the Society for Neuroscience* **26**, 10967-10983, doi:10.1523/jneurosci.2572-06.2006 (2006).
18 Solly, S. K. *et al.* Myelin/oligodendrocyte glycoprotein (MOG) expression is associated with myelin deposition. *Glia* **18**, 39-48, doi:10.1002/(sici)1098-1136(199609)18:1<39::aid-glia4>3.0.co;2-z (1996).
19 Madhavarao, C. N. *et al.* Immunohistochemical localization of aspartoacylase in the rat central nervous system. *The Journal of comparative neurology* **472**, 318-329, doi:10.1002/cne.20080 (2004).
20 Aggarwal, S. *et al.* Myelin membrane assembly is driven by a phase transition of myelin basic proteins into a cohesive protein meshwork. *PLoS biology* **11**, e1001577, doi:10.1371/journal.pbio.1001577 (2013).
21 Hildebrand, C., Remahl, S., Persson, H. & Bjartmar, C. Myelinated nerve fibres in the CNS. *Prog Neurobiol* **40**, 319-384, doi:10.1016/0301-0082(93)90015-k (1993).
22 Pan, Z. *et al.* A common ankyrin-G-based mechanism retains KCNQ and NaV channels at electrically active domains of the axon. *The Journal of neuroscience : the official journal of the Society for Neuroscience* **26**, 2599-2613, doi:10.1523/JNEUROSCI.4314-05.2006 (2006).
23 Poliak, S. *et al.* Juxtaparanodal clustering of Shaker-like K+ channels in myelinated axons depends on Caspr2 and TAG-1. *The Journal of cell biology* **162**, 1149-1160, doi:10.1083/jcb.200305018 (2003).
24 Wang, S. S. *et al.* Functional trade-offs in white matter axonal scaling. *The Journal of neuroscience : the official journal of the Society for Neuroscience* **28**, 4047-4056, doi:10.1523/JNEUROSCI.5559-05.2008 (2008).
25 Yeung, M. S. *et al.* Dynamics of oligodendrocyte generation and myelination in the human brain. *Cell* **159**, 766-774, doi:10.1016/j.cell.2014.10.011 (2014).
26 Makinodan, M., Rosen, K. M., Ito, S. & Corfas, G. A critical period for social experience-dependent oligodendrocyte maturation and myelination. *Science* **337**, 1357-1360, doi:10.1126/science.1220845 (2012).
27 Gibson, E. M. *et al.* Neuronal activity promotes oligodendrogenesis and adaptive myelination in the mammalian brain. *Science* **344**, 1252304, doi:10.1126/science.1252304 (2014).
28 PdR, H. Tercera aportacion al conocimiento morfologico e interpretacion funcional de la oligodendroglıa. *Mem Real Soc Esp Hist Nat* **14**, 5-122 (1928).
29 Marques, S. *et al.* Transcriptional Convergence of Oligodendrocyte Lineage Progenitors during Development. *Developmental cell* **46**, 504-517.e507, doi:10.1016/j.devcel.2018.07.005 (2018).

30 Spitzer, S. O. *et al.* Oligodendrocyte Progenitor Cells Become Regionally Diverse and Heterogeneous with Age. *Neuron* **101**, 459-471.e455, doi:10.1016/j.neuron.2018.12.020 (2019).
31 Umemori, H., Sato, S., Yagi, T., Aizawa, S. & Yamamoto, T. Initial events of myelination involve Fyn tyrosine kinase signalling. *Nature* **367**, 572-576, doi:10.1038/367572a0 (1994).
32 Charles, P. *et al.* Negative regulation of central nervous system myelination by polysialylated-neural cell adhesion molecule. *Proceedings of the National Academy of Sciences of the United States of America* **97**, 7585-7590, doi:10.1073/pnas.100076197 (2000).
33 Wang, S. *et al.* Notch receptor activation inhibits oligodendrocyte differentiation. *Neuron* **21**, 63-75 (1998).
34 Lee, S. *et al.* A culture system to study oligodendrocyte myelination processes using engineered nanofibers. *Nature methods* **9**, 917-922, doi:10.1038/nmeth.2105 (2012).
35 Remahl, S. & Hildebrand, C. Changing relation between onset of myelination and axon diameter range in developing feline white matter. *J Neurol Sci* **54**, 33-45 (1982).
36 Goebbels, S. *et al.* A neuronal PI(3,4,5)P3-dependent program of oligodendrocyte precursor recruitment and myelination. *Nat Neurosci*, doi:10.1038/nn.4425 (2016).
37 Stevens, B., Porta, S., Haak, L. L., Gallo, V. & Fields, R. D. Adenosine: a neuron-glial transmitter promoting myelination in the CNS in response to action potentials. *Neuron* **36**, 855-868 (2002).
38 Yuan, X., Eisen, A. M., McBain, C. J. & Gallo, V. A role for glutamate and its receptors in the regulation of oligodendrocyte development in cerebellar tissue slices. *Development (Cambridge, England)* **125**, 2901-2914 (1998).
39 Ishibashi, T. *et al.* Astrocytes promote myelination in response to electrical impulses. *Neuron* **49**, 823-832, doi:10.1016/j.neuron.2006.02.006 (2006).
40 Goldstein, B., Takeshita, H., Mizumoto, K. & Sawa, H. Wnt signals can function as positional cues in establishing cell polarity. *Developmental cell* **10**, 391-396, doi:10.1016/j.devcel.2005.12.016 (2006).
41 Huang, Y. L. & Niehrs, C. Polarized Wnt signaling regulates ectodermal cell fate in Xenopus. *Developmental cell* **29**, 250-257, doi:10.1016/j.devcel.2014.03.015 (2014).
42 Schneider, J., Arraf, A. A., Grinstein, M., Yelin, R. & Schultheiss, T. M. Wnt signaling orients the proximal-distal axis of chick kidney nephrons. *Development (Cambridge, England)* **142**, 2686-2695, doi:10.1242/dev.123968 (2015).
43 Kitagawa, M. *et al.* An F-box protein, FWD1, mediates ubiquitin-dependent proteolysis of beta-catenin. *The EMBO journal* **18**, 2401-2410, doi:10.1093/emboj/18.9.2401 (1999).
44 Sawa, H. Control of cell polarity and asymmetric division in C. elegans. *Curr Top Dev Biol* **101**, 55-76, doi:10.1016/B978-0-12-394592-1.00003-X (2012).
45 Stamos, J. L., Chu, M. L., Enos, M. D., Shah, N. & Weis, W. I. Structural basis of GSK-3 inhibition by N-terminal phosphorylation and by the Wnt receptor LRP6. *eLife* **3**, e01998, doi:10.7554/eLife.01998 (2014).

46 Hovanes, K. *et al.* Beta-catenin-sensitive isoforms of lymphoid enhancer factor-1 are selectively expressed in colon cancer. *Nat Genet* **28**, 53-57, doi:10.1038/88264 (2001).
47 Shimogori, T., VanSant, J., Paik, E. & Grove, E. A. Members of the Wnt, Fz, and Frp gene families expressed in postnatal mouse cerebral cortex. *The Journal of comparative neurology* **473**, 496-510, doi:10.1002/cne.20135 (2004).
48 Peifer, M., McCrea, P. D., Green, K. J., Wieschaus, E. & Gumbiner, B. M. The vertebrate adhesive junction proteins beta-catenin and plakoglobin and the Drosophila segment polarity gene armadillo form a multigene family with similar properties. *The Journal of cell biology* **118**, 681-691, doi:10.1083/jcb.118.3.681 (1992).
49 Alok, A. *et al.* Wnt proteins synergize to activate beta-catenin signaling. *Journal of cell science* **130**, 1532-1544, doi:10.1242/jcs.198093 (2017).
50 Ke, J. *et al.* Structure and function of Norrin in assembly and activation of a Frizzled 4-Lrp5/6 complex. *Genes & development* **27**, 2305-2319, doi:10.1101/gad.228544.113 (2013).
51 Chang, T. H. *et al.* Structure and functional properties of Norrin mimic Wnt for signalling with Frizzled4, Lrp5/6, and proteoglycan. *eLife* **4**, doi:10.7554/eLife.06554 (2015).
52 Zhou, Y. & Nathans, J. Gpr124 controls CNS angiogenesis and blood-brain barrier integrity by promoting ligand-specific canonical wnt signaling. *Developmental cell* **31**, 248-256, doi:10.1016/j.devcel.2014.08.018 (2014).
53 Kakugawa, S. *et al.* Notum deacylates Wnt proteins to suppress signalling activity. *Nature* **519**, 187-192, doi:10.1038/nature14259 (2015).
54 Caneparo, L. *et al.* Dickkopf-1 regulates gastrulation movements by coordinated modulation of Wnt/beta catenin and Wnt/PCP activities, through interaction with the Dally-like homolog Knypek. *Genes & development* **21**, 465-480, doi:10.1101/gad.406007 (2007).
55 Cruciat, C. M. *et al.* Requirement of prorenin receptor and vacuolar H+-ATPase-mediated acidification for Wnt signaling. *Science* **327**, 459-463, doi:10.1126/science.1179802 (2010).
56 Song, H. H., Shi, W., Xiang, Y. Y. & Filmus, J. The loss of glypican-3 induces alterations in Wnt signaling. *The Journal of biological chemistry* **280**, 2116-2125, doi:10.1074/jbc.M410090200 (2005).
57 Chenn, A. Wnt/beta-catenin signaling in cerebral cortical development. *Organogenesis* **4**, 76-80 (2008).
58 Boitard, M. *et al.* Wnt signaling regulates multipolar-to-bipolar transition of migrating neurons in the cerebral cortex. *Cell reports* **10**, 1349-1361, doi:10.1016/j.celrep.2015.01.061 (2015).
59 Bocchi, R. *et al.* Perturbed Wnt signaling leads to neuronal migration delay, altered interhemispheric connections and impaired social behavior. *Nature communications* **8**, 1158, doi:10.1038/s41467-017-01046-w (2017).
60 Ye, F. *et al.* HDAC1 and HDAC2 regulate oligodendrocyte differentiation by disrupting the beta-catenin-TCF interaction. *Nat Neurosci* **12**, 829-838, doi:10.1038/nn.2333 (2009).

61 Fancy, S. P. *et al.* Dysregulation of the Wnt pathway inhibits timely myelination and remyelination in the mammalian CNS. *Genes & development* **23**, 1571-1585, doi:10.1101/gad.1806309 (2009).
62 Langseth, A. J. *et al.* Wnts influence the timing and efficiency of oligodendrocyte precursor cell generation in the telencephalon. *The Journal of neuroscience : the official journal of the Society for Neuroscience* **30**, 13367-13372, doi:10.1523/JNEUROSCI.1934-10.2010 (2010).
63 Fancy, S. P. *et al.* Axin2 as regulatory and therapeutic target in newborn brain injury and remyelination. *Nat Neurosci* **14**, 1009-1016, doi:10.1038/nn.2855 (2011).
64 Dai, Z. M. *et al.* Stage-specific regulation of oligodendrocyte development by Wnt/beta-catenin signaling. *The Journal of neuroscience : the official journal of the Society for Neuroscience* **34**, 8467-8473, doi:10.1523/jneurosci.0311-14.2014 (2014).
65 Lang, J. *et al.* Adenomatous polyposis coli regulates oligodendroglial development. *The Journal of neuroscience : the official journal of the Society for Neuroscience* **33**, 3113-3130, doi:10.1523/jneurosci.3467-12.2013 (2013).
66 Corda, D. *et al.* The emerging physiological roles of the glycerophosphodiesterase family. *The FEBS journal* **281**, 998-1016, doi:10.1111/febs.12699 (2014).
67 Labasque, M. & Faivre-Sarrailh, C. GPI-anchored proteins at the node of Ranvier. *FEBS letters* **584**, 1787-1792, doi:10.1016/j.febslet.2009.08.025 (2010).
68 Heider, S., Dangerfield, J. A. & Metzner, C. Biomedical applications of glycosylphosphatidylinositol-anchored proteins. *Journal of lipid research* **57**, 1778-1788, doi:10.1194/jlr.R070201 (2016).
69 Novitch, B. G., Wichterle, H., Jessell, T. M. & Sockanathan, S. A requirement for retinoic acid-mediated transcriptional activation in ventral neural patterning and motor neuron specification. *Neuron* **40**, 81-95, doi:10.1016/j.neuron.2003.08.006 (2003).
70 Matas-Rico, E. *et al.* Glycerophosphodiesterase GDE2 Promotes Neuroblastoma Differentiation through Glypican Release and Is a Marker of Clinical Outcome. *Cancer cell* **30**, 548-562, doi:10.1016/j.ccell.2016.08.016 (2016).
71 Park, S. *et al.* GDE2 promotes neurogenesis by glycosylphosphatidylinositol-anchor cleavage of RECK. *Science* **339**, 324-328, doi:10.1126/science.1231921 (2013).
72 van Veen, M. *et al.* Glycerophosphodiesterase GDE2/GDPD5 affects pancreas differentiation in zebrafish. *Int J Biochem Cell Biol* **94**, 71-78, doi:10.1016/j.biocel.2017.11.015 (2018).
73 Gallazzini, M., Ferraris, J. D. & Burg, M. B. GDPD5 is a glycerophosphocholine phosphodiesterase that osmotically regulates the osmoprotective organic osmolyte GPC. *Proceedings of the National Academy of Sciences of the United States of America* **105**, 11026-11031, doi:10.1073/pnas.0805496105 (2008).
74 Corda, D. *et al.* The developmentally regulated osteoblast phosphodiesterase GDE3 is glycerophosphoinositol-specific and modulates cell growth. *The Journal of biological chemistry* **284**, 24848-24856, doi:10.1074/jbc.M109.035444 (2009).

75 van Veen, M. *et al.* Negative regulation of urokinase receptor activity by a GPI-specific phospholipase C in breast cancer cells. *eLife* **6**, doi:10.7554/eLife.23649 (2017).
76 Dobrowolski, M. *et al.* GDE3 regulates oligodendrocyte precursor proliferation via release of soluble CNTFRalpha. *Development (Cambridge, England)* **147**, doi:10.1242/dev.180695 (2020).
77 Sabharwal, P., Lee, C., Park, S., Rao, M. & Sockanathan, S. GDE2 regulates subtype-specific motor neuron generation through inhibition of Notch signaling. *Neuron* **71**, 1058-1070, doi:10.1016/j.neuron.2011.07.028 (2011).
78 Rodriguez, M., Choi, J., Park, S. & Sockanathan, S. Gde2 regulates cortical neuronal identity by controlling the timing of cortical progenitor differentiation. *Development (Cambridge, England)* **139**, 3870-3879, doi:10.1242/dev.081083 (2012).
79 Louvi, A. & Artavanis-Tsakonas, S. Notch signalling in vertebrate neural development. *Nature reviews. Neuroscience* **7**, 93-102, doi:10.1038/nrn1847 (2006).
80 Muraguchi, T. *et al.* RECK modulates Notch signaling during cortical neurogenesis by regulating ADAM10 activity. *Nat Neurosci* **10**, 838-845, doi:10.1038/nn1922 (2007).
81 Shoemaker, L. D. & Arlotta, P. Untangling the cortex: Advances in understanding specification and differentiation of corticospinal motor neurons. *BioEssays : news and reviews in molecular, cellular and developmental biology* **32**, 197-206, doi:10.1002/bies.200900114 (2010).
82 Cave, C. *et al.* GDE2 is essential for neuronal survival in the postnatal mammalian spinal cord. *Molecular neurodegeneration* **12**, 8, doi:10.1186/s13024-017-0148-1 (2017).
83 Nave, K. A. & Werner, H. B. Myelination of the nervous system: mechanisms and functions. *Annual review of cell and developmental biology* **30**, 503-533, doi:10.1146/annurev-cellbio-100913-013101 (2014).
84 Nusse, R. & Clevers, H. Wnt/beta-Catenin Signaling, Disease, and Emerging Therapeutic Modalities. *Cell* **169**, 985-999, doi:10.1016/j.cell.2017.05.016 (2017).
85 Zhang, Y. *et al.* An RNA-sequencing transcriptome and splicing database of glia, neurons, and vascular cells of the cerebral cortex. *The Journal of neuroscience : the official journal of the Society for Neuroscience* **34**, 11929-11947, doi:10.1523/JNEUROSCI.1860-14.2014 (2014).
86 Cahoy, J. D. *et al.* A transcriptome database for astrocytes, neurons, and oligodendrocytes: a new resource for understanding brain development and function. *The Journal of neuroscience : the official journal of the Society for Neuroscience* **28**, 264-278, doi:10.1523/jneurosci.4178-07.2008 (2008).
87 Zhang, Y. *et al.* An RNA-sequencing transcriptome and splicing database of glia, neurons, and vascular cells of the cerebral cortex. **34**, 11929-11947, doi:10.1523/jneurosci.1860-14.2014 (2014).
88 Tasic, B. *et al.* Adult mouse cortical cell taxonomy revealed by single cell transcriptomics. *Nat Neurosci* **19**, 335-346, doi:10.1038/nn.4216 (2016).

89 Mayoral, S. R. & Chan, J. R. The environment rules: spatiotemporal regulation of oligodendrocyte differentiation. *Current opinion in neurobiology* **39**, 47-52, doi:10.1016/j.conb.2016.04.002 (2016).
90 Simon, C., Lickert, H., Gotz, M. & Dimou, L. Sox10-iCreERT2 : a mouse line to inducibly trace the neural crest and oligodendrocyte lineage. *Genesis (New York, N.Y. : 2000)* **50**, 506-515, doi:10.1002/dvg.22003 (2012).
91 Tatsumi, K. *et al.* Olig2-Lineage Astrocytes: A Distinct Subtype of Astrocytes That Differs from GFAP Astrocytes. *Front Neuroanat* **12**, 8, doi:10.3389/fnana.2018.00008 (2018).
92 Goebbels, S. *et al.* Genetic targeting of principal neurons in neocortex and hippocampus of NEX-Cre mice. *Genesis (New York, N.Y. : 2000)* **44**, 611-621, doi:10.1002/dvg.20256 (2006).
93 Kang, S. H., Fukaya, M., Yang, J. K., Rothstein, J. D. & Bergles, D. E. NG2+ CNS glial progenitors remain committed to the oligodendrocyte lineage in postnatal life and following neurodegeneration. *Neuron* **68**, 668-681, doi:10.1016/j.neuron.2010.09.009 (2010).
94 Kim, K. *et al.* Competitive PCR for quantitation of gonadotropin-releasing hormone mRNA level in a single micropunch of the rat preoptic area. *Mol Cell Endocrinol* **97**, 153-158, doi:10.1016/0303-7207(93)90222-6 (1993).
95 Bayraktar, O. A., Fuentealba, L. C., Alvarez-Buylla, A. & Rowitch, D. H. Astrocyte development and heterogeneity. *Cold Spring Harbor perspectives in biology* **7**, a020362, doi:10.1101/cshperspect.a020362 (2014).
96 Kaech, S. & Banker, G. Culturing hippocampal neurons. *Nature protocols* **1**, 2406-2415, doi:10.1038/nprot.2006.356 (2006).
97 Woodruff, R. H., Fruttiger, M., Richardson, W. D. & Franklin, R. J. Platelet-derived growth factor regulates oligodendrocyte progenitor numbers in adult CNS and their response following CNS demyelination. *Mol Cell Neurosci* **25**, 252-262, doi:10.1016/j.mcn.2003.10.014 (2004).
98 Zuchero, J. B. *et al.* CNS Myelin Wrapping Is Driven by Actin Disassembly. *Developmental cell* **34**, 152-167, doi:10.1016/j.devcel.2015.06.011 (2015).
99 Li, N., Sul, J. Y. & Haydon, P. G. A calcium-induced calcium influx factor, nitric oxide, modulates the refilling of calcium stores in astrocytes. *The Journal of neuroscience : the official journal of the Society for Neuroscience* **23**, 10302-10310 (2003).
100 Dedkova, E. N., Sigova, A. A. & Zinchenko, V. P. Mechanism of action of calcium ionophores on intact cells: ionophore-resistant cells. *Membr Cell Biol* **13**, 357-368 (2000).
101 Khawaled, R., Bruening-Wright, A., Adelman, J. P. & Maylie, J. Bicuculline block of small-conductance calcium-activated potassium channels. *Pflugers Archiv : European journal of physiology* **438**, 314-321, doi:10.1007/s004240050915 (1999).
102 Janda, C. Y., Waghray, D., Levin, A. M., Thomas, C. & Garcia, K. C. Structural basis of Wnt recognition by Frizzled. *Science* **337**, 59-64, doi:10.1126/science.1222879 (2012).

103 Liu, C. *et al.* Control of beta-catenin phosphorylation/degradation by a dual-kinase mechanism. *Cell* **108**, 837-847, doi:10.1016/s0092-8674(02)00685-2 (2002).
104 Bienz, M. beta-Catenin: a pivot between cell adhesion and Wnt signalling. *Current biology : CB* **15**, R64-67, doi:10.1016/j.cub.2004.12.058 (2005).
105 Cho, C., Smallwood, P. M. & Nathans, J. Reck and Gpr124 Are Essential Receptor Cofactors for Wnt7a/Wnt7b-Specific Signaling in Mammalian CNS Angiogenesis and Blood-Brain Barrier Regulation. *Neuron* **95**, 1056-1073 e1055, doi:10.1016/j.neuron.2017.07.031 (2017).
106 Bengoa-Vergniory, N., Gorrono-Etxebarria, I., Gonzalez-Salazar, I. & Kypta, R. M. A switch from canonical to noncanonical Wnt signaling mediates early differentiation of human neural stem cells. *Stem cells (Dayton, Ohio)* **32**, 3196-3208, doi:10.1002/stem.1807 (2014).
107 Harada, N. *et al.* Intestinal polyposis in mice with a dominant stable mutation of the beta-catenin gene. *The EMBO journal* **18**, 5931-5942, doi:10.1093/emboj/18.21.5931 (1999).
108 Lamprianou, S., Chatzopoulou, E., Thomas, J. L., Bouyain, S. & Harroch, S. A complex between contactin-1 and the protein tyrosine phosphatase PTPRZ controls the development of oligodendrocyte precursor cells. *Proceedings of the National Academy of Sciences of the United States of America* **108**, 17498-17503, doi:10.1073/pnas.1108774108 (2011).
109 Faissner, A., Heck, N., Dobbertin, A. & Garwood, J. DSD-1-Proteoglycan/Phosphacan and receptor protein tyrosine phosphatase-beta isoforms during development and regeneration of neural tissues. *Advances in experimental medicine and biology* **557**, 25-53, doi:10.1007/0-387-30128-3_3 (2006).
110 Dwyer, C. A., Katoh, T., Tiemeyer, M. & Matthews, R. T. Neurons and glia modify receptor protein-tyrosine phosphatase zeta (RPTPzeta)/phosphacan with cell-specific O-mannosyl glycans in the developing brain. *The Journal of biological chemistry* **290**, 10256-10273, doi:10.1074/jbc.M114.614099 (2015).
111 Saha, S., Anilkumar, A. A. & Mayor, S. GPI-anchored protein organization and dynamics at the cell surface. *Journal of lipid research* **57**, 159-175, doi:10.1194/jlr.R062885 (2016).
112 Cho, C., Smallwood, P. M. & Nathans, J. Reck and Gpr124 Are Essential Receptor Cofactors for Wnt7a/Wnt7b-Specific Signaling in Mammalian CNS Angiogenesis and Blood-Brain Barrier Regulation. *Neuron*, doi:10.1016/j.neuron.2017.07.031 (2017).
113 Nogusa, Y., Fujioka, Y., Komatsu, R., Kato, N. & Yanaka, N. Isolation and characterization of two serpentine membrane proteins containing glycerophosphodiester phosphodiesterase, GDE2 and GDE6. *Gene* **337**, 173-179, doi:10.1016/j.gene.2004.04.026 (2004).
114 Chenn, A. & Walsh, C. A. Regulation of cerebral cortical size by control of cell cycle exit in neural precursors. *Science* **297**, 365-369, doi:10.1126/science.1074192 (2002).
115 Munji, R. N., Choe, Y., Li, G., Siegenthaler, J. A. & Pleasure, S. J. Wnt signaling regulates neuronal differentiation of cortical intermediate progenitors. *The*

Journal of neuroscience : the official journal of the Society for Neuroscience **31**, 1676-1687, doi:10.1523/jneurosci.5404-10.2011 (2011).
116 Filmus, J., Capurro, M. & Rast, J. Glypicans. *Genome biology* **9**, 224, doi:10.1186/gb-2008-9-5-224 (2008).
117 Eubelen, M. *et al.* A molecular mechanism for Wnt ligand-specific signaling. *Science (New York, N.Y.)* **361**, doi:10.1126/science.aat1178 (2018).
118 Han, C., Yan, D., Belenkaya, T. Y. & Lin, X. Drosophila glypicans Dally and Dally-like shape the extracellular Wingless morphogen gradient in the wing disc. *Development (Cambridge, England)* **132**, 667-679, doi:10.1242/dev.01636 (2005).
119 Sakane, H., Yamamoto, H., Matsumoto, S., Sato, A. & Kikuchi, A. Localization of glypican-4 in different membrane microdomains is involved in the regulation of Wnt signaling. *Journal of cell science* **125**, 449-460, doi:10.1242/jcs.091876 (2012).
120 Lebensohn, A. M. *et al.* Comparative genetic screens in human cells reveal new regulatory mechanisms in WNT signaling. *eLife* **5**, doi:10.7554/eLife.21459 (2016).
121 Maurel, P., Rauch, U., Flad, M., Margolis, R. K. & Margolis, R. U. Phosphacan, a chondroitin sulfate proteoglycan of brain that interacts with neurons and neural cell-adhesion molecules, is an extracellular variant of a receptor-type protein tyrosine phosphatase. *Proceedings of the National Academy of Sciences of the United States of America* **91**, 2512-2516, doi:10.1073/pnas.91.7.2512 (1994).
122 Harroch, S. *et al.* A critical role for the protein tyrosine phosphatase receptor type Z in functional recovery from demyelinating lesions. *Nat Genet* **32**, 411-414, doi:10.1038/ng1004 (2002).
123 Badea, T. C., Wang, Y. & Nathans, J. A noninvasive genetic/pharmacologic strategy for visualizing cell morphology and clonal relationships in the mouse. *The Journal of neuroscience : the official journal of the Society for Neuroscience* **23**, 2314-2322 (2003).
124 Baxi, E. G. *et al.* Transfer of myelin-reactive th17 cells impairs endogenous remyelination in the central nervous system of cuprizone-fed mice. *The Journal of neuroscience : the official journal of the Society for Neuroscience* **35**, 8626-8639, doi:10.1523/jneurosci.3817-14.2015 (2015).
125 Andrews, S. FastQC: a quality control tool for high throughput sequence data. **Available online at**, http://www.bioinformatics.babraham.ac.uk/projects/fastqc (2010).
126 Pertea, G. Fqtrim: trimming and filtering of next-gen reads. **Available online at** http://ccb.jhu.edu/software/fqtrim/ (2010).
127 Kim, S. Y. *et al.* Diverging neural pathways assemble a behavioural state from separable features in anxiety. *Nature*, doi:10.1038/nature12018 (2013).
128 Trapnell, C. *et al.* Differential gene and transcript expression analysis of RNA-seq experiments with TopHat and Cufflinks. *Nature protocols* **7**, 562-578, doi:10.1038/nprot.2012.016 (2012).
129 http://www.gencodegenes.org/. **Reference gene annotation for the mouse genome**.

Biography

Bo-Ran Choi was born in Seoul, South Korea.

Bo-Ran attended Seoul National University College of Veterinary Medicine in South Korea where she majored in Veterinary Medicine. She earned her Master's (M.S.) degree at Seoul National University. During her M.S. studies, she worked under the supervision of Dr. Hee-Jong Woo where she investigated prion protein conversions induced by trivalent iron.

In 2014, Bo-Ran began her PhD at Johns Hopkins University School of Medicine under the mentorship of Dr. Shanthini Sockanathan.